Débora Elisa Peretti

Details on the Deterministic and Stochastic Stabilization of an Inverted Pendulum

Porto Alegre

2016

Débora Elisa Peretti

Details on the Deterministic and Stochastic Stabilization of an Inverted Pendulum

Master's thesis presented to Instituto de Física of Universidade Federal do Rio Grande do Sul as a partial requirement to a Master of Physics title.

Universidade federal do Rio Grande do Sul – UFRGS

Instituto de Física

Programa de Pós-Graduação em Física

Supervisor: Dr. Roberto da Silva

Collaborator: Dra. Sandra D. Prado

Porto Alegre

2016

"Contrariwise, if it was so, it might be;
and if it were so, it would be;
but as it isn't it ain't. That's logic."
(Tweedledee - 'Through the Looking Glass')

Abstract

In this work a quantitative and qualitative analysis of the dynamical stabilization of an inverted pendulum with a sinusoidal external perturbation applied at the suspension point is made. Initially, the external perturbation is composed of a single cosine, then a generalization is made using a sum of N cosines with different amplitudes and frequencies. Approximations are tested, and the time for which the inverted pendulum remains stable is explored when N is large, in order to recover the pattern of the case when $N = 1$. The specific case of periodic and almost periodic oscillations, when $N = 2$, is analysed and stability diagrams considering different frequencies and amplitudes are studied. Later, an additive Gaussian noise is added to the system so the degradation of the stability diagrams generated by different variances can be studied. All points of this work are corroborated by simulations, which numerically integrate the system's equation of motion through a fourth order Runge-Kutta method. Algorithms and extra details on the integration methods used are explored in a publication of this work, which is presented in this thesis as an appendix.

Keywords: Inverted pendulum. Dynamic stabilization. Parametric excitation. Gaussian noise.

Resumo

Neste trabalho, uma análise quantitativa e qualitativa para a estabilização dinâmica de um pêndulo invertido com uma força externa senoidal aplicada no ponto de suspensão é feita. Inicialmente, a perturbação externa é composta de um único cosseno, então uma generalização é feita, usando uma soma de N cossenos com diferentes amplitudes e frequências. Aproximações são testadas e o tempo durante o qual o pêndulo invertido permanece estável é explorado quando N é grande, a fim de recuperar o padrão do caso onde $N = 1$. O caso específico de oscilações periódicas e quase periódicas, quando $N = 2$, é analisado e diagramas de estabilidade considerando diferentes frequências e amplitudes são estudados. Depois, um ruído Gaussiano additivo é adicionado ao sistema para que a degradação dos diagramas de estabilidade gerados por variâncias diferentes possam ser estudados. Todos os pontos deste trabalho são corroborados por simulações, as quais integram numericamente as equações de movimento do sistema através do método de Runge-Kutta de quarta ordem. Os algoritmos e detalhes extras dos métodos de integração usados são explorados numa publicação deste trabalho, a qual está apresentada, nesta dissertação, como um apêndice.

Palavras-chave: Pêndulo invertido. Estabilização dinâmica. Excitação paramétrica. Ruído Gaussiano.

Contents

1 Introduction

The pendulum is a widely known physical model that has been studied in many textbooks and papers due to its importance in the history of Physics. One of the many uses of a pendulum is the pendulum clock. The fact that the simple pendulum is a harmonic oscillator is its main advantage; it swings back and forth in a precise time depending on its length. It was conceived by Galileo Galilei and invented by Christiaan Huygens in 1656.

A pendulum has two equilibrium positions: one stable and one unstable. The latter is located above the suspension point. The system at this position is generally known as an inverted pendulum. Since this is an unstable equilibrium position, any perturbation on the system will cause the pendulum to leave its original configuration and turn into a pendulum. But by applying a suitable choice of force at the suspension point, the inverted position may be stabilized, so the system oscillates around the now stable equilibrium position.

Oscillations can be classified into three different categories (BUTIKOV et al., 1999):

- **Free (natural):** occurs when a system is left isolated after an initial action.
- **Forced:** when an oscillator is subjected to an external influence whose effect over the system can be expressed by an extra term (a time-dependent periodic or quasi-periodic function, for example) on the differential equation of motion which describes the system. After a transient period, the forced oscillation becomes stationary and acquires the period of the external influence. When the frequency of the external force is close to the natural one, the final amplitude may assume high values. This phenomenon is called resonance.
- **Parametric:** consists of a periodic variation of a system's parameter, to which the motion is sensible.

The inverted pendulum and its stability are largely explored in Physics, Engineering, Biology and many other areas due to its technological importance (IBRAHIM, 2006). It is related to rocket or missile guidance, where the center of gravity is located behind the center of drag, causing aerodynamic instability (NASA, 2014); the interaction of inertia forces, hydrodynamic forces, and drag contributions makes the dynamical analysis of ocean structures similar to an inverted pendulum (SHLESINGER; SWEAN, 1998); the body posture of a biped walking can be regarded as a simple linear inverted pendulum, which has been the focus of many robotics studies (YANG; PENG; SONG,

2013; KAJITA et al., 2010); random fluctuations in the spatial curvature provide an additional steadying mechanism to the stability of photons trajectories in cosmological models, and behave as an inverted pendulum with an excitation at its point of suspension (DETTMANN; KEATING; PRADO, 2004).

There are two ways of stabilizing an inverted pendulum: by feedback or controlling mechanism (YANG; PENG; SONG, 2013; YAMAKAWA, 1989), or by rapidly oscillating the pivot (KAPITZA, 1965). The latter is called the Kapitza's pendulum, and when the oscillation is sufficiently strong, the pendulum may recover from perturbations in a counterintuitive way.

Considering an inverted pendulum composed of a light rod of length l with a heavy small bob of mass m, as can be seen in Figure 1, and assuming the rod has negligible mass, so all the mass of the system is concentrated on the bob, the Lagrangian of the system can be written as:

$$L(\theta, \dot{\theta}, f, \dot{f}) = \frac{1}{2}ml^2\dot{\theta}^2 + \frac{1}{2}m\dot{f}^2 - ml\dot{f}\dot{\theta}\sin(\theta) - mgl\cos(\theta) - mgf(t). \tag{1.1}$$

Thefore, most general equation, which describes the motion of the bob is given by:

$$\frac{d^2\theta}{dt^2} + \beta\frac{d\theta}{dt} - \omega_0^2\left(1 - \frac{1}{g}\ddot{f}(t)\right)\sin(\theta) = \xi(t), \tag{1.2}$$

where β is the damping constant, $\omega_0 = \sqrt{g/l}$ is the angular frequency of free oscillations (natural frequency), $\ddot{f}(t)$ is an acceleration caused by an external perturbation $f(t)$, which has only a vertical component applied at the suspension point, and $\xi(t)$ is an additive noise. In this present work, damping effects will be neglected ($\beta = 0$). Therefore, the system is conservative, if there is no additive noise ($\xi(t) = 0$).

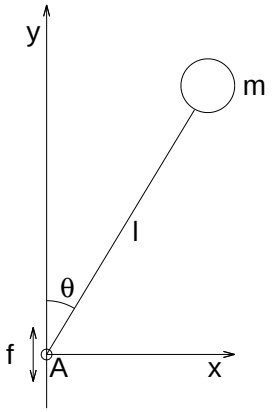

Figure 1 – Inverted pendulum composed of a heavy bob of mass m, a light rigid rod of length l, and f is the external perturbation applied at the suspension point.

When the frequency of the external force is approximately twice the natural frequency of the system, the lower state of equilibrium ($y < 0$) becomes unstable and the system leaves it, and the upper state of equilibrium ($y > 0$) becomes stable. This phenomenon is known as parametric resonance. This type of dynamic stability was first pointed out by Stephenson (1908). Kapitza (1965) has the first known work with a simple theoretical solution that he himself experimentally investigated.

However, oscillatory motions of the support are not the only way of stabilizing the system (SETHNA, 1973). Liu & Willms (1994) stabilized an inverted undamped pendulum by applying impulses in the y-direction corresponding to kicking it. This perturbation causes a change on angular velocity without changing the position: every time the pendulum starts to fall from the upper stability position, it is kicked back so it may stay close to the equilibrium position.

The main purpose of this work is to understand the stabilizing patterns of an inverted pendulum over infinite periods of time by using a deterministic periodic or almost periodic external perturbation ($f(t) \neq 0$) applied at the pivot. Stability diagrams will be constructed to study the permanence of the system at the upside-down position considering different sets of parameters. A Gaussian additive noise will be added to the system ($\xi(t) \neq 0$) and the effects on the diagrams will be analysed.

Since the inverted pendulum with an external force composed of one cosine has already been studied by several authors (KAPITZA, 1965; BUTIKOV, 2001; IBRAHIM, 2006; BUTIKOV et al., 1999; LANDAU; LIFSCHITZ, 1966; FENN; BAYNE; SINCLAIR, 1998), in Chapter 2, a review of these papers is presented and complemented by simulations and additional results.

On Chapter 3 a generalization of the calculations performed in the previous Chapter will be extended for a sum of N cosines, instead of a single one. Simulations will corroborate the mathematical results found. Two different aspects of the problem will be analysed: by randomly sorting frequencies, with the proper amplitude scaling, it will be shown that the time for which the system remains stable reproduces the same pattern as the behaviour of one cosine of Chapter 2; and by randomly sorting frequencies and amplitude inside defined ranges the optimal value of N so the system has a higher probability of stabilization will be found.

Chapter 4 presents the inverted pendulum with periodic or almost periodic external forces. Using the generalized results found on Chapter 3, the specific case of two cosines $N = 2$ is studied, and stability diagrams for the parameters of amplitude and frequency are constructed. The results will be compared to the ones established by Bogdanoff & Citron (1965). Since for almost periodic external forces there is no defined period, an analysis of possible choices of period will be performed to check if there is any that better reproduces the numerical results.

At last, on Chapter 5, a study of additive external Gaussian noise is presented. First a review of the works made by Bogdanoff & Citron (1965), Mitchell (1972), Sethna (1973) and Howe (1974), which presented only a stochastic external perturbation applied at the suspension point. Then, a Gaussian noise is added to the inverted pendulum along with the deterministic external force of a sum of cosines, differently from previous works, which only consider the stochastic component, so the examination of the destruction of the stability diagrams can be made.

Final remarks and comments are made on Chapter 6, where prospects for the continuity of this work will be presented.

2 The Inverted Pendulum under a Periodic Excitation of a Single Cosine

This Chapter is focused on an inverted pendulum with an external periodic excitation applied at the suspension point in the form of a single cosine of amplitude a and frequency Ω. Characteristics and some analysis of this system will be presented here.

2.1 The System

The equation of motion of an inverted pendulum considering a periodic external perturbation $f(t) = a\cos(\Omega t)$ only on the y-direction applied at the suspension point A (Figure 2), in the absence of friction ($\beta = 0$), from (1.2) is given by:

$$\ddot{\theta} - \left[\omega_0^2 - \frac{a\Omega^2}{l}\cos(\Omega t)\right]\sin(\theta) = 0 \tag{2.1}$$

where a is the amplitude of the external perturbation and Ω is its frequency. Using the approximation $\sin(\theta) \approx \theta$ for small angles, equation (2.1) can be rewritten as:

$$\ddot{\theta} - \left[\omega_0^2 - \frac{a\Omega^2}{l}\cos(\Omega t)\right]\theta = 0. \tag{2.2}$$

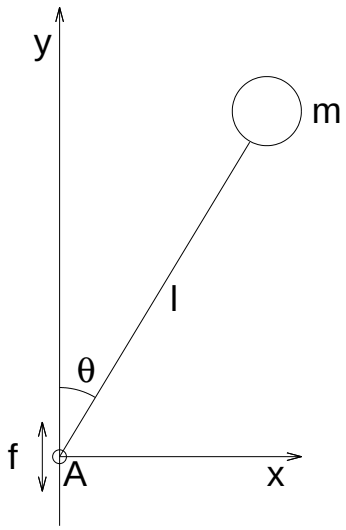

Figure 2 – Inverted pendulum composed of a heavy bob of mass m and a light rigid rod of length l with a vibration f applied at the suspension axis A, commonly known as “Kapitza’s Pendulum”.

Figure 3 shows the evolution of the angular position of an inverted pendulum for arbitrary angles (top plot, by numerically integrating equation (2.1)), and the behaviour of the external perturbation applied at the pendulum's suspension point. The parameters chosen for this figure were: amplitude $a = 0.17$ m, and frequency $\Omega = 30$ rad/s. The time evolution of equation (2.2), is not shown in Figure 3 because it has the exact same behaviour as the equation for arbitrary angles.

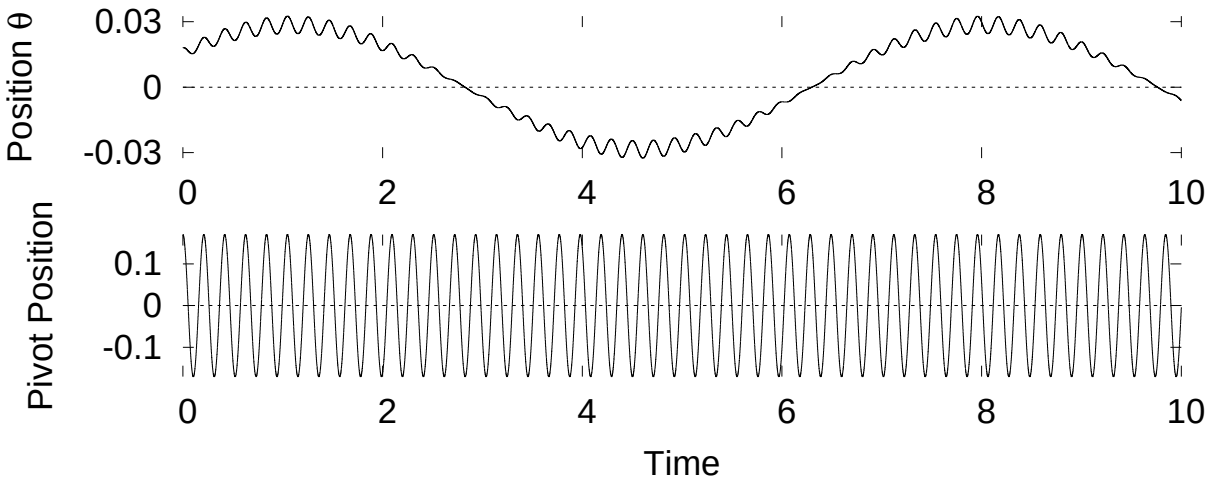

Figure 3 – Plots of the position versus time of the bob of an inverted pendulum for arbitrary angles (top), and the behaviour of the external perturbation composed of one cosine of amplitude $a = 0.17$ m and frequency $\Omega = 30$ rad/s. (Simulation parameters: $g = 9.81$ m/s^2, $l = 1.2$ m, $\omega_0 = 2.86$ Hz, $\theta_0 = 0.018$ rad.)

2.2 Stabilizing an Inverted Pendulum

To explain the stability of an inverted pendulum whose pivot is oscillating at a high frequency, consider that gravity provides a restoring torque $\tau_{gr} = mgl\sin(\theta)$. When the suspension point has a vertical acceleration it is convenient to analyse the motion using a non inertial reference frame. Due to the acceleration of the reference frame, another force acts on the pendulum: the force of inertia $-m\ddot{f}$, where $f(t) = a\cos(\Omega t)$ is the time dependent external perturbation. The minus signal appears due to the relative movement of the coordinate system in which the bob moves (ARNOLD, 1989). This force of inertia is given by:

$$\begin{aligned} F_{in}(t) &= -m\ddot{f} \\ &= ma\Omega^2\cos(\Omega t) \end{aligned} \tag{2.3}$$

The torque generated by this force F_{in} must be added to the torque of the gravitational force. The direction of this force of inertia is:

- Downward: when $f(t) < 0$, i.e., when the axis is below the middle point of the oscillation. Therefore during the corresponding of half the period of oscillation, this additional is equivalent to a strengthening of the gravitational force.
- Upward: when $f(t) > 0$. During the other half-period the action of the external force is equivalent to weakening the gravitational force.

In the case of rapid oscillations, the mean value of the force of inertia evaluated over the small period of an oscillation is zero, but the mean value of the torque is not. This nonzero mean torque explains the stabilization of the pendulum at the upside-down position.

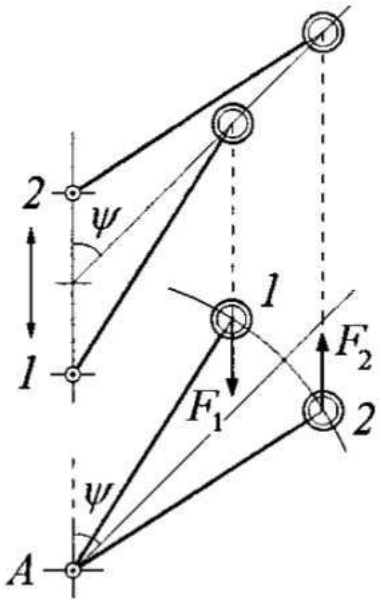

Figure 4 – Forces of inertia exerted on the pendulum in the noninertial reference frame at the extreme positions 1 and 2 of the oscillating axis A (adapted from Butikov (2001) "On the dynamic stabilization of an inverted pendulum" *Am. J. Phys.*; Vol 69, No. 6, June 2001, page 3).

To better understand the influence of the force of inertial upon the system, gravity must be disregarded. The rod is displaced by an arbitrary angle ψ from the direction of the oscillation, and the axis sways between the extremes 1 and 2, as can be seen in the upper part of Figure 4. In the noninertial reference frame (lower part of Figure 4) associated with the vibrating line the bob moves between positions 1 and 2 on an arc of a circle whose centre coincides with the axis A of the pendulum. When the pivot is moved below the point of suspension A, the force of inertia F_1 on the bob is directed downwards. On the other extreme (position 2), the force of inertia F_2 has the same magnitude but is directed upwards. However, the torque of force F_2 is larger than the torque of force F_1,

since the arm of force in position 2 is larger. Therefore the mean force of inertia creates a torque that tends to turn the pendulum up, on the direction in which the rod stays parallel to the axis of oscillation. This torque depends only on the deflection angle of the pendulum to the direction of vibration of the pivot.

2.3 Lower Boundary of Stability and Maximum Angle Deflection

Taking gravity into consideration, the inverted pendulum is stable given that the mean torque of the force of inertia τ_{in} is larger than the torque of gravity τ_{gr}, so the stability condition is:

$$|\tau_{in}| > |\tau_{gr}|.$$

Considering that the motion of a pendulum whose axis vibrates with high frequency is a superposition of "slow" ψ and "fast" δ components, the main interest is on the "slow" component, whose variation during a period of constrained vibrations is small.

The bob is deflected by an instantaneous value $\theta(t)$, that is a sum of the components $\psi(t) = \langle\theta(t)\rangle$ and δ, which has mean value equals to zero. This angle δ oscillates with high frequency Ω and has an amplitude proportional to $\sin[\psi(t)]$:

$$\begin{aligned}\theta(t) &= \psi(t) + \delta(t) \\ &= \psi(t) - \frac{f(t)}{l}\sin(\psi) \\ &= \psi(t) - \frac{a}{l}\cos(\Omega t)\sin(\psi).\end{aligned}$$

Considering a small δ, the following expansion is valid:

$$\begin{aligned}\sin(\theta) &= \sin(\psi + \delta) \\ &= \sin(\psi)\cos(\delta) + \cos(\psi)\sin(\delta) \\ &\approx \sin(\psi) + \delta\cos(\psi).\end{aligned}$$

Time averages will be taken on the interval of a period T by using:

$$\langle g(t)\rangle = \frac{1}{T}\int_0^T g(t)dt \tag{2.4}$$

The torque of the force of gravity τ_{gr} is taken as the time average over a period of rapid oscillations of the axis:

$$\begin{aligned}\langle -mgl\sin(\theta)\rangle &= -mgl\langle\sin(\psi + \delta)\rangle \\ &= -mgl\sin(\psi),\end{aligned} \tag{2.5}$$

while the torque of the inertial force is given by:

$$\begin{aligned}\tau_{in} &= -l\langle F_{in}\rangle\langle\sin(\psi+\delta)\rangle \\ &= -l[ma\Omega^2\cos(\Omega t)]\left[\frac{a}{l}\cos(\Omega t)\sin(\psi)\right]\cos(\psi) \\ &= -\frac{1}{2}ma^2\Omega^2\sin(\psi)\cos(\psi). \end{aligned} \tag{2.6}$$

The minus sign in (2.6) shows that it is a restorer torque. This explains the physical reason for the dynamic stabilization of the inverted pendulum, and that it does not depend on the restriction for small values of the angle θ.

Comparing the right-hand sides of equations (2.5) and (2.6) it can be observed that the torque of the force of inertia can exceed, in magnitude, the gravitational's one, which tends to tip the pendulum down, when the following condition is satisfied:

$$a\Omega > \sqrt{2gl}. \tag{2.7}$$

This condition gives the lower boundary of the dynamical stability (BUTIKOV, 2001).

The maximum value for the angle of deflection from the inverted vertical position $\theta_{max} = \psi_0$ for which the pendulum will not return to that position can be estabilished by equating both right-hand sides of (2.5) and (2.6) considering $\psi = \psi_0$:

$$\begin{aligned} -mgl\sin(0-\psi_0) &= -\frac{1}{2}ma^2\Omega^2\sin(0-\psi_0)\cos(0-\psi_0) \\ \cos(\psi_0) &= \frac{2gl}{a^2\Omega^2} \\ \cos(\theta_{max}) &= \frac{2gl}{a^2\Omega^2}. \end{aligned} \tag{2.8}$$

When the pendulum is displaced from the vertical by an angle that does not exceed θ_{max} it executes relatively small oscillations around the inverted position. This slow motion occurs under both mean torques from the forces of inertia and gravity. Rapid oscillations have the frequency of the forced vibrations of the axis and they overlap the slow motion of the pendulum.

All these results concern the smooth motion of the pendulum with an axis that vibrates quickly and were found without the use of the differential equation for the system under consideration. As they were found by the decomposition of the motion on slow oscillations and fast vibrations, these results are approximated and valid only when the amplitude of the vibration restricted to the axis is small in comparison to the pendulum's length ($a \ll l$), and when the driving frequency is much larger than the natural frequency ($\Omega \gg \omega_0$).

It cannot be expected from this approach an explanation for the chaotic modes and parametrical instability. This approach forecasts the lower limit of the pendulum's stability but does not give an upper boundary, which is related to the ordinary parametric resonance of the non inverted pendulum, which will be explored in the next section.

2.4 Upper Boundary of Stability and Parametric Resonance

In previous studies (BUTIKOV, 2001), it was shown that in certain parts of the parameter space, the pendulum whose axis vibrates with high frequency is trapped in an n-periodic oscillation instead of gradually approaching the equilibrium position by the process of damped oscillations. In these oscillations, the phase trajectory repeats itself after n driving periods T. Since these motions have period nT, this phenomenon is called a subharmonic resonance of nth order. The origin of these oscillations does not depend on gravity.

Simulations show (BUTIKOV, 2001) that, for small angles, period-2 oscillations have a very simple spectral composition and they occur at the upper boundary of dynamic stability: the fundamental harmonic whose frequency equals $\Omega/2$ with a small addition of the third harmonic with frequency $3\Omega/2$. Hence, a possible periodic solution to equation (2.2) which corresponds to the upper boundary of stability can be written as:

$$\theta = A_1 \sin\left(\frac{\Omega t}{2}\right) + A_3 \sin\left(\frac{3\Omega t}{2}\right). \tag{2.9}$$

It is important to notice that equation 2.2 does not necessarily have a periodic solution, equation (2.9) is an Ansatz for a periodic solution given by Butikov (2001).

The Ansatz (2.9) suggested by Butikov (2001) is due to the behaviour of the pendulum at the upper boundary condition. This leads to the attainment of a critical amplitude:

$$a = \frac{l\left(\left[117 + 232\left(\frac{\omega_0}{\Omega}\right)^2 + 80\left(\frac{\omega_0}{\Omega}\right)^4\right]^{1/2} - 9 - 4\left(\frac{\omega_0}{\Omega}\right)^2\right)}{4}. \tag{2.10}$$

It is important to notice that this equation is being pragmatically used as a suitable comparison with numerical results in this work. Further investigations of equation (2.10) are still required.

Diagram on Figure 5 shows numerical results and theoretical boundaries of stability. Green points are sets of parameters for which the system is stable while red dots represent unstable sets. Black curve shows the lower boundary and the blue one, the upper boundary. It can be seen that there is a great agreement between theory and simulation on the limit $a \ll l$. The diagram was constructed following the procedure presented on Tables 1 and 2 of Appendix C (SILVA; PERETTI; PRADO, 2016).

The phenomenon known as parametric resonance happens when the amplitude of oscillation of the system caused by the periodic modulation of a parameter increases consistently, so the equilibrium becomes unstable and the system is no longer steadily executing oscillations, with increasing amplitude.

Parametric excitation can only occur if there exists already a natural oscillation in the system. The strongest parametric vibration happens when the modulation cicle

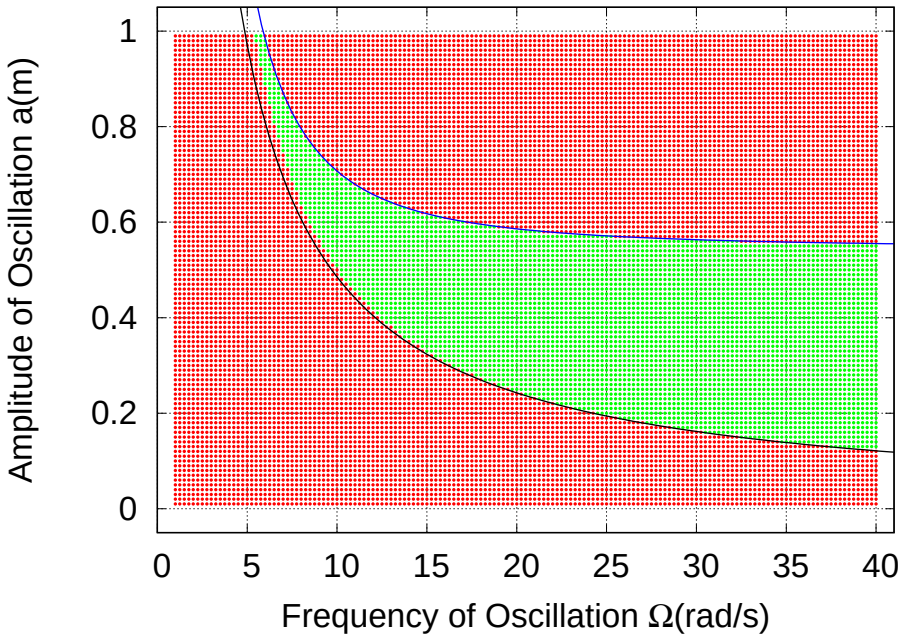

Figure 5 – Stability diagram for the parameters a and Ω for small angles (simulation parameters: $l = 1.2$ m, $g = 9.81$ m/s^2, $\omega_0 = 2.86$ Hz, and $\theta_0 = 0.018$ rad). Green points are sets of parameters for which the system is stable while red dots represent unstable sets. Black curve shows the lower boundary and blue curve, the upper boundary.

repeats itself twice during one period of the natural oscillation of the system, i.e. when parametrical modulation of frequency is twice the system's natural frequency. Thus, the condition for parametric resonance to happen is

$$\Omega = \frac{2\omega_0}{n} \tag{2.11}$$

where $n = 1, 2, ...$ is the order of parametrical resonance. The larger the order of parametric resonance, the smaller the quantity of energy delivered to the oscillatory system over a period is. Resonances of even order are weaker (BUTIKOV et al., 1999).

2.5 Effective Potential

The effective potential function $U_{eff}(\psi)$ of the system is related to the mean total torque $\tau(\psi)$ applied on the pendulum. The torque is defined as the partial derivative of this potential function: $\tau(\psi) = -dU_{eff}(\psi)/d\psi$. Such effective potential function was first introduced by Landau & Lifschitz (1966) and experimental investigations of this effective potential were made to prove its efficiency (FENN; BAYNE; SINCLAIR, 1998). The total torque expression is written as the sum of (2.5) and (2.6):

$$\tau = -mgl\sin(\psi) - \frac{1}{2}ma^2\Omega^2\sin(\psi)\cos(\psi). \tag{2.12}$$

Therefore an expression for the effective potential function can be set up for this system:

$$\begin{aligned} U_{eff} &= -\int_{\pi}^{\psi} \tau(\psi')d\psi' \\ &= mgl(-\cos(\psi'))|_{\pi}^{\psi} + \frac{1}{2}ma^2\Omega^2\left(-\frac{1}{2}\cos(2\psi')\right)\Big|_{\pi}^{\psi} \\ U_{eff} &= mgl(1+\cos(\psi)) + \frac{1}{4}ma^2\Omega^2(1-\cos(2\psi)) \end{aligned} \tag{2.13}$$

Figure 6 shows the form of effective potential (red solid curve) (2.13) and the corresponding potentials (blue dashed line is the inertial potential and green dash-dot is the gravitational) of each torque. It can be seen that at $\psi = \pi$ the minima of the gravitational U_{gr} and inertial U_{in} potentials coincide generating the principal minimum of the total potential. This minimum corresponds to the stable equilibrium position of a regular pendulum. The next minimum of U_{in} happens at $\psi = 0$ where U_{gr} has a maximum, corresponding to the equilibrium position of the inverted pendulum. If condition (2.7) is true, the magnitude of U_{in} is larger than U_{gr}, then the effective potential has a local minimum at $\psi = 0$. The slopes of the additional well at $\psi = 0$ are not as steep as the main one at $\psi = \pm\pi$.

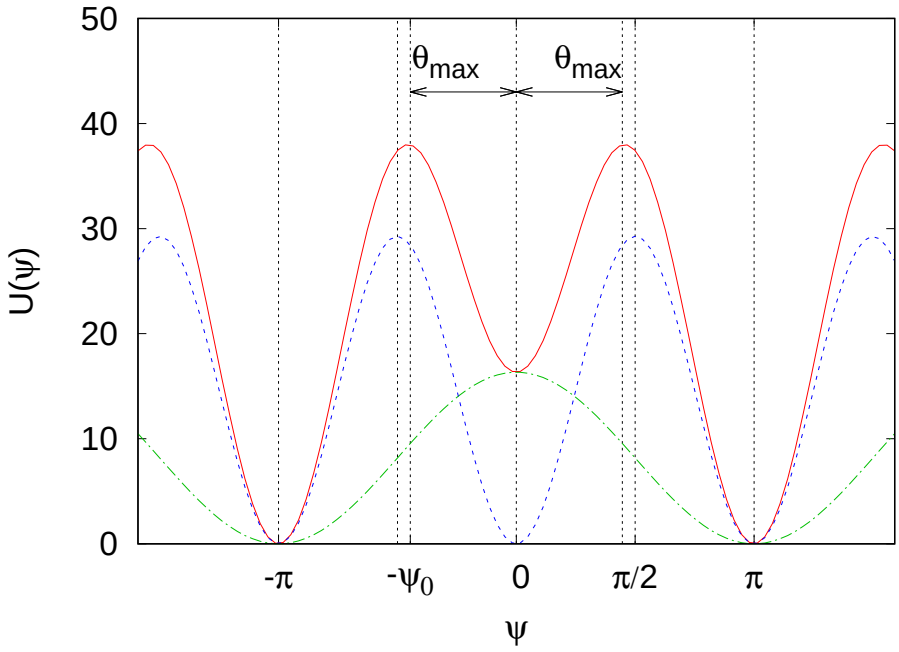

Figure 6 – Plots of the gravitational potential energy U_{gr} (green dash-dot line), mean potential energy of the force of inertia U_{in} (blue dashed line), and the total potential energy $U_{eff}(\psi)$ for the pendulum with a vertically oscillating axis (red solid line). Maximum deflection angle θ_{max} can also be seen. (Simulation parameters: $m = 1$ kg, $g = 9.81$ m/s^2, $l = 1.2$ m, $a = 0.17$ m, and $\Omega = 45$ rad/s.)

The affirmation that stability happens when U_{in} is larger than U_{gr} is only true while the upper stability condition is not achieved. Above it, the amplitude of the inertial potential is still larger than the gravitational potential, but the system is no longer stable. This approach of effective angle does not predict the upper boundary either.

The peaks of the potential barrier between the two wells occur at the deflections $\pm\psi_0$, from $\psi = \pm\pi$ (or $\pm\theta_{max}$ from $\psi = 0$). At these positions, gravity's mean torque is balanced by force of inertia's mean torque. However, these equilibrium positions are unstable: the slightest perturbation will make the pendulum fall to one of the wells and oscillate there from one peak to another. It remains for a longer time near the peak of the potential barrier at the deflection and then moves rapidly towards the other one, where it remains for few moments before returning to the rapid motion.

When the amplitude of the pivot's vibration increases beyond a critical value a_{max}, which is not small when compared to the pendulum's length l, the dynamically stabilized inverted position of the pendulum loses its stability. Consequently this case occurs beyond the limits of applicability of the approach based on the effective potential of an inverted pendulum, as well as the loss of stability of the non inverted pendulum on the conditions of ordinary parametric resonance.

2.6 Arbitrary Angles

The lower boundary of stability and the effective potential were found for arbitrary angles, i.e. without the use of the approximation $\sin\theta \approx \theta$, but the upper limit is known only for small angles. Although there is no analytical expression for it for arbitrary angles, it can be clearly seen on Figure 7. It can also be seen that the upper boundary is larger than that for small angles, which shows the necessity of numerically solving the complete equation (2.1) instead of (2.2). As in Figure 5, green points are sets of parameters for which the system is stable while red dots represent unstable sets. Black curve shows the lower boundary of stability and blue curve represents the upper for small angles. As Figure 5, this diagram was constructed following the procedure presented on Tables 1 and 2 of Appendix C (SILVA; PERETTI; PRADO, 2016).

Without the use of the approximation for small angles $\sin\theta \approx \theta$, the simulations are able to portray a more realistic experiment. Figure 7 shows the importance of numerically integrating the complete equation (2.1), since there are sets of amplitude a and frequency Ω that are stable (green) but are not contained on the region foreseen by the theoretical approach for small angles.

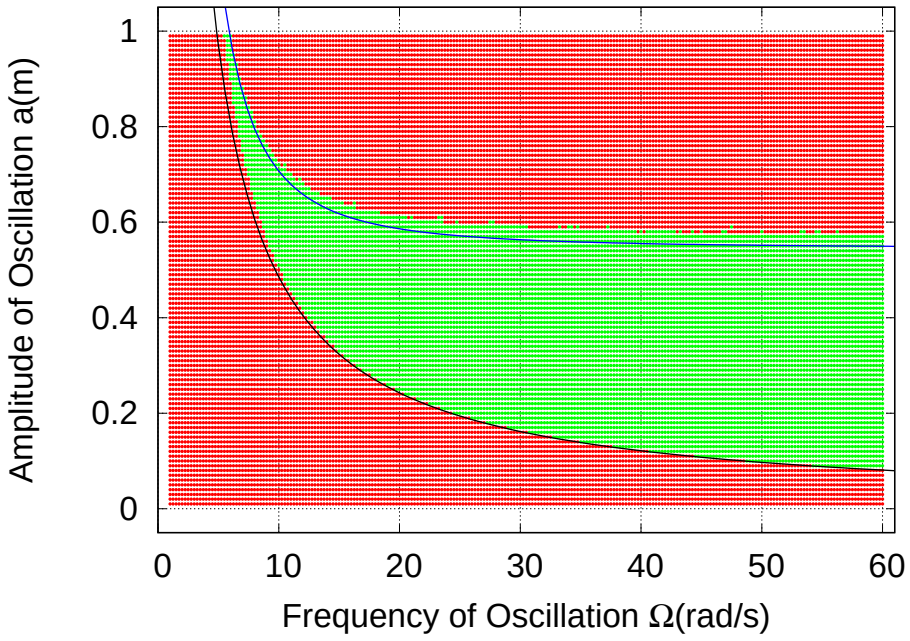

Figure 7 – Stability diagram for the parameters a and Ω for arbitrary angles (simulation parameters: $l = 1.2$ m, $g = 9.81$ m/s^2, $\omega_0 = 2.86$ Hz, and $\theta_0 = 0.018$ rad). Green points are sets of parameters for which the system is stable while red dots represent unstable sets. Black curve shows the lower boundary of stability and blue curve represents the upper one for small angles.

2.7 Initial Angle

Figure 8 presents four stability diagrams of an inverted pendulum for arbitrary angles using different initial angles. Green points represent sets of parameters for which the system is stable while red ones represent unstable. Black curves show the lower boundary of stability and blue curves represent the upper limit for small angles. Top left diagram corresponds to initial angle equal to $\theta_0 = 0.018$ rad, top right $\theta_0 = 0.518$ rad, bottom left $\theta_0 = 1.0$ rad, and bottom right $\theta_0 = 1.5$ rad. These plots were made using the complete equation of motion (2.1). It can be seen that the larger the initial angle, the smaller the stable region of the diagram is. There are no stable sets of parameters when the initial angle is $\theta_0 = 1.5$ rad.

As a complementary reading, one finds the stabilization of an inverted pendulum using a different external periodic function at Appendix A, where there is a comparison of the stability boundary (2.7) with the boundary found for this other external function.

In this Chapter, the aspects of an inverted pendulum with a periodic oscillation of a single cosine of amplitude a and frequency Ω at the suspension point were analysed. Stability conditions were established and diagrams of stability were constructed with the intentions of better understanding the behaviour of this system.

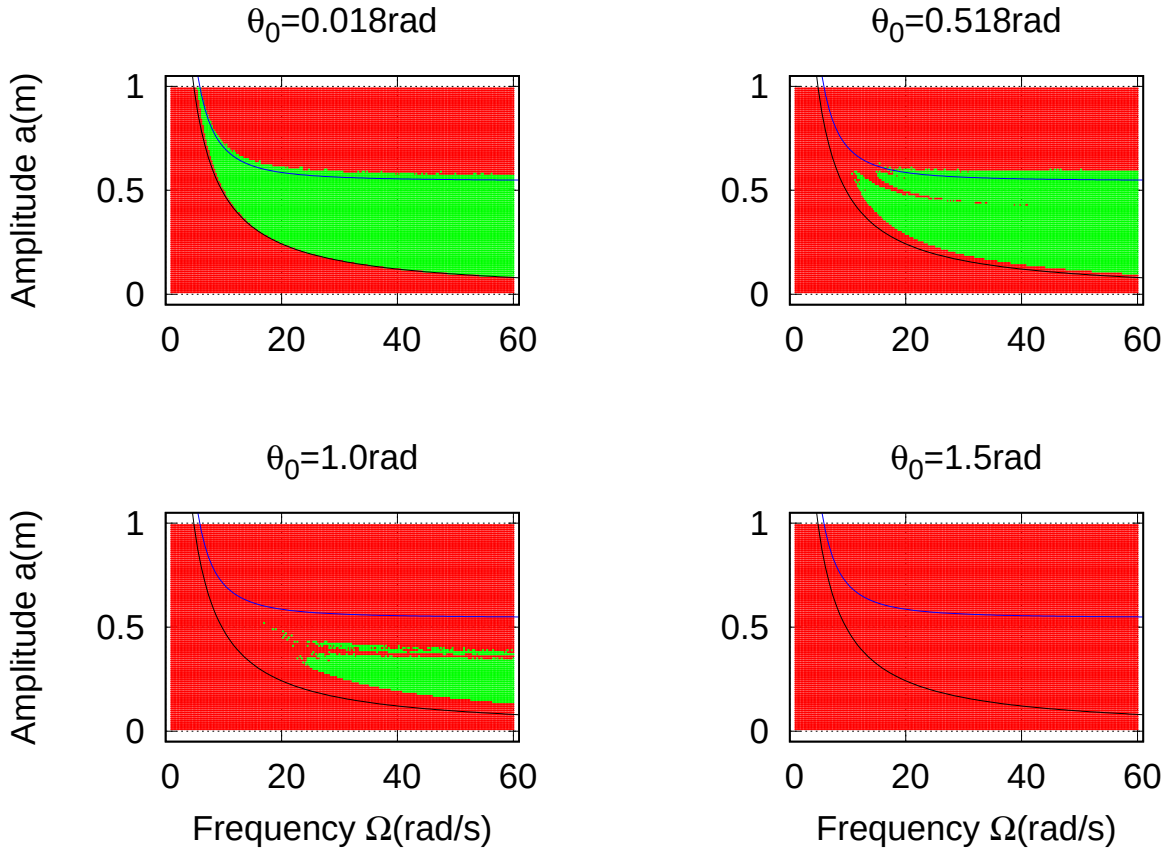

Figure 8 – Stability diagram for the parameters a and Ω for arbitrary angles (simulation parameters: $l = 1.2$ m, $g = 9.81$ m/s^2 and $\omega_0 = 2.86$ Hz). Green points are the sets of parameters for which the system is stable while red points represent instability. Black curves show the lower boundary of stability and blue curves represent the upper boundary for small angles. Top left corresponds to an initial angle of $\theta_0 = 0.018$ rad; top right $\theta_0 = 0.518$ rad; bottom left, $\theta_0 = 1$ rad; and bottom right $\theta_0 = 1.5$ rad. No stable set of parameters are found on the last diagram.

3 Generalization

This Chapter is focused on an inverted pendulum with an external periodic excitation given by a sum of N cosines of amplitudes a_i and frequencies Ω_i applied at its suspension point. The methods used on the previous Chapter will be adapted for this generalization. Characteristics and some analysis of this system will be presented here.

3.1 Sum of Cosines

An external function given as the sum of N cosines of amplitudes a_1, a_2, ..., a_N and frequencies Ω_1, Ω_2, ..., Ω_N is applied at the suspension point:

$$f(t) = \sum_{i=1}^{N} a_i \cos(\Omega_i t)$$

and the force of inertia corresponding to this perturbation is:

$$F_{in}(t) = m \sum_{i=1}^{N} a_i \Omega_i^2 \cos(\Omega_i t). \tag{3.1}$$

The equation of motion for this inverted pendulum in the absence of friction is then given by:

$$\ddot{\theta} - \left[\omega_0^2 - \frac{1}{l}\sum_{i=1}^{N} a_i \Omega_i^2 \cos(\Omega_i t)\right] \sin(\theta) = 0, \tag{3.2}$$

By using the approximation for small angles, the equation of motion is written as:

$$\ddot{\theta} - \left[\omega_0^2 - \frac{1}{l}\sum_{i=1}^{N} a_i \Omega_i^2 \cos(\Omega_i t)\right] \theta = 0. \tag{3.3}$$

This equation has the form of a second-order linear ordinary differential equation known as Hill equation, which is named after George William Hill (1886). Because of the large determinants involved on Hill's method to find the solution for these equations when N is large, it is not a suitable method for the purposes of this work (BOGDANOFF, 1962). Mathieu equations, as equation (2.2), are an important special case of Hill equations since they are useful for treating a variety of problems in applied mathematics, including wave motion in a periodic media and exact plane wave solutions in general relativity (MATHIEU, 1868). The solution of a Hill equation may be given by Floquet theory, due to Gaston Floquet (1883), which gives a canonical form for each fundamental matrix solution of this common linear system by making a coordinate change that transforms the periodic system into a traditional linear system with constant real coefficients. Although it is very interesting, Floquet theory is not practical, hence the need of numerically integrating the equations of motion so the stability of the system may be analysed.

Keeping in mind that the stability condition used is that the module of the inertial torque is larger than of the gravitational one, the lower boundary of stability for this new system can be found. Since the external perturbation no longer has a known period of oscillation the mean value of the inertial torque over a period must be carefully calculated using 2.4, where it is supposed that there it a period T. Therefore:

$$\begin{aligned}\tau_{in} &= < -lF_{in}\sin(\psi+\delta) > \\ &= -\left\langle m\left[\sum_{i=1}^{N} a_i\Omega_i^2\cos(\Omega_i t)\right](\sin\psi+\delta\cos\psi)\right\rangle \\ &= -ml\left\langle\left[\sum_{i=1}^{N} a_i\Omega_i^2\cos(\Omega_i t)\right]\left[\frac{1}{l}\sum_{i=1}^{N} a_i\cos(\Omega_i t)\right]\right\rangle\sin\psi\cos\psi\end{aligned}$$

$$\begin{aligned}\tau_{in} &= -m\sin\psi\cos\psi\left\langle\left[\sum_{i=1}^{N} a_i^2\Omega_i^2\cos^2(\Omega_i t)+\sum_{i\neq j=1}^{N} a_i a_j\Omega_i^2\cos(\Omega_i t)\cos(\Omega_j t)\right]\right\rangle \\ &= -m\sin\psi\cos\psi\left[\sum_{i=1}^{N} a_i^2\Omega_i^2 < \cos^2(\Omega_i t) > + \sum_{i\neq j=1}^{N} a_i a_j\Omega_i^2 < \cos(\Omega_i t)\cos(\Omega_j t) >\right]\end{aligned}$$

$$\begin{aligned}\tau_{in} = -m\sin\psi\cos\psi\Bigg[&\sum_{i=1}^{N}\frac{a_i^2\Omega_i^2}{2}\left(\frac{\sin(2\Omega_i T)}{2\Omega_i T}+1\right)+ \\ &\sum_{i\neq j=1}^{N}\frac{a_i a_j\Omega_i^2}{2T}\left(\frac{\sin((\Omega_i+\Omega_j)T)}{\Omega_i+\Omega_j}+\frac{\sin((\Omega_i-\Omega_j)T)}{\Omega_i-\Omega_j}\right)\Bigg],\end{aligned} \tag{3.4}$$

while gravitational torque remains the same as in (2.5). The stability condition of this system is now:

$$\begin{aligned}&\sum_{i=1}^{N} a_i^2\Omega_i^2\left(\frac{\sin(2\Omega_i T)}{2\Omega_i T}+1\right)+ \\ &\sum_{i\neq j=1}^{N}\frac{a_i a_j\Omega_i^2}{T}\left(\frac{\sin((\Omega_i+\Omega_j)T)}{\Omega_i+\Omega_j}+\frac{\sin((\Omega_i-\Omega_j)T)}{\Omega_i-\Omega_j}\right) > 2gl.\end{aligned} \tag{3.5}$$

Along with this stability condition, Bogdanoff & Citron (1965) stated that the difference among all frequencies must be large for the system to be steady. There are other methods to find condition (3.5), and one of them, by using pertubative analysis, is presented in Appendix B.

The maximum value for the angle deflection from the inverted position can also be found. Equating the right side of equations (2.5) and (3.4) and using $\theta_{max} = \psi_0$:

$$\begin{aligned}\cos(\theta_{max}) = 2gl\Bigg[&\sum_{i=1}^{N} a_i^2\Omega_i^2\left(\frac{\sin(2\Omega_i T)}{2\Omega_i T}+1\right)+ \\ &\sum_{i\neq j=1}^{N}\frac{a_i a_j\Omega_i^2}{T}\left(\frac{\sin((\Omega_i+\Omega_j)T)}{\Omega_i+\Omega_j}+\frac{\sin((\Omega_i-\Omega_j)T)}{\Omega_i-\Omega_j}\right)\Bigg]^{-1}.\end{aligned} \tag{3.6}$$

Again these results concern the smooth motion of an inverted pendulum with a quickly vibrating axis and were found without the use of a differential equation for the system under consideration, therefore they are valid for all values of θ. Since they were found by the decomposition of the motion into slow oscillations and fast vibrations, these results are approximated and valid only when the amplitudes of vibration are small compared to the pendulum length ($\{a_i\}_{i=1}^N \ll l$), and the driving frequencies are larger than the natural frequency ($\{\Omega_i\}_{i=1}^N \gg \omega_0$). An upper boundary might be expected in this case too. However it is not known in the literature and since it is not the main concern in this work, it will not be explored.

Using the definition previously made for the potential function $U(\psi)$, and integrating over a mean period T, the effective potential of this system is given by:

$$U_{eff} = mgl(1+\cos(\psi)) + \frac{m}{4}\left[\sum_{i=1}^{N} a_i^2\Omega_i^2\left(\frac{\sin(2\Omega_i T)}{2\Omega_i T}+1\right) + \sum_{i\neq j=1}^{N}\frac{a_i a_j \Omega_i^2}{T}\left(\frac{\sin((\Omega_i+\Omega_j)T)}{\Omega_i+\Omega_j}+\frac{\sin((\Omega_i-\Omega_j)T)}{\Omega_i-\Omega_j}\right)\right](1-\cos(2\psi)). \quad (3.7)$$

Since the dependence of U_{eff} on the angle ψ is the same as in (2.13), the graph's form is the same as Figure 6.

3.2 Close Frequencies

There is a trivial case when the excitation frequencies have such close values that the period of oscillation can be found by the average value of the set $\{T_i\}_{i=1}^N$. In this case, the stability condition resumes to a simple one:

$$\sum_{i=1}^{N} a_i^2\Omega_i^2 > 2gl. \quad (3.8)$$

This case simplifies all equations found in section 3.1, since the period is known. The maximum deflection angle and the effective potential become:

$$\cos(\theta_{max}) = \frac{2gl}{\sum_{i=1}^{N} a_i^2\Omega_i^2} \quad (3.9)$$

and

$$U_{eff} = mgl(1+\cos(\psi)) + \frac{m}{4}\sum_{i=1}^{N} a_i^2\Omega_i^2(1-\cos(2\psi)) \quad (3.10)$$

respectively.

3.3 Random Frequencies

If the frequencies are randomly chosen inside defined ranges, and are equally distributed according to a Probability Density Function, the external perturbation can be substituted by its average, which is written as:

$$\overline{f(t)} = \overline{\cos(\Omega t)} \sum_{i=1}^{N} a_i \tag{3.11}$$

where

$$\overline{\cos(\Omega t)} = \int_0^\infty \cos(\Omega t) h(\Omega) d\Omega$$

and $h(\Omega)$ is the PDF which corresponds to the distribution of the frequencies. As a standard case, an uniform distribution can be used and the mean value assumes the following expression:

$$\begin{aligned} \overline{\cos(\Omega t)} &= \frac{1}{\Omega_{max} - \Omega_{min}} \int_{\Omega_{min}}^{\Omega_{max}} \cos(\Omega t) d\Omega \\ &= \frac{\sin(\Omega_{max} t) - \sin(\Omega_{min} t)}{(\Omega_{max} - \Omega_{min}) t}. \end{aligned} \tag{3.12}$$

The time dependence on equation (3.12) suggests that as time increases, a loss of stability must occur. Hence, it is interesting to consider a time-dependent amplitude. Therefore, by rewriting the amplitudes as a explicitly time dependent $a_i = a(t)$:

$$\sum_{i=1}^{N} a_i = N a(t),$$

equation (3.11) is then given by:

$$\overline{f}(t) = N a(t) \left(\frac{\sin(\Omega_{max} t) - \sin(\Omega_{min} t)}{(\Omega_{max} - \Omega_{min}) t} \right). \tag{3.13}$$

In this case, by denoting

$$h(t|\Omega) = \frac{a(t)}{t} \sin(\Omega t) \tag{3.14}$$

one can find:

$$\frac{d^2 h}{dt^2} = \ddot{a}(t) \sin(\Omega t) + 2\dot{a}(t) \left[\frac{\Omega \cos(\Omega t)}{t} - \frac{\sin(\Omega t)}{t^2} \right] + a(t) \left[\frac{2 \sin(\Omega t)}{t^3} - \frac{2\Omega \cos(\Omega t)}{t^2} - \frac{\Omega^2 \sin(\Omega t)}{t} \right].$$

A simple choice is to consider a linear dependence on the amplitude as $a(t) = Ct$, where C is a constant, up to first order terms $\frac{d^2 h}{dt^2} = -CN\Omega^2 \sin(\Omega t)$ is found. Rescaling $CN = a\Omega_{max}$:

$$\ddot{\overline{f}}(t) = -\frac{a\Omega_{max}^3}{\Omega_{max} - \Omega_{min}} \sin(\Omega_{max} t) + \frac{a\Omega_{min}^2 \Omega_{max}}{\Omega_{max} - \Omega_{min}} \sin(\Omega_{min} t) \tag{3.15}$$

If minimum frequency is equal to zero ($\Omega_{min} = 0$), equation (3.15) resumes to:

$$\ddot{\overline{f}}(t) = -a\Omega_{max}^2 \sin(\Omega_{max} t) \tag{3.16}$$

which reproduces, in average, the same results as case $N = 1$ and, therefore, it is expected that the stabilization condition obtained:

$$a^2 > \frac{2gl}{\Omega_{max}^2} \tag{3.17}$$

should be recovered.

To numerically validate this approximation, one may rewrite the external perturbation by considering that the amplitude is now dependent on the time, finding:

$$f(t) = \sum_{i=1}^{N} a_i t \cos(\Omega_i t). \tag{3.18}$$

The second derivative of equation (3.18) is

$$\ddot{f}(t) = -\sum_{i=1}^{N} \Omega_i^2 a_i t \cos(\Omega_i t) - 2\sum_{i=1}^{N} \Omega_i a_i \sin(\Omega_i t)$$

and, with this, the equation of motion associated with the system is given by

$$\ddot{\theta} - \left[\omega_0^2 - \sum_{i=1}^{N}\left(\frac{a_i t \Omega^2}{l}\cos(\Omega_i t) + \frac{2a_i\Omega_i}{l}\sin(\Omega_i t)\right)\right]\sin\theta = 0. \tag{3.19}$$

By numerically integrating equation (3.19) via a forth order Runge-Kutta method (following procedures shown in Tables 1 and 4 of Appendix C (SILVA; PERETTI; PRADO, 2016)), Figure 9 can be constructed, where it is shown the pendulum's stability time, i.e., the time for which the inverted pendulum remains stable, as a function of the maximum frequency Ω_{max} and maximum amplitude a_{max}. This Figure corroborates the results found previously, that the pattern of stability is as the one found for the deterministic case of $N = 1$, which implies that, by using the assumptions that the frequencies are randomly chosen according from an uniform distribution, and that the amplitude is linearly dependent on time, the system with a perturbation of N cosines resumes to the case of one cosine for a finite amount of time.

The main problem with this analysis is that the time proportional terms contribute to destabilize the system so the system remains stable only for a finite time, as can be seen on Figure 9. The bigger the number N of cosines used, the higher is the time during which the system remains stable and the better the agreement with the case when $N = 1$, since the highest stability times present approximately the same form. Red sets of amplitude and frequency remain stable for less time than green ones.

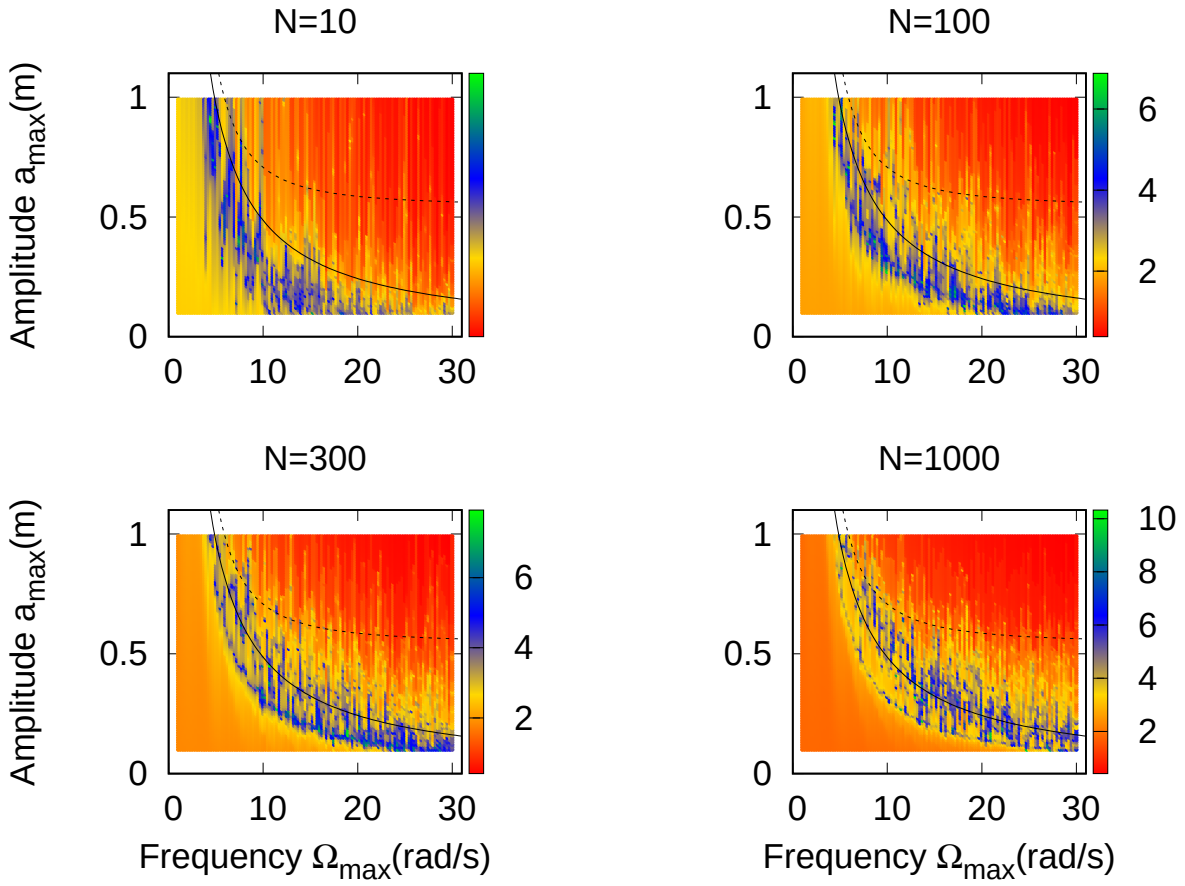

Figure 9 – Stability time diagram of an inverted pendulum using the PDF approximation (simulation parameters: $l = 1.2$ m, $g = 9.81$ m/s^2, $\omega_0 = 2.86$ Hz, and $\theta_0 = 0.018$ rad). It can be seen that the PDF approximation makes the system resume to approximately the same results as $N = 1$, in the previous Chapter. The more close to red the colour of the point, the smaller the time for which the inverted pendulum remains stable, while green sets of amplitude and frequency represent the highest times. Time scale is set in seconds. First diagram shows no scale since it does not remain stable for more than 2 seconds.

3.4 Stabilization Probability

Having made the generalization of the external function as a sum of N cosines, the remaining question is: which value of N gives the highest probability of stabilization?

Simulating for each value of N, varying from 1 to 20, N_{run} times the time evolution of the inverted pendulum for different randomly chosen values of amplitudes a_i and frequencies Ω_i via a fourth-order Runge-Kutta method (following procedures presented on Tables 1 and 5 of Appendix C (SILVA; PERETTI; PRADO, 2016)), the stability probability p_{stab} for different random values of amplitudes and frequencies chosen between fixed

ranges $[0, a_{max}]$ and $[0, \Omega_{max}]$, respectively, is calculated using:

$$p_{stab} = \frac{n_{stab}}{N_{run}} \tag{3.20}$$

where n_{stab} is the number of times the system stabilized.

Figure 10 presents the stabilization probability of N cosines when the maximum amplitude is fixed at $a_{max} = 0.17$ m and different maximum value for frequencies are set. One can see that the higher the maximum frequency, the higher the probability of stabilization is and that by fixing an upper value for the amplitude and ranging the frequency Ω_{max}, the optimal value of N does not change.

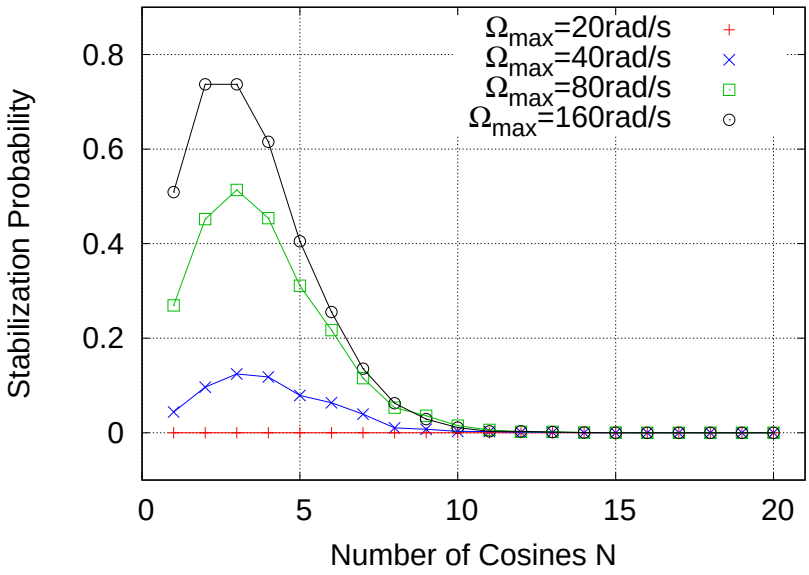

Figure 10 – Stabilization probability of an inverted pendulum (simulation parameters: $l = 1.2$ m, $g = 9.81$ m/s^2, $\omega_0 = 2.86$ Hz, $\theta_0 = 0.018$ rad, and $N_{run} = 2000$) for different numbers of cosines N used on equation (3.2), keeping the maximum amplitude fixed at $a_{max} = 0.17$ m and changing the maximum value of frequency Ω_{max}. Red crosses represent maximum frequency $\Omega_{max} = 20$ rad/s; blue crosses, $\Omega_{max} = 40$ rad/s; green squares, $\Omega_{max} = 80$ rad/s; and black circles, $\Omega_{max} = 160$ rad/s.

Keeping the maximum frequency fixed at $\Omega_{max} = 80$ rad/s and ranging maximum amplitudes, Figure 11 shows the stability probability of our system. It can be seen that the smaller the maximum amplitude, the larger the number of cosines in (3.2) that can be used to stabilize the system is. Therefore, the maximum value of a_{max} influences the optimal number of cosines N. Red crosses represent maximum amplitude $a_{max} = 0.08$ m; blue crosses, $a_{max} = 0.17$ m; green squares, $a_{max} = 0.34$ m; and black circles, $a_{max} = 0.68$ m.

Now, with maximum frequency and amplitude fixed at respectively $\Omega_{max} = 80$ rad/s and $a_{max} = 0.34$ m, a study of the effects of the initial angle on the stabilization probability is made. Figure 12 shows the stabilization probability for different values of number

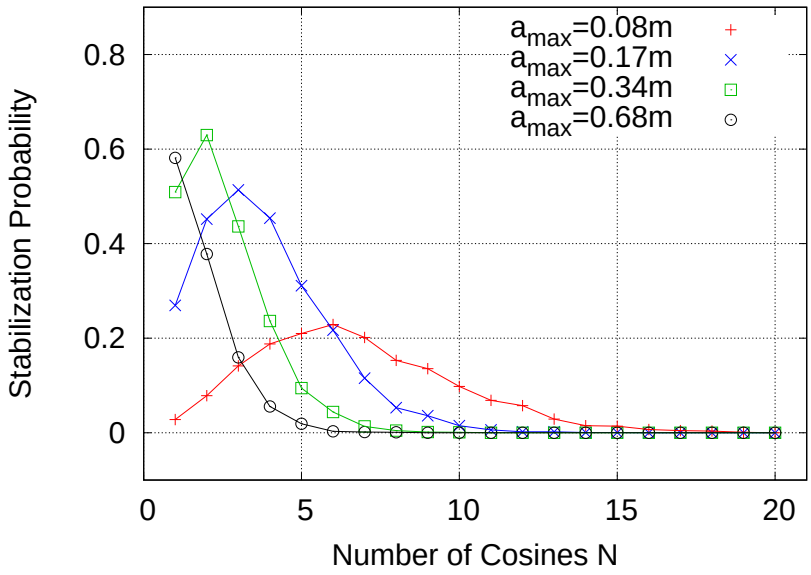

Figure 11 – Stabilization probability of an inverted pendulum (simulation parameters: $l = 1.2$ m, $g = 9.81$ m/s^2, $\omega_0 = 2.86$ Hz, $\theta_0 = 0.018$ rad, and $N_{run} = 2000$) for different numbers of cosines N used on equation (3.2), keeping the maximum frequency Ω_{max} fixed at 80 rad/s and changing the maximum value of amplitude a_{max}. Red crosses represent maximum amplitude $a_{max} = 0.08$ m; blue crosses, $a_{max} = 0.17$ m; green squares, $a_{max} = 0.34$ m; and black circles, $a_{max} = 0.68$ m.

of cosines N in equation (3.2) for two different initial angles $\theta_0 = 0.018$ rad (red squares) and $\theta_0 = 0.518$ rad (blue circles). It can be seen that the change on the initial angle does not affect the optimal number of cosines.

This Chapter introduced a generalized form of the previous one. Here, a sum of N cosines was used and the results found on the previous chapter were generalized. It is also shown a way of associating the case when $N = 1$ with N large, where frequencies where randomly sorted from a range and amplitude was rescaled. Finally, the best value of N was found for different ranges of amplitudes, frequencies, and initial angles.

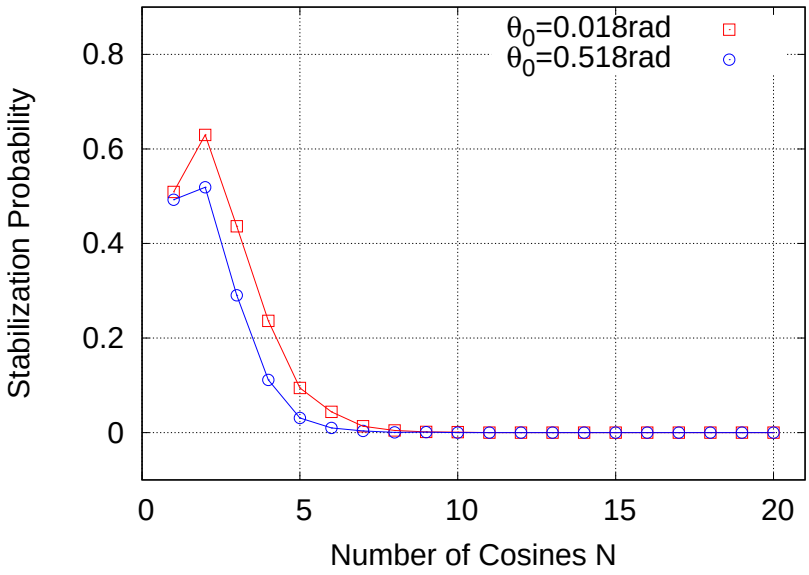

Figure 12 – Stabilization probability of an inverted pendulum (simulation parameters: $l = 1.2$ m, $g = 9.81$ m/s^2, $\omega_0 = 2.86$ Hz, and $N_{run} = 2000$) for different numbers of cosines N used on equation (3.2), keeping maxima frequency $\Omega_{max} = 80$ rad/s and amplitude $a_{max} = 0.34$ m fixed for two different initial angles. Red squares represent $\theta_0 = 0.018$ rad; and blue circles, $\theta_0 = 0.518$ rad.

4 Periodic and Almost Periodic Base Motion

This Chapter shows the aspects of the system for the special case when $N = 2$, when there may be a periodic or non periodic base motion. The results found in the previous Chapter will be rewritten for this specific case, and some characteristics of the system will be pointed out.

4.1 Two Cosines

The generalization performed in the previous chapter is considered for the specific case of two cosines $N = 2$. The external perturbation at the suspension point is given by a sum of two cosines of amplitudes a_1 and a_2, and frequencies Ω_1 and Ω_2. The expected effect is that the two cosines of different frequencies interfere with each other causing a destabilization on the system when the two frequencies are close (HEMP; SETHNA, 1968). Therefore, the external perturbation can be written as:

$$f(t) = a_1 \cos(\Omega_1 t) + a_2 \cos(\Omega_2) \tag{4.1}$$

and the force of inertia is written as:

$$F_{in}(t) = m(a_1 \Omega_1^2 \cos(\Omega_1 t) + a_2 \Omega_2^2 \cos(\Omega_2 t)). \tag{4.2}$$

Hence, in the absence of friction ($\beta = 0$), the equation of motion is given by

$$\ddot{\theta} - \left[\omega_0^2 - \frac{1}{l}(a_1 \Omega_1^2 \cos(\Omega_1 t) + a_2 \Omega_2^2 \cos(\Omega_2 t))\right] \sin\theta = 0, \tag{4.3}$$

and for small angles

$$\ddot{\theta} - \left[\omega_0^2 - \frac{1}{l}(a_1 \Omega_1^2 \cos(\Omega_1 t) + a_2 \Omega_2^2 \cos(\Omega_2 t))\right] \theta = 0 \tag{4.4}$$

where ω_0 is the natural frequency of oscillation of the system, and l is the length of the inverted pendulum.

Figure 13 shows the evolution of the position of an inverted pendulum in time for arbitrary angles: top plot corresponds to numerically integrating equation (4.3); and middle plot considers the approximated equation of motion for small angles, equation (4.4). Bottom plot shows the behaviour of the external perturbation composed of two cosines. It can be seen that the behaviour of the position as a function of time is very different when we consider arbitrary angles or small angles. Hence the importance of not using the approximation on simulations.

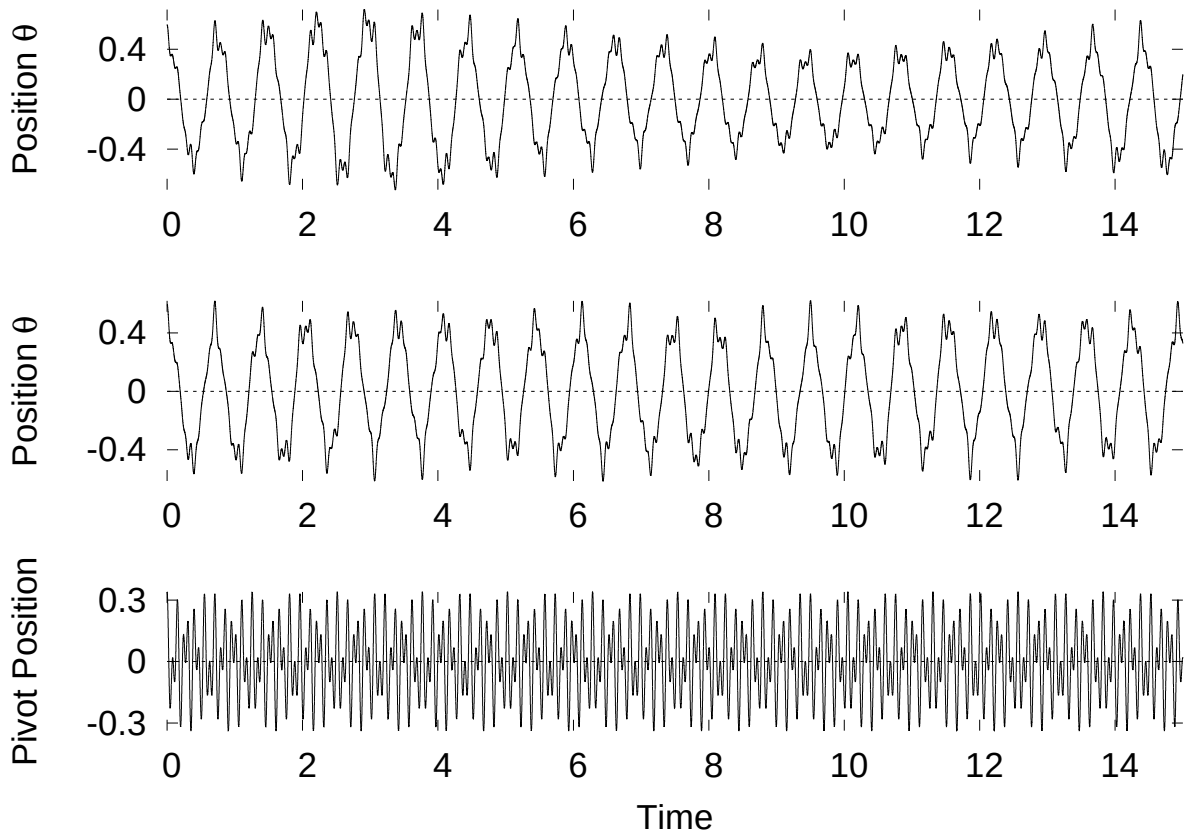

Figure 13 – Plots of position versus time of the bob of an inverted pendulum for arbitrary angles (top plot), and using the approximation of small angles (middle plot). Bottom plot shows the behaviour of the external perturbation composed of two cosines of same amplitude $a_1 = a_2 = 0.17$ m and different frequencies $\Omega_1 = 45$ rad/s and $\Omega_2 = 80$ rad/s. Simulation parameters: $g = 9.81$ m/s^2, $l = 1.2$ m, $\omega_0 = 2.86$ Hz, $\theta_0 = 0.018$ rad.

Since stability condition established in Chapter 2 is still valid, substituting $N = 2$ in equation (3.4), the inertial torque of the system can be obtained:

$$\tau_{in} = -m \sin\psi \cos\psi \left[\frac{a_1^2 \Omega_1^2}{2} \left(\frac{\sin(2\Omega_1 T)}{2\Omega_1 T} + 1 \right) + \frac{a_2^2 \Omega_2^2}{2} \left(\frac{\sin(2\Omega_2 T)}{2\Omega_2 T} + 1 \right) + \frac{a_1 a_2}{2T} (\Omega_1^2 + \Omega_2^2) \left(\frac{\sin((\Omega_1 + \Omega_2)T)}{\Omega_1 + \Omega_2} + \frac{\sin((\Omega_1 - \Omega_2)T)}{\Omega_1 - \Omega_2} \right) \right] \quad (4.5)$$

where m is the mass of the pendulum's bob, and T is the period of the external perturbation applied at the suspension point. Gravitational torque remains still the same as in

equation (2.5), therefore the system's stability condition is estabilished:

$$a_1^2\Omega_1^2\left(\frac{\sin(2\Omega_1 T)}{2\Omega_1 T}+1\right)+a_2^2\Omega_2^2\left(\frac{\sin(2\Omega_2 T)}{2\Omega_2 T}+1\right)+ \\ \frac{a_1a_2}{T}(\Omega_1^2+\Omega_2^2)\left(\frac{\sin((\Omega_1+\Omega_2)T)}{\Omega_1+\Omega_2}+\frac{\sin((\Omega_1-\Omega_2)T)}{\Omega_1-\Omega_2}\right)>2gl. \quad (4.6)$$

These results were found assuming that there is a period T for the system.

From previous Chapter's equation (3.6), maximum angle of deflection is:

$$\cos(\theta_{max})=2gl\left[a_1^2\Omega_1^2\left(\frac{\sin(2\Omega_1 T)}{2\Omega_1 T}+1\right)+a_2^2\Omega_2^2\left(\frac{\sin(2\Omega_2 T)}{2\Omega_2 T}+1\right)+ \\ \frac{a_1a_2}{T}(\Omega_1^2+\Omega_2^2)\left(\frac{\sin((\Omega_1+\Omega_2)T)}{\Omega_1+\Omega_2}+\frac{\sin((\Omega_1-\Omega_2)T)}{\Omega_1-\Omega_2}\right)\right]. \quad (4.7)$$

An upper stability boundary when using (4.1) is also unknown in the literature and it is not the main concern in this work, hence it will not be explored.

Substituting $N=2$ in equation (3.7), the expression of the effective potential for this case is

$$U_{eff}=mgl(1+\cos\psi)+\frac{1}{4}\left[a_1^2\Omega_1^2\left(\frac{\sin(2\Omega_1 T)}{2\Omega_1 T}+1\right)+a_2^2\Omega_2^2\left(\frac{\sin(2\Omega_2 T)}{2\Omega_2 T}+1\right)+ \\ +\frac{a_1a_2}{T}(\Omega_1^2+\Omega_2^2)\left(\frac{\sin((\Omega_1+\Omega_2)T)}{\Omega_1+\Omega_2}+\frac{\sin((\Omega_1-\Omega_2)T)}{\Omega_1-\Omega_2}\right)\right](1-\cos(2\psi)) \quad (4.8)$$

The shape of the potential function does not change with the different number of cosines used on the external function, since it dependes only on the angle ψ. As the stability condition (4.6), the amplitude of the effective potential depends on a chosen period for the system, since it does not necessarily has a known one.

Using the close frequencies approximation, stability condition (4.6) becomes:

$$a_1^2\Omega_1^2+a_2^2\Omega_2^2>2gl \quad (4.9)$$

Rewriting equation (4.9) as an equality:

$$\frac{a_1^2}{2gl}\Omega_1^2+\frac{a_2^2}{2gl}\Omega_2^2=1$$

an ellipse equation is found for the lower boundary of stability. When we fix two values of amplitudes and range frequencies, a stability diagram can be constructed for the excitations frequencies Ω_1 and Ω_2 by numerically integrating equation (4.3) via a forth order Runge-Kutta method. All diagrams from this Chapter were constructed following the procedure presented on Tables 1 and 3 of Appendix C (SILVA; PERETTI; PRADO, 2016).

Figure 14 shows two different stability diagrams for frequencies with different fixed amplitudes. The diagram on the left has amplitudes $a_1 = 0.17$ m and $a_2 = 0.34$ m while the one on the right has $a_1 = 0.15$ m and $a_2 = 0.5$ m. Green points represent sets of frequencies for which the system is stable, and red dots represent unstable ones. Black curve shows the ellipse cited above as the lower boundary of stability using the approximation for close frequencies (4.9).

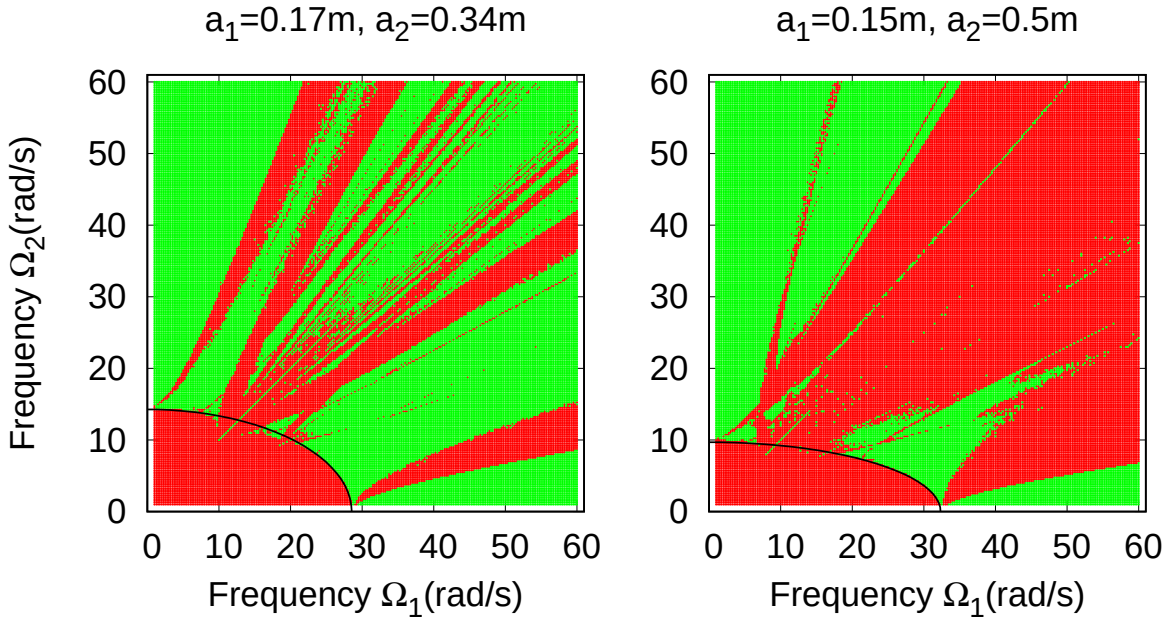

Figure 14 – Stability diagram for different sets of frequencies with amplitudes fixed at $a_1 = 0.17$ m and $a_2 = 0.34$ m on the left diagram, and $a_1 = 0.15$ m and $a_2 = 0.5$ m on the right (simulation parameters: $g = 9.81$ m/s^2, $l = 1.2$ m, $\omega_0 = 2.86$ Hz, and $\theta_0 = 0.018$ rad). Green points represent stable sets of frequencies, and red ones represent unstable. Black curve represents the lower boundary of stability given by equation (4.9).

At the diagonal of these diagrams (when frequencies Ω_1 and Ω_2 are exactly the same), the system resumes to the same case of one cosine, as discussed on Chapter 2, with frequency $\Omega = \Omega_1 = \Omega_2$ and amplitude $a = a_1 + a_2$. On the diagram where $a = 0.5$ m, the lower (2.7) and upper (2.10) boundaries can be seen, since the green points at the diagonal do not go all the way to the end. The diagram on the left needs a larger range of frequencies to show the upper limit.

In Figure 14 it is interesting to notice that high values of frequencies do not necessarily mean stability. Branches of unstable regions that reminds Arnold tongues (ARNOLD, 1989) appear on the region above the lower stability condition. Sets of fractal dimensions may present here (OTT, 2002).

Around the diagonal, where frequencies are close, beating phenomenon is observed. This phenomenon explains the stable sets of frequencies found below the lower boundary

(4.9), more clearly seen on the left diagram of Figure 14. When two adjacent frequencies cause beating, stability is only possible if there is damping and it is sufficiently large to prevent the pendulum from falling during long periods of low amplitude of the support motion (HOWE, 1974).

Now, fixing values for the frequencies Ω_1 and Ω_2, four stability diagrams for different sets of amplitudes a_1 and a_2 are constructed on Figure 15. At top left, frequencies are fixed at $\Omega_1 = 10$ rad/s and $\Omega_2 = 20$ rad/s; top right, $\Omega_1 = 20$ rad/s and $\Omega_2 = 80$ rad/s; bottom left, $\Omega_1 = 80$ rad/s and $\Omega_2 = 160$ rad/s; and bottom right, $\Omega_1 = 10$ rad/s and $\Omega_2 = 160$ rad/s. Green points represent stable sets of amplitudes, while red ones, unstable. Since frequencies are too high, the axes of the ellipses that give the lower boundary of stability for close frequencies (4.9) are too small to appear on those diagrams and, therefore there is no expected behaviour for them. Additional regions of instability can be seen when the difference between the frequencies is smaller, although some stability is present even when the difference is arbitrarily small (HOWE, 1974).

All chosen sets of fixed frequencies in Figure 15 are multiple values, i.e., $\Omega_2 = n\Omega_1$, therefore the period of function (4.1) is known for each set, and is equal to $T = 2\pi/\Omega_1$. Because of it, expression (4.9) is no longer an approximation and is now an exact condition.

Figure 16 shows two stability diagrams for different sets of amplitudes with fixed frequencies that are not multiple values of each other. The values of the axes of the ellipses that give the lower boundary of stability according to (4.9) are too small to appear in these diagrams.

4.2 Equal Amplitudes

An interesting case happens when the amplitudes a_1 and a_2 of perturbation (4.1) are equal, and shall be called $a_1 = a_2 = a$. The lower boundary of stability (4.6) becomes

$$\Omega_1^2\left(\frac{\sin(2\Omega_1 T)}{2\Omega_1 T}+1\right)+\Omega_2^2\left(\frac{\sin(2\Omega_2 T)}{2\Omega_2 T}+1\right)+ \\ +\frac{(\Omega_1^2+\Omega_2^2)}{T}\left(\frac{\sin((\Omega_1+\Omega_2)T)}{\Omega_1+\Omega_2}+\frac{\sin((\Omega_1-\Omega_2)T)}{\Omega_1-\Omega_2}\right)>\frac{2gl}{a^2}. \quad (4.10)$$

Using the approximation for close frequencies, expression (4.10) is

$$\Omega_1^2+\Omega_2^2=\frac{2gl}{a^2}, \quad (4.11)$$

which is the equation of a circle with radius equals to $(2gl/a^2)^{1/2}$. Figure 17 shows two stability diagrams for different sets of frequencies and different fixed amplitudes: $a = 0.17$ m (left) and $a = 0.34$ m (right). Green points represent stable sets of frequencies, while red ones represent unstable sets. Black curve gives the lower boundary of stability given by (4.11).

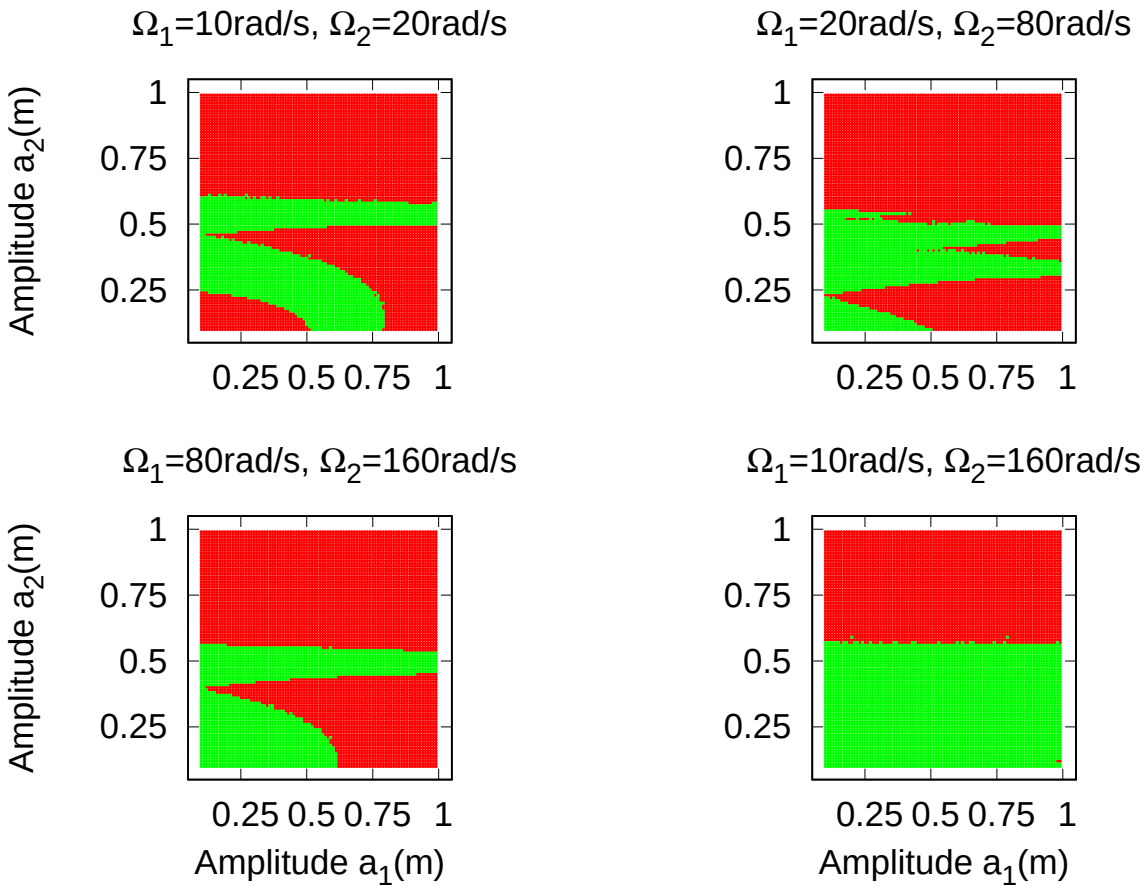

Figure 15 – Stability diagram for different sets of amplitudes with frequencies fixed at $\Omega_1 = 10$ rad/s and $\Omega_2 = 20$ rad/s at top left, $\Omega_1 = 20$ rad/s and $\Omega_2 = 80$ rad/s at top right, $\Omega_1 = 80$ rad/s and $\Omega_2 = 160$ rad/s at bottom left, and $\Omega_1 = 10$ rad/s and $\Omega_2 = 160$ rad/s at bottom right (simulation parameters: $g = 9.81$ m/s^2, $l = 1.2$ m, $\omega_0 = 2.86$ Hz, and $\theta_0 = 0.018$ rad). Green points represent stable sets of amplitudes, while red ones, unstable sets.

Figure 17 shows that when amplitudes a_1 and a_2 are equal, the stability diagram for frequencies becomes symmetric with a symmetry axis at the diagonal. As can be seen, the smaller the amplitude, more stable sets of frequencies are found and sets of fractal dimensions seem to be present.

4.3 Equal Frequencies

By making the frequencies equal, $\Omega_1 = \Omega_2 = \Omega$, the system resumes to the case when $N = 1$ with an amplitude of $a = a_1 + a_2$, and the lower boundary of stability becomes:

$$a_1^2 + a_2^2 > \frac{2gl}{\Omega^2}. \tag{4.12}$$

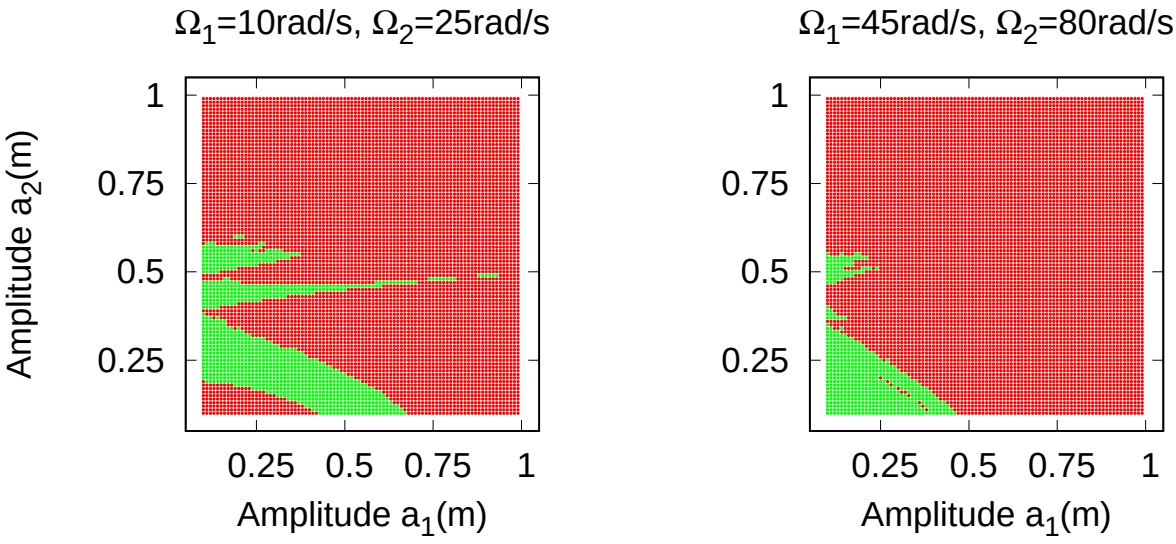

Figure 16 – Stability diagram for different sets of amplitudes with frequencies fixed at $\Omega_1 = 10$ rad/s and $\Omega_2 = 25$ rad/s on the left diagram, and $\Omega_1 = 45$ rad/s and $\Omega_2 = 80$ rad/s on the right (simulation parameters: $g = 9.81$ m/s^2, $l = 1.2$ m, $\omega_0 = 2.86$ Hz, and $\theta_0 = 0.018$ rad). Green points represent stable sets of amplitudes while red ones, unstable sets.

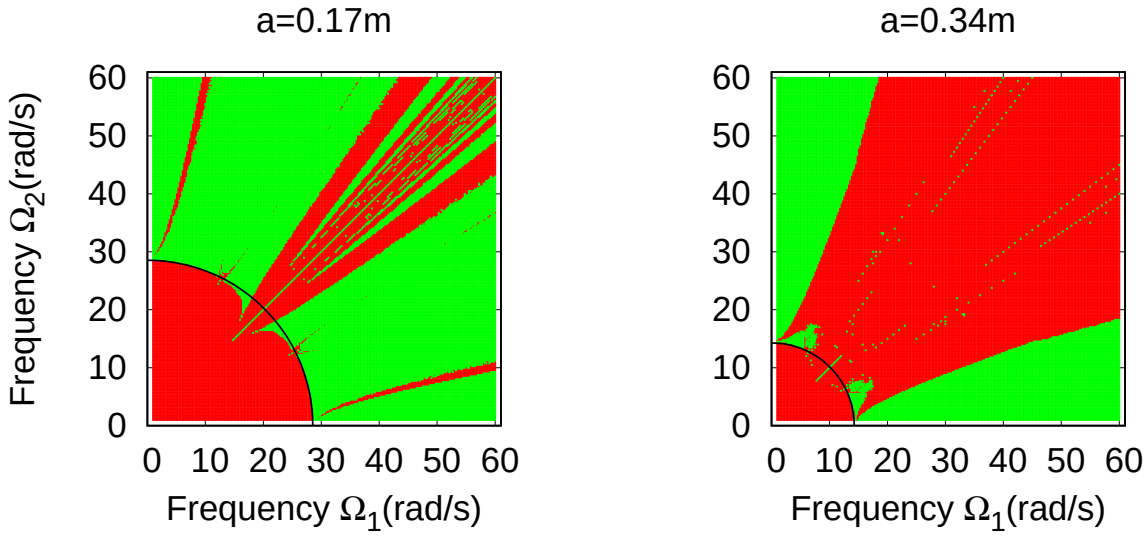

Figure 17 – Stability diagram for different sets of frequencies with amplitudes fixed at $a = 0.17$ m on the left diagram, and $a = 0.34$ m on the right (simulation parameters: $g = 9.81$ m/s^2, $l = 1.2$ m, $\omega_0 = 2.86$ Hz, and $\theta_0 = 0.018$ rad). Green points represent stable sets of frequencies, and red points, unstable. Black curve represents the lower boundary of stability given by (4.11).

Again, this represents an equation of a circle but with radius equals to $(2gl/\Omega^2)^{1/2}$. Since frequencies Ω have high values, this stability boundary circle is too small to appear on Figure 18, and therefore, the behaviour of the stability diagrams is unknown. The only expected aspect was a symmetry with axis at the diagonal, which can be seen.

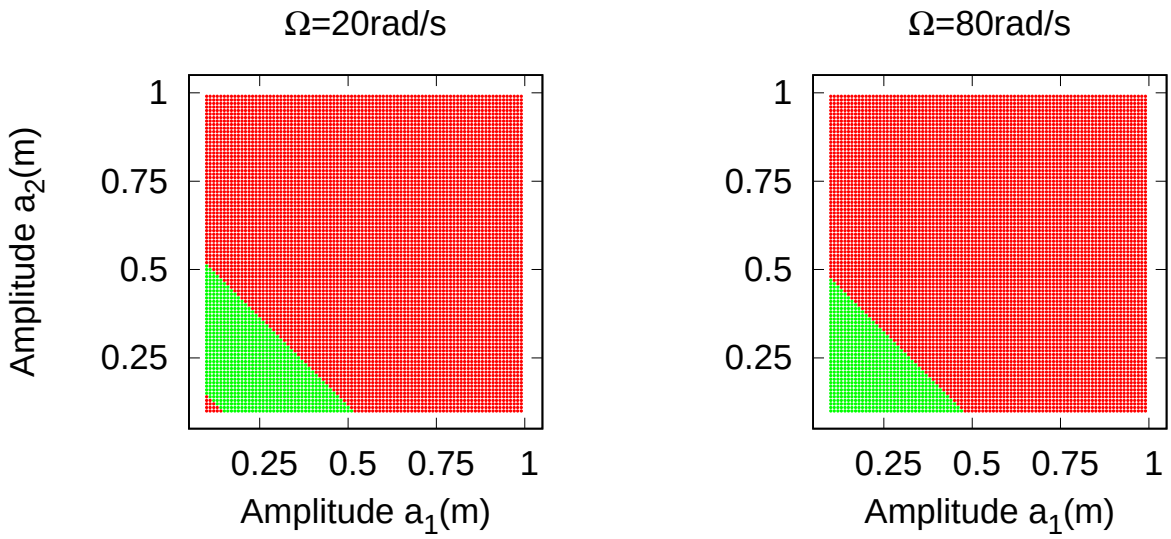

Figure 18 – Stability diagram for different sets of amplitudes with equal frequencies fixed at $\Omega = 20$ rad/s on the left diagram, and $\Omega = 80$ rad/s on the right (simulations parameters: $g = 9.81$ m/s^2, $l = 1.2$ m, $\omega_0 = 2.86$ Hz, and $\theta_0 = 0.018$ rad). Green points represent stable sets of amplitudes while red ones, unstable.

Figure 18 shows two stability diagrams for sets of amplitudes with fixed frequencies $\Omega = 20$ rad/s on the left, and $\Omega = 80$ rad/s on the right. Green points represent stable sets of amplitudes, while red represents unstable sets. Simulations have shown that for frequencies above $\Omega = 25$ rad/s, the stability diagram does not change for any frequency.

4.4 A Study of Periods

Since most sets of frequencies do not have a definite period, values of period can be chosen so an approximated behaviour can be predicted. The lower boundary of stability (4.6) depends on the period T and, therefore the choice of variable T is important so the established boundaries are closer to their real behaviour. Four reasonable choices were made in this work and are represented on Figure 19.

Figure 19 shows four stability diagrams for frequencies with fixed amplitudes at $a_1 = a_2 = 0.17$ m for different choices of period T. Again, green points represent stable sets of frequencies, and red points, unstable ones. Black curve limits the lower boundary of stability by equation (4.11). Each period is related to a frequency as in

$$T_i = \frac{2\pi}{\Omega_i}. \tag{4.13}$$

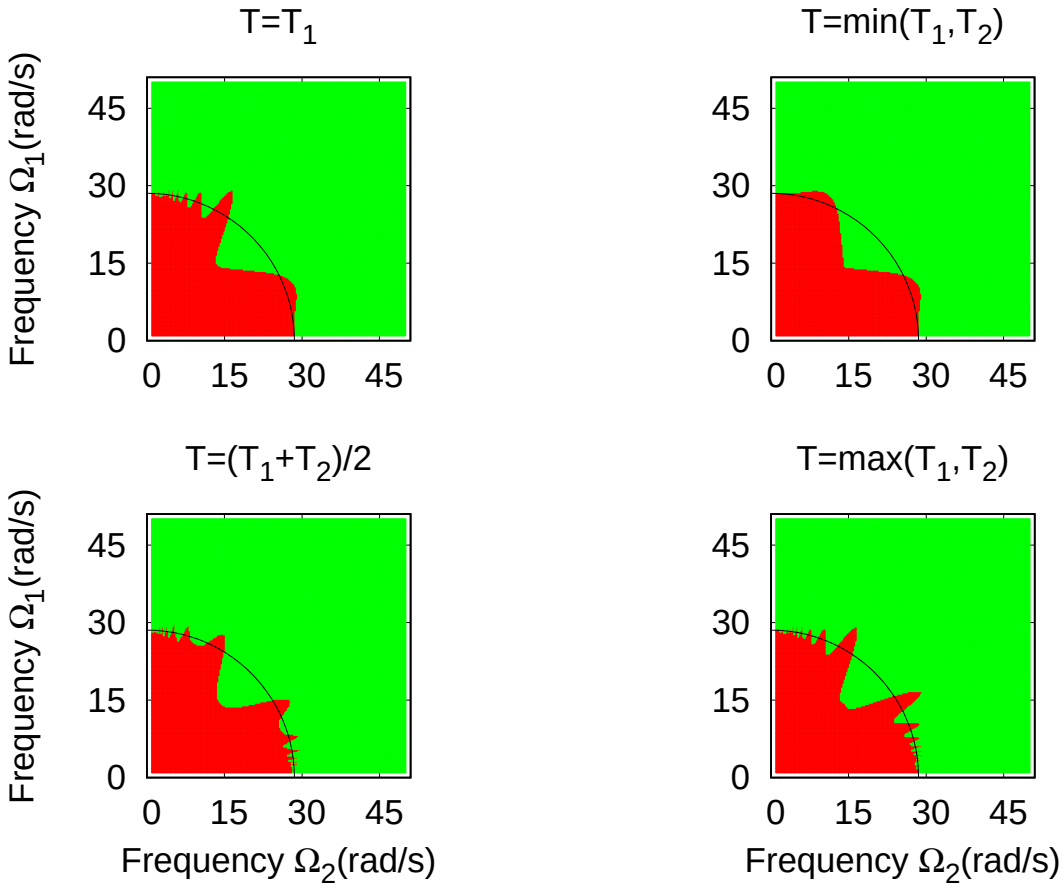

Figure 19 – Stability diagrams for frequencies with amplitudes fixed at $a_1 = a_2 = a = 0.17$ m using (4.6) for four different choices of period $T_i = 2\pi/\Omega_i$ (simulation parameters: $g = 9.81$ m/s^2, $l = 1.2$ m, $\omega_0 = 2.86$ Hz, and $\theta_0 = 0.018$ rad). Top left diagram considers period $T = T_1$; top right, the smallest value between T_1 and T_2; at bottom left, period is taken as the mean period value; and bottom right considers the maximum value between T_1 and T_2. Green points represent stable sets of frequencies while red dots, unstable. Black curve shows the lower boundary of stability given by (4.11).

The choices made here were: the period being equal to the period of one of the frequencies $T = T_1$ (top left diagram); the minimum value between periods T_1 and T_2 (top right); the mean value of periods $T = (T_1 + T_2)/2$; and the maximum value between periods (bottom right). From these plots and by a qualitative analysis, the best choice of period seems to be the maximum value between T_1 and T_2, since there seems to be a better agreement with left diagram from Figure 17.

In this Chapter, the specific case for $N = 2$ was analysed. Stability condition and diagrams were constructed for different combinations of amplitudes and frequencies so the many aspects of this system could be seen. Since external function (4.1) not necessarily has a defined value for the period, a few reasonable choices were made, tested, and it was

established that the best choice of period is the highest value between the periods.

5 External Stochastic Excitation

This Chapter starts by showing a brief review of previous works where the stability condition was obtained for the inverted pendulum under a stochastic external excitation with special conditions. Then, it will be shown how the addition of a Gaussian noise affect the stability diagrams found in the previous Chapters.

5.1 Stochastic Excitation

Several authors have found that the inverted pendulum with a random parametric excitation applied at the suspension point is a stable system over an infinite interval of time if there is a damping coefficient (MITCHELL, 1972; SETHNA, 1973; HOWE, 1974).

Mitchell (1972) used the method of averaging to find the following stability condition:

$$\sigma_{\xi}^{2} > gl \tag{5.1}$$

where σ_{ξ}^{2} is the variance of the suspension point velocity. Though equation (5.1) is independent of a damping coefficient, numerical simulations have shown that the pendulum's stability is dependent on a sufficiently large damping at the base motion (MITCHELL, 1972), which is a sample function from a stochastic process with a high pass power spectral density function. The stochastic base of motion used on his experiments was a white noise generator, and he experimentally found out that the larger the variance of the base acceleration, the more stable the pendulum becomes.

Using an arbitrary support motion, Sethna (1973) stated that the vertically up position of an inverted pendulum can be made stable as long as the vertical support motion is fast, the average of the square of the support velocity exceeds the square of the velocity plus one, and the damping is linear.

Howe (1974) found the same stability condition (5.1) but assuming that the damping could also be small by making the change of variable

$$\theta = \left[1 + \frac{\xi(t)}{l}\right]\phi. \tag{5.2}$$

Although ϕ changes very little during the averaging period, it produces a term that contributes with a nonzero value. Over many periods of oscillation, this nonzero contribution accumulates and eventually alters significantly the motion of the system.

Bogdanoff and Citron (IBRAHIM, 2006) found through experiments that an inverted pendulum cannot be stabilized using only a Gaussian random noise as an external

excitation, regardless of the spectral shape. It is important to notice that this experiment considered nonzero damping.

5.2 Mixed Excitation

Considering an additive Gaussian noise of variance σ^2 applied on an inverted pendulum, additionally to the deterministic sum of cosines excitation at the suspension point, a study is made on the new stability diagrams, which show the probability of the system being stable p_{stab} for sets of amplitudes a_i and frequencies Ω_i after N_{run} iterations. This probability is given by equation (3.20). The plots constructed have a colour scale graduated accordingly to p_{stab}: the closer to green the point, the more stable the set of parameters is (SILVA; PERETTI; PRADO, 2016).

Considering the first case of an external perturbation of one cosine but now with an additive noise, the equation of motion becomes:

$$\ddot{\theta} - \left[\omega_0^2 - \frac{a\Omega^2}{l}\cos(\Omega t)\right]\sin\theta = \xi(t) \tag{5.3}$$

where $\xi(t)$ is, in this case, a Gaussian noise of zero mean and variance σ^2. Figure 20 shows four diagrams for different values of variance: top left is $\sigma = 1$; top right, $\sigma = 2$; bottom left, $\sigma = 8$; and bottom right, $\sigma = 10$. The diagrams were constructed by numerically integrating equation (5.3) via a fourth order Runge-Kutta method, following the procedures described in Tables 1, and 2 or 3 of Appendix C (SILVA; PERETTI; PRADO, 2016).

Figure 20 shows that the additive noise does not change considerably the form of the stability diagram from Figure 7. The increase of the variance produces the effect of destabilizing some sets of amplitudes and frequencies that were stable before, increasing the unstable region. The destruction of the diagrams starts at the borders of the stable region of Figure 7, and penetrates further as variance increases. However, it can be seen that using a perturbation on the form of a cosine is a very efficient way of stabilizing an inverted pendulum since the additive Gaussian noise was not very effective to destabilize it even with a large variance.

When using a deterministic excitation of two cosines with an additive Gaussian random noise, the equation of motion becomes:

$$\ddot{\theta} - \left[\omega_0^2 - \frac{a_1\Omega_1^2}{l}\cos(\Omega_1 t) - \frac{a_2\Omega_2^2}{l}\cos(\Omega_2 t)\right]\sin\theta = \xi(t) \tag{5.4}$$

where, again, $\xi(t)$ is a Gaussian noise of zero mean and variance σ^2. Since the behaviour of the system does not change much with the addition of the noise, as can be seen by comparing Figures 7 and 20, for the case of two cosines the study will be made for only one value of variance, but for different parameters.

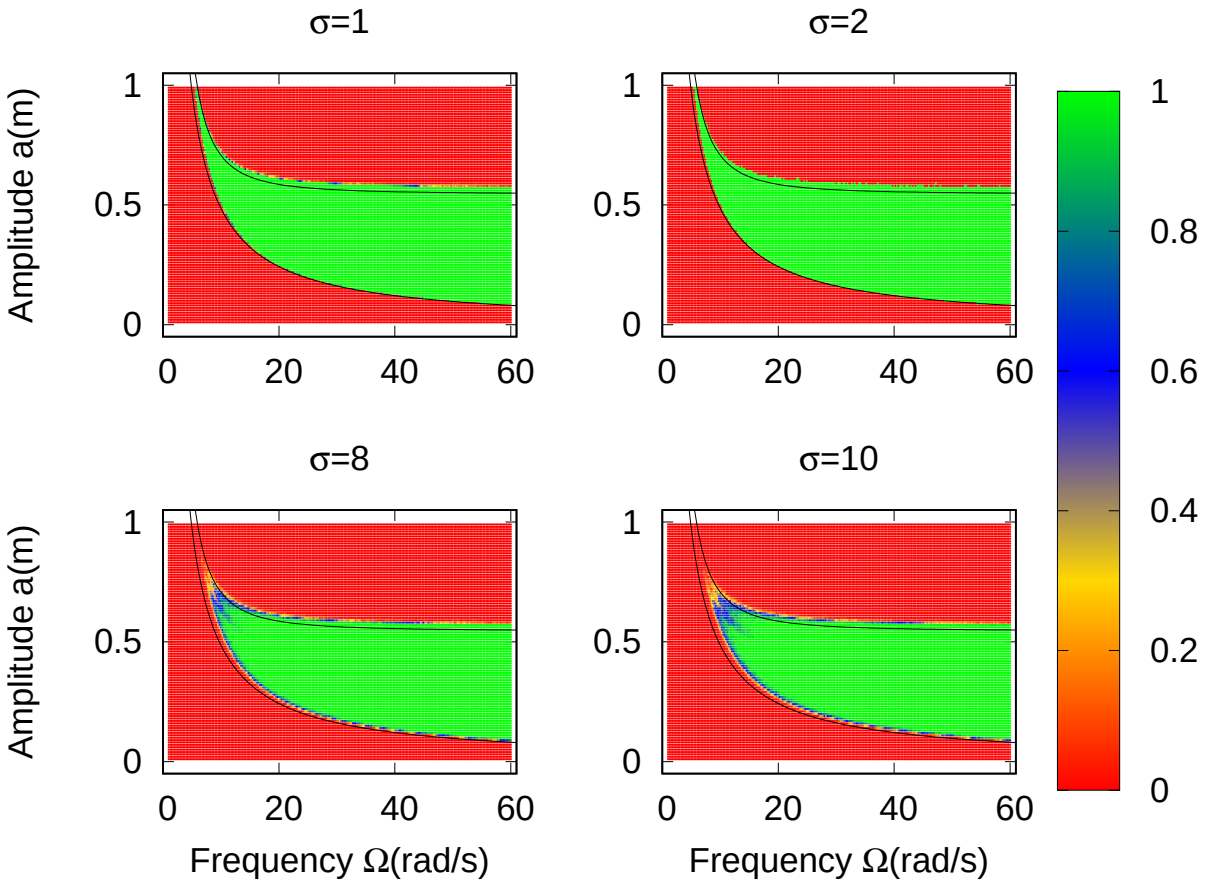

Figure 20 – Stability diagram for the parameters amplitude a and frequency of oscillation Ω with a Gaussian noise of mean zero and variance σ (simulation parameters: $l = 1.2$ m, $g = 9.81$ m/s^2, $\omega_0 = 2.86$ Hz, $\theta_0 = 0.018$ rad, $N_{run} = 50$). The colour scale is graduated accordingly to p_{stab}: the closer to green the point, the more stable is the set of parameters. Top left diagram shows the stability diagram when $\sigma = 1$; top right, $\sigma = 2$; bottom left, $\sigma = 8$; and bottom right, $\sigma = 10$. The solid black curve shows the lower boundary of stability (2.7), and the dashed curve shows the upper boundary (2.10).

Figure 21 shows the effects of a Gaussian additive noise on a system with a deterministic excitation of two cosines of amplitudes $a = 0.17$ m (diagram on the left) and $a = 0.34$ m (on the right). This figure suggests that when the amplitudes of the cosines are higher, the system is less sensitive to degradations. An increase on the unstable region can be seen above the stability boundary given by equation (4.11), plotted as a black solid line, but the addition of the noise does not create new regions of stability.

Figure 22 also shows the effects of a Gaussian additive noise on a system with a deterministic excitation of two cosines but with different fixed frequencies $\Omega_1 = 20$ rad/s and $\Omega_2 = 80$ rad/s (diagram on the left), and $\Omega_1 = 10$ rad/s and $\Omega_2 = 25$ rad/s (on the right). These diagrams suggest that the greater the difference between the frequencies, the

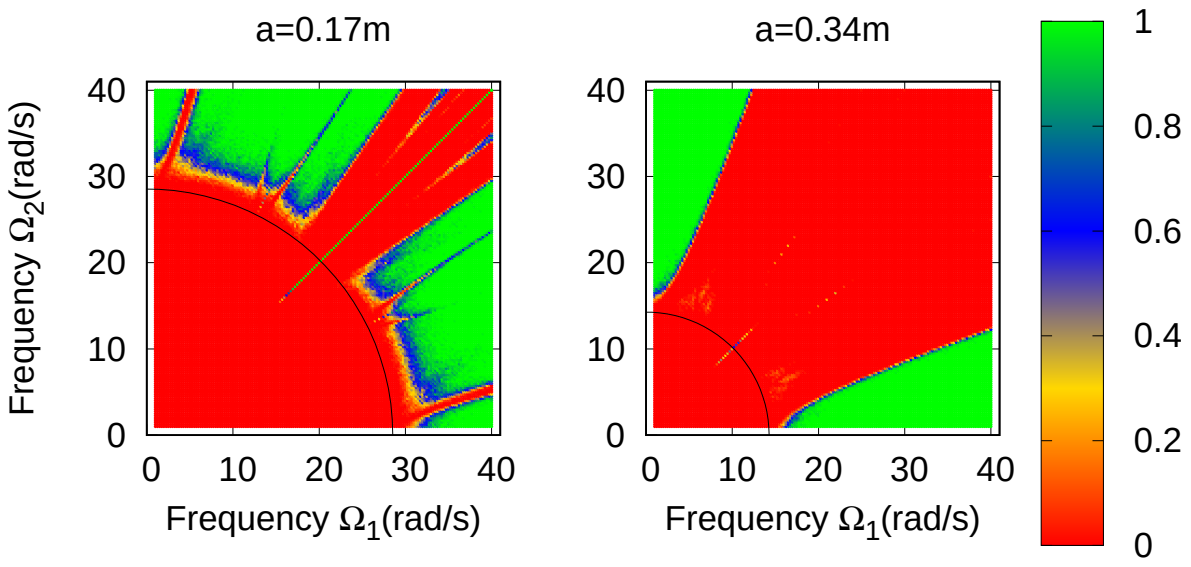

Figure 21 – Stability diagram for different sets of frequencies with fixed amplitudes at $a = 0.17$ m (left) and $a = 0.34$ m (right) (simulation parameters: $g = 9.81$ m/s^2, $l = 1.2$ m, $\omega_0 = 2.86$ Hz, $\theta_0 = 0.018$ rad, $N_{run} = 50$, and $\sigma = 10$). The colour scale is graduated accordingly to p_{stab}: the closer to green the point, the more stable the set of frequencies is. Black curve shows the lower boundary of stability given by (4.11).

more stable the system is, which agrees with the statements made by Howe (1974), since the Gaussian additive noise proved to be more efficient to degrade the stability diagram on the right than the one on the left.

In this Chapter, a review of some works previously made on the stabilization of an inverted pendulum with a random noise applied at the suspension point was made. Then, at the suspension point is applied an external perturbation of N cosines, and an additive Gaussian noise is introduced in the system. The effects of this additive noise are seen on diagrams that show the stability probability for different sets of parameters.

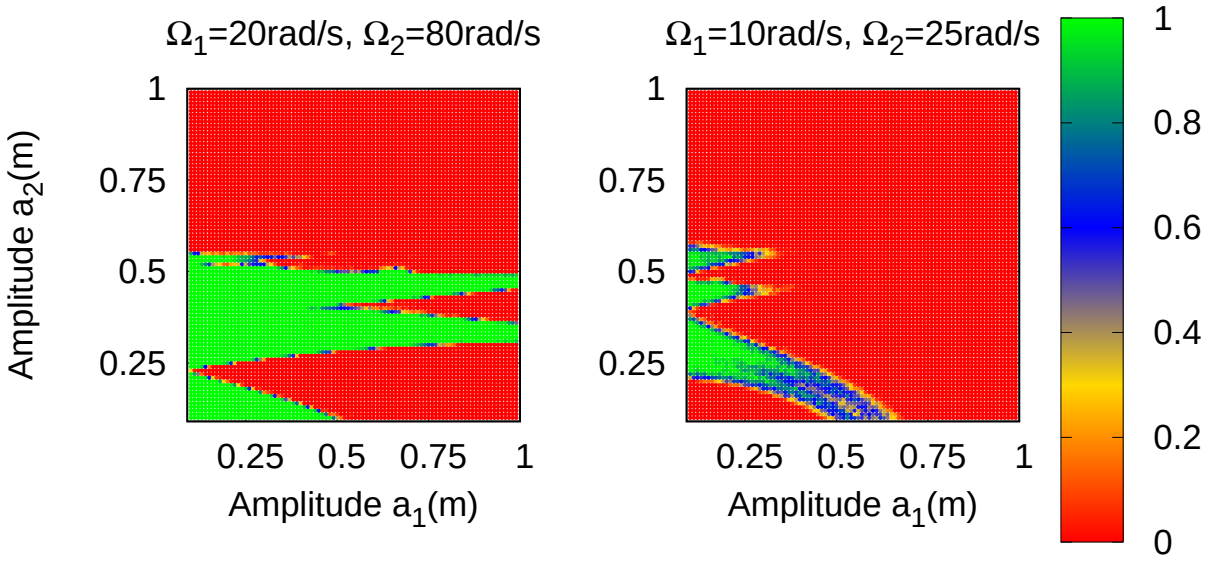

Figure 22 – Stability diagram for different sets of amplitudes with fixed frequencies at $\Omega_1 = 20$ rad/s and $\Omega_2 = 80$ rad/s (left), and $\Omega_1 = 10$ rad/s and $\Omega_2 = 25$ rad/s (right) (simulation parameters: $g = 9.81$ m/s^2, $l = 1.2$ m, $\omega_0 = 2.86$ Hz, $\theta_0 = 0.018$ rad, $N_{run} = 50$, and $\sigma = 10$). The colour scale is graduated accordingly to p_{stab}: the closer to green the point, the more stable the set of amplitudes.

6 Conclusions and Final Remarks

The main purpose of this work was to study the phenomenon related to the stabilization of an inverted pendulum over large periods of time. By making a deterministic analysis, it has been proved that periodic external forces on the form of a sum of N cosines may be very effective on steadying this system, and that an additive Gaussian noise is not sufficient to significantly destabilize it, although further studies on the effects of the Gaussian noise are still to be made.

In Chapter 2, a review of an inverted pendulum with an external force in the form of a cosine of amplitude a and frequency Ω based on previous articles was made. The lower and upper boundaries of stability (2.7) and (2.10) respectively, maximum angle of deflection (2.8), and effective potential (2.13) were established. The importance of not using the small angles approximation $\sin\theta \approx \theta$ can be seen in the stability diagram in Figure 7, since equation (2.10) was the only one where this approach was used, and it is not respected by the numerical integration of the equation of motion (2.1) through a fourth order Runge-Kutta. A study of the influence of the initial angle on the system was made and appears on Figure 8.

All methods introduced on Chapter 2 were used to make the generalization for a sum of N cosines on Chapter 3. The condition of stability (3.5), maximum angle (3.6) of deflection, and an equation for the system's effective potential (3.7) were found and approximations were made. Using the appropriate rescaling of the amplitude and choosing the appropriate intervals of frequencies, it was shown that an inverted pendulum with external force (3.18) can reduce to the case of $N = 1$ cosine. Then, still by choosing random values of frequencies, a study was made to find the best value of N for the highest stabilization probability. The drawn conclusions were: increasing the maximum frequency Ω_{max}, the optimal value of N does not change; the smaller the value of the maximum amplitude, the more number of cosines are needed to amount the probability of stabilizing the system; and the choice of initial angle does not have any effect on the value of N.

For the specific case of $N = 2$ cosines, generalized equations from Chapter 3 were rewritten on Chapter 4. Different values of amplitudes were set so their influence on the stability diagram of frequencies, which presents complex patterns, could be observed. The same happens for the amplitude but in this case, an analysis was made to observe the influence of periodic and almost periodic sets of frequencies on the diagrams. The larger the difference between amplitudes a_1 and a_2, the less stable sets of frequencies there were, while the opposite happens for frequencies: the larger the difference between frequencies

Ω_1 and Ω_2, the more stable sets of frequencies were found. When the amplitudes are exactly the same, the diagram has an axis of symmetry at its diagonal. When frequencies are exactly the same, the system resumes to the case when $N = 1$ with an amplitude of $a = a_1 + a_2$. When the system has no defined period, an approximation for its value can be made. Four possible values were chosen, and it was stated that the best value for a period choice is the maximum value between T_1 and T_2.

A review of previous works of an inverted pendulum with random parametric excitations was made on Chapter 5, and it stated that the condition of stability was dependent on the variance of the suspension point's velocity of the inverted pendulum. Then the influence of a Gaussian additive noise on the system along with the external deterministic excitations was studied. A destruction of the stability diagram was expected, but that it would not be so strong was not. Even the increase of noise variance up to a value of $\sigma = 10$ was not enough to deform the diagrams on a significant manner.

This work covers many aspects of an inverted pendulum with deterministic and stochastic parametric excitations, but further studies can still be made, as the introduction of different periodic external forces and the influence of other stochastic noises. A more precise solution for equation (2.1) can be sought using a better approximation as $\sin\theta \approx \theta - \frac{\theta^3}{6}$ so the upper boundary (2.10) could fit better for arbitrary angles. Regarding the generalization of N cosines, distinct probability density functions could also be tested. Chaotic modes may be present in the system and have not been explored so far. An examination can also be made by considering the motion of the pivot in more than one direction. A truly stochastic superposition of cosines also must be better explored. Further works on this system are already in progress.

Bibliography

ARNOLD, V. I. *Mathematical methods of classical mechanics*. [S.l.]: Springer Science & Business Media, 1989. 121–122 p. Cited 4 times on pages 16, 40, 59, and 61.

BOGDANOFF, J.; CITRON, S. Experiments with an inverted pendulum subject to random parametric excitation. *The Journal of the Acoustical Society of America*, Acoustical Society of America, v. 38, n. 3, p. 447–452, 1965. Cited 3 times on pages 13, 14, and 28.

BOGDANOFF, J. L. Influence on the behavior of a linear dynamical system of some imposed rapid motions of small amplitude. *The Journal of the Acoustical Society of America*, Acoustical Society of America, v. 34, n. 8, p. 1055–1062, 1962. Cited on page 27.

BUTIKOV, E. I. On the dynamic stabilization of an inverted pendulum. *American Journal of Physics*, American Association of Physics Teachers, v. 69, n. 7, p. 755–768, 2001. Cited 4 times on pages 13, 17, 19, and 20.

BUTIKOV, E. I. et al. Parametric resonance. *Computing in Science & Engineering*, IEEE, v. 1, n. 3, p. 76–83, 1999. Cited 3 times on pages 11, 13, and 21.

DETTMANN, C.; KEATING, J.; PRADO, S. Stochastic stabilization of cosmological photons. *Journal of Physics A: Mathematical and General*, IOP Publishing, v. 37, n. 30, p. L377, 2004. Cited on page 12.

FENN, J. G.; BAYNE, D. A.; SINCLAIR, B. D. Experimental investigation of the "effective potential" of an inverted pendulum. *American Journal of Physics*, American Association of Physics Teachers, v. 66, n. 11, p. 981–984, 1998. Cited 2 times on pages 13 and 21.

FLOQUET, G. Sur les équations différentielles linéaires à coefficients périodiques. In: *Annales scientifiques de l'École normale supérieure*. [S.l.: s.n.], 1883. v. 12, p. 47–88. Cited on page 27.

HEMP, G. W.; SETHNA, P. On dynamical systems with high frequency parametric excitation. *International Journal of Non-Linear Mechanics*, Elsevier, v. 3, n. 3, p. 351–365, 1968. Cited on page 37.

HILL, G. W. On the part of the motion of the lunar perigee which is a function of the mean motions of the sun and moon. *Acta mathematica*, Springer, v. 8, n. 1, p. 1–36, 1886. Cited on page 27.

HOWE, M. The mean square stability of an inverted pendulum subject to random parametric excitation. *Journal of Sound and Vibration*, Elsevier, v. 32, n. 3, p. 407–421, 1974. Cited 4 times on pages 14, 41, 47, and 50.

IBRAHIM, R. A. Excitation-induced stability and phase transition: a review. *Journal of Vibration and Control*, SAGE Publications, v. 12, n. 10, p. 1093–1170, 2006. Cited 3 times on pages 11, 13, and 47.

KAJITA, S. et al. Biped walking stabilization based on linear inverted pendulum tracking. In: IEEE. *Intelligent Robots and Systems (IROS), 2010 IEEE/RSJ International Conference on*. [S.l.], 2010. p. 4489–4496. Cited on page 12.

KAPITZA, P. L. *Collected papers of P.L. Kapitza*. London: Pergamon Press, 1965. 714–726 p. Cited 3 times on pages 12, 13, and 63.

LANDAU, L.; LIFSCHITZ, L. *Physique théorique-Mécanique*. [S.l.]: Mir, 1966. Cited 4 times on pages 13, 21, 63, and 65.

LIU, X.; WILLMS, A. Impulsive stabilizability of autonomous systems. *Journal of Mathematical Analysis and Applications*, Elsevier, v. 187, n. 1, p. 17–39, 1994. Cited on page 13.

MATHIEU, E. Mémoire sur le mouvement vibratoire d'une membrane de forme elliptique. *Journal de mathématiques pures et appliquées*, p. 137–203, 1868. Cited on page 27.

MITCHELL, R. Stability of the inverted pendulum subjected to almost periodic and stochastic base motion—an application of the method of averaging. *International Journal of Non-Linear Mechanics*, Elsevier, v. 7, n. 1, p. 101–123, 1972. Cited 2 times on pages 14 and 47.

NASA. *Rocket Stability*. 2014. Online; accessed on 26-October-2015. Disponível em: <https://spaceflightsystems.grc.nasa.gov/education/rocket/rktstab.html>. Cited on page 11.

OTT, E. *Chaos in dynamical systems*. [S.l.]: Cambridge university press, 2002. Cited on page 40.

SETHNA, P. Method of averaging for systems bounded for positive time. *Journal of Mathematical Analysis and Applications*, Elsevier, v. 41, n. 3, p. 621–631, 1973. Cited 3 times on pages 13, 14, and 47.

SHLESINGER, M. F.; SWEAN, T. *Stochastically excited nonlinear ocean structures*. [S.l.]: World Scientific, 1998. Cited on page 11.

SILVA, R. da; PERETTI, D. E.; PRADO, S. D. Deterministic and stochastic aspects of the stability in an inverted pendulum under a generalized parametric excitation. *accepted at Applied Mathematical Modelling, arXiv:1603.01261*, 2016. Cited 7 times on pages 20, 23, 31, 32, 39, 48, and 67.

STEPHENSON, A. Xx. on induced stability. *The London, Edinburgh, and Dublin Philosophical Magazine and Journal of Science*, Taylor & Francis, v. 15, n. 86, p. 233–236, 1908. Cited on page 13.

YAMAKAWA, T. Stabilization of an inverted pendulum by a high-speed fuzzy logic controller hardware system. *Fuzzy sets and Systems*, Elsevier, v. 32, n. 2, p. 161–180, 1989. Cited on page 12.

YANG, R.; PENG, Y.; SONG, Y. Stability and hopf bifurcation in an inverted pendulum with delayed feedback control. *Nonlinear Dynamics*, Springer, v. 73, n. 1-2, p. 737–749, 2013. Cited on page 12.

Appendix

APPENDIX A – A Different External Function

The external function used to stabilize an inverted pendulum does not necessarily need to be $\cos(\Omega t)$ or $\sin(\Omega t)$. Arnold (1989) stabilized an inverted pendulum using a function of period 2τ defined in Figure 23. The function is periodic and defined separately within each half period.

The system used here is the same as before: a light rod of length l with a bob of mass m attached to it. This pendulum oscillates vertically with a periodic function, whose acceleration is $\pm c$ (where $c = 8a/\tau^2$)(ARNOLD, 1989).

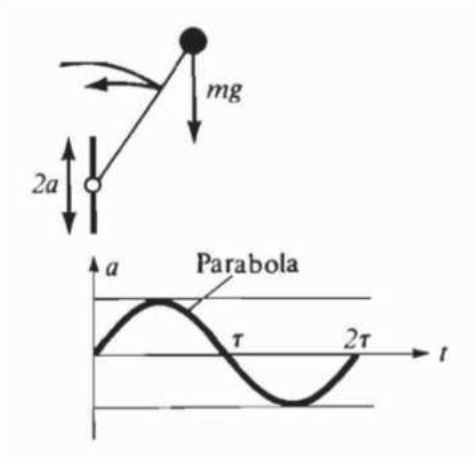

Figure 23 – Inverted pendulum with an oscillatory suspension point (adapted from Arnold (1989), "Mathematical Methods of Classical Mechanics", Springer, 2nd edition, September 5, 1997, page 121).

Using the known points of Figure 23, the function that describes the motion of the pendulum's suspension point can be found. During the first half period ($0 < t < \tau$) the acceleration is $c = -8a/\tau^2$. Therefore:

$$\begin{aligned} \frac{d^2y_1}{dt^2} &= -\frac{8a}{\tau^2} \\ y_1(t) &= -\frac{4at^2}{\tau^2} + \frac{4at}{\tau}. \end{aligned} \tag{A.1}$$

During the second half period ($\tau < t < 2\tau$), the acceleration is $c = +8a/\tau^2$. Therefore:

$$\begin{aligned} \frac{d^2y_2}{dt^2} &= +\frac{8a}{\tau^2} \\ y_2(t) &= -\frac{4at^2}{\tau^2} - \frac{12at}{\tau} + 8a. \end{aligned} \tag{A.2}$$

The equation which describes the coordinates of the bob is written as:

$$x = l\sin\theta \tag{A.3}$$
$$y = l\cos\theta + y_i \tag{A.4}$$

where $i = 1, 2$ and y_i are equations (A.1) and (A.2). Using (A.3) and (A.4) the Lagrangian of the system is:

$$L = \frac{ml^2\dot{\theta}^2}{2} + \frac{m\dot{y}_i^2}{2} - ml\dot{\theta}\dot{y}_i\sin\theta - mg(l\cos\theta + y_i). \tag{A.5}$$

Replacing (A.5) in the Euler-Lagrange equation:

$$\ddot{\theta} - \frac{\ddot{y}_i}{l}\sin\theta - \frac{y_i\theta}{l}\cos\theta - \frac{g}{l}\sin\theta = 0.$$

And approximating for small angles:

$$\ddot{\theta} = (\omega^2 \pm d^2)\theta \tag{A.6}$$

where $\omega^2 = g/l$ e $d^2 = c/l$.

For a function defined at each half period the transformation matrix A is written as the product of two matrices, each defined at a half period. Starting with the first half period, the equation of motion is given by:

$$\begin{aligned}\ddot{\theta} - (\omega^2 - d^2)\theta &= 0\\ \ddot{\theta} + (d^2 - \omega^2)\theta &= 0\\ \ddot{\theta} + \Lambda^2\theta &= 0.\end{aligned} \tag{A.7}$$

where $\Lambda^2 = d^2 - \omega^2$. The solutions to (A.7) and its first derivative are:

$$\theta(t) = c_1\cos(\Lambda t) + c_2\sin(\Lambda t), \tag{A.8}$$
$$\dot{\theta}(t) = -c_1\Lambda\sin(\Lambda t) + c_2\Lambda\cos(\Lambda t). \tag{A.9}$$

The solution for the initial conditions $\theta = 1$ and $\dot{\theta} = 0$ yields $c_1 = 1$ and $c_2 = 0$. Therefore:

$$\begin{aligned}\theta(t) &= \cos(\Lambda t),\\ \dot{\theta}(t) &= -\Lambda\sin(\Lambda t).\end{aligned}$$

While the solution with initial conditions $\theta = 0$ and $\dot{\theta} = 1$ yields other values for the constants $c_1 = 0$ and $c_2 = 1/\Lambda$. Therefore

$$\begin{aligned}\theta(t) &= \frac{1}{\Lambda}\sin(\Lambda t),\\ \dot{\theta}(t) &= \cos(\Lambda t).\end{aligned}$$

With these solutions the matrix of transformation A_2 can be written as:

$$A_2 = \begin{bmatrix} \cos(\Lambda\tau) & \frac{1}{\Lambda}\sin(\Lambda\tau) \\ -\Lambda\sin(\Lambda\tau) & \cos(\Lambda\tau) \end{bmatrix}. \tag{A.10}$$

During the other half period the equations of motion are:

$$\begin{aligned} \ddot{\theta} - (d^2 + \omega^2)\theta = 0 \\ \ddot{\theta} - k^2\theta = 0 \end{aligned} \tag{A.11}$$

where $k^2 = d^2 + \omega^2$. The solutions to (A.11) and its first derivative are:

$$\theta(t) = c_3\cosh(kt) + c_4\sinh(kt), \tag{A.12}$$

$$\dot{\theta}(t) = kc_3\sinh(kt) + kc_4\cosh(kt). \tag{A.13}$$

Initial conditions $\theta = 1$ and $\dot{\theta} = 0$ yield $c_3 = 1$ and $c_4 = 0$, then:

$$\begin{aligned} \theta(t) &= \cosh(kt), \\ \dot{\theta}(t) &= k\sinh(kt). \end{aligned}$$

While initial conditions $\theta = 0$ and $\dot{\theta} = 1$ yield $c_3 = 0$ and $c_4 = 1/k$. Therefore,

$$\begin{aligned} \theta(t) &= \frac{1}{k}\sinh(kt), \\ \dot{\theta}(t) &= \cosh(kt). \end{aligned}$$

With these solutions the matrix A_1 is written as:

$$A_1 = \begin{bmatrix} \cosh(k\tau) & \frac{1}{k}\sinh(k\tau) \\ k\sinh(k\tau) & \cosh(k\tau) \end{bmatrix}. \tag{A.14}$$

The system's total transformation matrix A is the product of A_1 and A_2:

$$A = \begin{bmatrix} \cos(\Lambda\tau)\cosh(k\tau) + \frac{k}{\Lambda}\sin(\Lambda\tau)\sinh(k\tau) & \frac{1}{k}\cos(\Lambda\tau)\sin(k\tau) + \frac{1}{\Lambda}\sin(\Lambda\tau)\cosh(k\tau) \\ -\Lambda\sin(\Lambda\tau)\cosh(k\tau) + k\cos(\Lambda\tau)\sinh(k\tau) & -\frac{\Lambda}{k}\sinh(k\tau)\sin(\Lambda\tau) + \cos(\Lambda\tau)\cosh(k\tau) \end{bmatrix}. \tag{A.15}$$

And the trace of this matrix is

$$\mathrm{Tr}A = 2\cos(\Lambda\tau)\cosh(k\tau) + \left(\frac{k}{\Lambda} - \frac{\Lambda}{k}\right)\sin(\Lambda\tau)\sinh(k\tau). \tag{A.16}$$

If A is the matrix of linear mapping of the plane on itself, which preserves area ($\det(A) = 1$) then the mapping of A is stable if $|\mathrm{Tr}A| < 2$ (ARNOLD, 1989). This condition is satisfied for sufficiently rapid oscillations of the suspension point ($c > g$). Dimensionless variables ϵ and μ are here introduced such that:

$$\frac{a}{l} = \epsilon^2 < 1 \tag{A.17}$$

$$\frac{g}{c} = \mu^2 < 1. \tag{A.18}$$

Substituting on k and Λ and remembering that $|c| = 8a/\tau^2$:

$$\begin{aligned} k\tau &= \sqrt{\frac{c}{l} + gl}\tau \\ &= 2\epsilon\sqrt{2}\sqrt{1+\mu^2} \end{aligned} \tag{A.19}$$

$$\begin{aligned} \Lambda\tau &= \sqrt{\frac{c}{l} - \frac{g}{l}}\tau \\ &= 2\epsilon\sqrt{2}\sqrt{1-\mu^2} \end{aligned} \tag{A.20}$$

$$\begin{aligned} \frac{k}{\Lambda} &= \frac{\sqrt{1+\mu^2}}{\sqrt{1-\mu^2}} \\ \frac{\Lambda}{k} &= \frac{\sqrt{1-\mu^2}}{\sqrt{1+\mu^2}} \\ \frac{k}{\Lambda} - \frac{\Lambda}{k} &= 2\mu^2 + O(\mu^4). \end{aligned}$$

Expanding sines and cosines in power series and substituting (A.19) and (A.20) up to fourth order of ϵ and μ:

$$\begin{aligned} \sinh(k\tau) &= 2\epsilon\sqrt{2}\sqrt{1+\mu^2} + \frac{8}{3}\epsilon^3\sqrt{2}(1+\mu^2)^{3/2} + O(\epsilon^4+\mu^4) \\ \sin(\Lambda\tau) &= 2\epsilon\sqrt{2}\sqrt{1-\mu^2} - \frac{8}{3}\epsilon^3\sqrt{2}(1-\mu^2)^{3/2} + O(\epsilon^4+\mu^4) \\ \cosh(k\tau) &= 1 + 4\epsilon^2(1+\mu^2) + \frac{8}{3}\epsilon^4(1+\mu^2)^2 + O(\epsilon^4+\mu^4) \\ \cos(\Lambda\tau) &= 1 - 4\epsilon^2(1-\mu^2) + \frac{8}{3}\epsilon^4(1-\mu^2)^2 + O(\epsilon^4+\mu^4). \end{aligned}$$

Finally, neglecting higher order terms:

$$\begin{aligned} \left(\frac{k}{\Lambda} - \frac{\Lambda}{k}\right)\sinh(k\tau)\sin(\Lambda\tau) &= 16\epsilon^2\mu^4 \\ \cosh(k\tau)\cos(\Lambda\tau) &= 1 + 8\epsilon^2\mu^2 - 16\epsilon^4 + \frac{16}{3}\epsilon^4. \end{aligned}$$

Replacing in (A.16) and remembering the stability condition:

$$2\left(1 + 8\epsilon^2\mu^2 - 16\epsilon^4 + \frac{16}{3}\epsilon^4\right) + 16\epsilon^4\mu^2 < 2$$

$$\epsilon^2 < \frac{2}{3}\mu^2.$$

From definitions (A.17) and (A.18), and recalling that $\omega^2 = g/l$ and $\tau^2 = 8a/c$, and the relation between period and frequency is $\tau = 1/\Omega$:

$$\begin{aligned} \frac{3}{2}\omega^2 &< \frac{ca}{l^2} \\ \frac{1}{2\tau} &> \sqrt{\frac{3}{64}}\omega\frac{l}{a} \\ \Omega &> \frac{2}{a}\sqrt{\frac{3gl}{64}}, \end{aligned} \tag{A.21}$$

which is the condition of stability.

APPENDIX B – Perturbative Analysis

The equation of motion (3.2) of an inverted pendulum with an external force given by a sum of N cosines applied at the suspension point can be rewritten as:

$$\frac{d^2\theta}{dt^2} = \frac{g}{l}\left(1 + \frac{1}{g}\sum_{i=1}^{N} a_i\Omega_i^2\cos(\Omega_i t)\right)\sin\theta \tag{B.1}$$

where g is gravity, l is the pendulum's length, and a_i are the amplitudes and Ω_i are the frequencies of the external force's cosines.

The motion of a particle under the influence of a constant field U (the gravitational field in this case) and a force which varies with a high frequency may be studied by perturbative analysis (LANDAU; LIFSCHITZ, 1966; KAPITZA, 1965). The equation of motion of a particle in a field written in terms of the angular coordinate is:

$$m\ddot{\theta} = -\frac{dU}{d\theta} + f(\theta). \tag{B.2}$$

By comparing (B.1) and (B.2), on may conclude that

$$U = \frac{g}{l}cos\theta,$$

which is the potential associated with gravity, and

$$f(\theta) = -\frac{\sin\theta}{l}\sum_{i=1}^{N} a_i\Omega_i^2\cos(\Omega_i t),$$

which is related to the external force due to the vibration of the pivot.

Again, the assumption that the movement can be separated into two components (a slow component $\psi(t)$ of large amplitude and low frequency, and a fast component $\delta(t)$ of small amplitude and high frequency), the motion of the pendulum is described by:

$$\theta(t) = \psi(t) + \delta(t). \tag{B.3}$$

Expanding the terms on the right-hand side of (B.2) via Taylor expansion, one has:

$$\begin{aligned}
\frac{\partial U}{\partial\theta} &= \left.\frac{\partial U}{\partial\theta}\right|_{\theta=\psi} + \left.\frac{\partial^2 U}{\partial\theta^2}\right|_{\theta=\psi}\delta + \frac{1}{2}\left.\frac{\partial^3 U}{\partial\theta^3}\right|_{\theta=\psi}\delta^2 + \ldots \\
\frac{\partial f}{\partial\theta} &= f(\psi) + \left.\frac{\partial f}{\partial\theta}\right|_{\theta=\psi}\delta + \left.\frac{\partial^2 f}{\partial\theta^2}\right|_{\theta=\psi}\delta^2 + \ldots.
\end{aligned}$$

Considering up to first order terms, from equations (B.2) and (B.3), one finds:

$$\ddot{\psi} + \ddot{\delta} = -\left.\frac{\partial U}{\partial\theta}\right|_{\theta=\psi} - \left.\frac{\partial^2 U}{\partial\theta^2}\right|_{\theta=\psi}\delta + f(\psi) + \left.\frac{\partial f}{\partial\theta}\right|_{\theta=\psi}\delta. \tag{B.4}$$

Perturbative effects are associated with the terms with δ, hence they are disregarded. Comparing the remaining terms of (B.4) with the associations made using (B.1) and (B.2), one can see that:

$$\ddot{\delta} = f(\psi) = -\frac{-\sin\theta}{l}\sum_{i=1}^{N} a_i\Omega_i^2\cos(\Omega_i t). \tag{B.5}$$

Integrating equation(B.5) twice:

$$\begin{aligned}\dot{\delta} &= \frac{\sin\theta}{l}\sum_{i=1}^{N} a_i\Omega_i\sin(\Omega_i t) + C_1\\ \delta &= \frac{\sin\theta}{l}\sum_{i=1}^{N} a_i\cos(\Omega_i t) + C_1 t + C_0.\end{aligned}$$

If δ is an oscillating term, constants C_0 and C_1 must be zero, otherwise δ would increase with time. For any set of frequencies $\Omega_{i\,i=1}^{N}$, the resultant superposition may not necessarily result in a periodic motion. For that to occur, there must exist a period T such that $\Omega_i T = 2\pi n_i$ and $\Omega_j T = 2\pi n_j$ for every pair $i \neq j = 1, ..., N$:

$$\frac{\Omega_i}{\Omega_j} = \frac{T_j}{T_i} = \frac{n_i}{n_j}. \tag{B.6}$$

The ratio between frequencies must be a rational number where n_i and n_j are the smallest integers.

Taking the time average of equation (B.4) and supposing that the non-perturbed terms do not change on first order approximation, one finds:

$$\ddot{\psi} \approx -\left.\frac{\partial U}{\partial\theta}\right|_{\theta=\psi} + \left\langle \left.\frac{\partial f}{\partial\theta}\right|_{\theta=\psi}\delta \right\rangle. \tag{B.7}$$

Computing separately the second term of the right-hand side of equation (B.7):

$$\begin{aligned}\left.\frac{\partial f}{\partial\theta}\right|_{\theta=\psi} &= -\frac{\cos\psi}{l}\sum_{i=1}^{N} a_i\Omega_i^2\cos(\Omega_i t)\\ \left\langle \left.\frac{\partial f}{\partial\theta}\right|_{\theta=\psi}\delta \right\rangle &= \left\langle -\frac{\cos\psi}{l^2}\left(\sum_{i=1}^{N} a_i\Omega_i^2\cos(\Omega_i t)\right)\left(\sum_{i=1}^{N} a_i\cos(\Omega_i t)\right)\sin\psi \right\rangle\\ &= -\frac{\cos\psi\sin\psi}{l^2}\left(\sum_{i=1}^{N} a_i\Omega_i^2\langle\cos^2(\Omega_i t)\rangle + \right.\\ &\quad \left. + \sum_{i\neq j=1}^{N} a_i a_j\Omega_i^2\langle\cos(\Omega_i t)\cos(\Omega_j t)\rangle\right)\\ \langle\cos^2(\Omega_i t)\rangle &= \frac{1}{T}\int_0^T \cos^2(\Omega_i t)dt = \frac{\sin(2\Omega_i T)}{4\Omega_i T} + \frac{1}{2} = \frac{1}{2}\left(\frac{\sin(2\Omega_i T)}{2\Omega_i T} + 1\right)\end{aligned}$$

$$\begin{aligned}
\langle \cos(\Omega_i T)\cos(\Omega_j T)\rangle &= \frac{1}{T}\int_0^N \cos(\Omega_i t)\cos(\Omega_j t)dt \\
&= \frac{1}{(\Omega_i+\Omega_j)(\Omega_i-\Omega_j)T}\left[\frac{(\Omega_i-\Omega_j)}{2}\sin((\Omega_i+\Omega_j)T) + \right. \\
&\quad \left. + \frac{(\Omega_i+\Omega_j)}{2}\sin((\Omega_i-\Omega_j)T)\right] \\
&= \frac{1}{2T}\left[\frac{\sin((\Omega_i+\Omega_j)T)}{\Omega_i+\Omega_j} + \frac{\sin((\Omega_i-\Omega_j)T)}{\Omega_i-\Omega_j}\right] \\
\left\langle \left.\frac{\partial f}{\partial\theta}\right|_{\theta=\psi}\delta \right\rangle &= -\frac{\sin(2\Psi)}{2l^2}\left[\frac{1}{2}\sum_{i=1}^{N} a_i^2\Omega_i^2\left(\frac{\sin(2\Omega_i T)}{2\Omega_i T}+1\right) + \right. \\
&\quad \left. + \sum_{i\neq j=1}^{N}\frac{a_i a_j\Omega_i^2}{2T}\left(\frac{\sin((\Omega_i+\Omega_j)T)}{\Omega_i+\Omega_j} + \frac{\sin((\Omega_i-\Omega_j)T)}{\Omega_i-\Omega_j}\right)\right]
\end{aligned}$$

Landau & Lifschitz (1966) state that

$$\ddot{\psi} = -\frac{\partial U_{eff}}{\partial\theta},$$

where U_{eff} is the effective potential of the system. Therefore:

$$\ddot{\psi} = -\left.\frac{\partial U}{\partial\theta}\right|_{\theta=\psi} + \left\langle \left.\frac{\partial f}{\partial\theta}\right|_{\theta=\psi}\delta\right\rangle. \tag{B.8}$$

From (B.8), an expression for the effective potential can be found:

$$\begin{aligned}
U_{eff} = \frac{g}{l}\cos\Psi - \frac{\cos(2\Psi)}{4l^2}&\left[\frac{1}{2}\sum_{i=1}^{N} a_i^2\Omega_i^2\left(\frac{\sin(2\Omega_i T)}{2\Omega_i T}+1\right) + \right. \\
&\left. + \sum_{i\neq j=1}^{N}\frac{a_i a_j\Omega_i^2}{2T}\left(\frac{\sin((\Omega_i+\Omega_j)T)}{\Omega_i+\Omega_j} + \frac{\sin((\Omega_i-\Omega_j)T)}{\Omega_i-\Omega_j}\right)\right]
\end{aligned} \tag{B.9}$$

The stability condition requires that the second derivative of the effective potential (B.9) must be bigger than zero. Using this condition and $\Psi = 0$, the stability condition of the inverted pendulum with an external force of N cosines applied at the suspension point is:

$$\begin{aligned}
&\sum_{i=1}^{N} a_i^2\Omega_i^2\left(\frac{\sin(2\Omega_i T)}{2\Omega_i T}+1\right) + \\
&\quad + \sum_{i\neq j=1}^{N}\frac{a_i a_j\Omega_i^2}{T}\left(\frac{\sin((\Omega_i+\Omega_j)T)}{\Omega_i+\Omega_j} + \frac{\sin((\Omega_i-\Omega_j)T)}{\Omega_i-\Omega_j}\right) > 2gl
\end{aligned} \tag{B.10}$$

APPENDIX C – Accepted Paper of this Work

The following pages contain the paper (SILVA; PERETTI; PRADO, 2016) of this work, accepted at *Applied Mathematical Modelling*.

Deterministic and stochastic aspects of the stability in an inverted pendulum under a generalized parametric excitation

Roberto da Silva, Debora E. Peretti, Sandra D. Prado

Institute of Physics, Federal University of Rio Grande do Sul, Av. Bento Gonçalves, 9500, Porto Alegre, 91501-970, RS, Brazil
E-mail:rdasilva@if.ufrgs.br

Abstract

In this paper, we explore the stability of an inverted pendulum under a generalized parametric excitation described by a superposition of N cosines with different amplitudes and frequencies, based on a simple stability condition that does not require any use of Lyapunov exponent, for example. Our analysis is separated in 3 different cases: $N = 1$, $N = 2$, and N very large. Our results were obtained via numerical simulations by fourth-order Runge Kutta integration of the non-linear equations. We also calculate the effective potential also for $N > 2$. We show then that numerical integrations recover a wider region of stability that are not captured by the (approximated) analytical method of the effective potential. We also analyze stochastic stabilization here: firstly, we look the effects of external noise in the stability diagram by enlarging the variance, and secondly, when N is large, we rescale the amplitude by showing that the diagrams for survival time of the inverted pendulum resembles the exact case for $N = 1$. Finally, we find numerically the optimal number of cosines corresponding to the maximal survival probability of the pendulum.

1. Introduction

The inverted pendulum, more precisely its stabilization mechanisms deserve a lot of attention from several correlated areas, including Physics, Mathematics, Biology, (see for example an interesting review [1]). However, the applications goes beyond, including the study of excitation effects in Ocean Structures [2], inverted pendulum robots [3] , a benchmark for testing control algorithms in the context of nonlinear programming [4], and many others.

Induced stability is a solved problem known since 1908 [5], but it was in the 1950s, with Kapiza [6], that this kind of stability was studied for the inverted pendulum system. Experimental results were obtained in the 1960s (see for example [7]) and even nowadays this problem still remains interesting [8].

The problem goes back to India, in the legend of an Indian magician who throws a rope to the sky. Apart from the fact a boy climbs the rope until he goes out of sight, the rope can in principle be kept suspended. A mathematical approach that considers a chain of $N-$segment inverted pendulums suggests an interesting explanation to the mystery of the Indian rope trick [9]. Given that $N \to \infty$ describes a perfectly flexible string, when the sum of lengths of the pendulums is fixed, Hurst showed that this chain is theoretically

controllable even in the limit of infinite N. Actually, Acheson [10] previously showed that such N finite linked inverted pendulums could be stabilized by parametric excitation.

The possible excitations/perturbations which may be capable of stabilizing an inverted pendulum, even for some time, have a large number of details which are not completely understood yet. Therefore, this apparent simple system, has a complexity that can be considered a challenging problem since some important stabilization problems in Engineering, as for instance, the stability of robot arms, the stability of populations in biology [1], or even the stabilization of photons deviation in Cosmology [11] require similar stabilization mechanisms.

An inverted pendulum (show in in Fig. 1) free of external forces, is unstable and the punctual mass m attached to the rigid massless rod will tend to oscillate around to the stable equilibrium position ($\theta = 180^0$), which corresponds to the usual pendulum problem).

In order to keep the pendulum upright, $\cos\theta > 0$, the frictionless hinge that attaches the rod to the suspension point, must vertically accelerated. Let us denote such acceleration by $a(t) = \ddot{z}(t)$, where $z(t)$ is a time-dependent excitation that controls the height of the pendulum suspension point P.

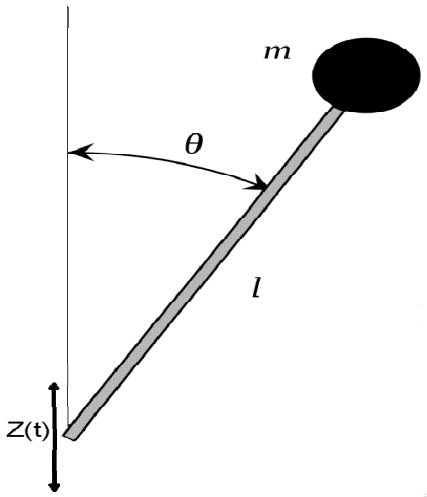

Figure 1: Inverted pendulum under a support excitation $z(t)$.

The Lagrangian of this problem can easily be written as:

$$\mathscr{L}(\theta,\dot{\theta},z,\dot{z}) = \frac{1}{2}ml^2\dot{\theta}^2 + \frac{1}{2}m\dot{z}^2 - ml\dot{z}\dot{\theta}\sin\theta - mgl\cos\theta - mgz(t). \tag{1}$$

It is worth emphasizing that all our results can be directly extended to an equivalent physical pendulum making simple associations. If we additionally consider a external excitation $\phi(t)$ we can derive the motion

equation

$$\ddot{\theta}(t) = \frac{g}{l}\left(1 + \frac{1}{g}\ddot{z}(t)\right)\sin\theta + \phi(t) \tag{2}$$

from the Lagrange equations.

Now, in order to generalize, we write $z(t) = z_{\text{det}}(t) + z_{\text{rand}}(t)$ and $\phi(t) = \phi_{\text{det}}(t) + \phi_{\text{rand}}(t)$ where subscripts "det" and "rand" denote the deterministic and stochastic time-dependent parts of the excitations/perturbations respectively. In this work, we focus our analysis into two important situations: $z_{\text{rand}}(t) = 0$ and $z_{\text{det}}(t) = \sum_{j=1}^{n} A_j \cos(\omega_j t)$, i.e., parametric sinusoidal excitation in the basis and $\phi_{\text{det}}(t) = 0$ and $\phi_{\text{rand}}(t) = N(\mu, \sigma)$ that denotes an external gaussian noise with mean μ and standard deviation σ. The more appropriate choice here is $\mu = 0$, given that we are mainly interested in the parametric stabilization of the inverted pendulum or in what we can call its survival time τ, which means the maximum time the pendulum remains upright or, mathematically, the time up to condition $\cos\theta < 0$ is satisfied. The condition $\mu \neq 0$ leads to a natural biased motion, which is not interesting here. In this work we consider to analyze how the stability condition is broken as function of the external noise dispersion σ.

Several authors [1, 12] have explored the case $N = 1$ using small angles approximation known as the effective potential method. However, even the well known case for one cosine, $N = 1$, deserves, in our opinion, some attention and alternative analysis. Therefore, firstly, we checked the literature based on numerical integration methods in order to verify the validity of previous results in the small oscillations regime and the initial conditions dependence, basically, the initial angle dependence. Particularly we also use these numerical integrations to observe the breaking of the stability region predicted by perturbative analysis and by parametric resonance (see Butikov [12]) when the external noise is turned on (i.e., $\phi \neq 0$). In this case we calculate the pendulum survival probability by considering different time evolutions (i.e, different evolutions meaning different seeds). A detailed connection between $N = 1$ and $N \to \infty$ is also explored when the pendulum amplitude grows linearly with time and is also rescaled with the number of cosines set in the parametric excitation.

In the second part of this work we analyze the superposition of two cosines, $N = 2$, which as far as we are concerned has not been explored yet. This case is interesting since the period of the composition is not always known so that the perturbative analysis is not able to describe the inverted pendulum stability regions correctly. Given such a problem, we analyze numerically the interesting case where the amplitudes are fixed and the frequencies: ω_1 and ω_2 are varied. The analytical results obtained via the effective potential method are compared with numerical simulations. We also analyze the effects of an analysis of the stability

breakdown considering different external noise dispersion σ in the numerical diagrams. Deviations from small oscillations behavior were considered in our analysis.

Finally, for $N > 2$, we look for optimization problems on the stability probability considering an ensemble of frequencies and amplitudes. The most remarkable detail in our analysis is the fact a simple choice for the stability criterion as, $\cos\theta > 0$, overcomes more laborious methods such as Liapunov exponent or other analysis to check stability conditions. So we organized our papers as it follows: in the next section we describe key points for a perturbative analysis extending our formulation for arbitrary N, which is known in literature as effective potential method. In section 3, we briefly show the numerical simulations which were developed. Our main results are presented in section 4. Some discussions and conclusions are finally presented in section 5.

2. Perturbative Analysis

We start our perturbative analysis by chosing the perturbative function $z(t) = \sum_{i=1}^{N} A_i \cos(\omega_i t)$, so that the Eq. 2 becomes

$$\frac{d^2\theta}{dt^2} = \frac{g}{l}\left(1 - \frac{1}{g}\sum_{i=1}^{N} A_i \omega_i^2 \cos(\omega_i t)\right)\sin\theta \tag{3}$$

where we set up $\phi(t) = 0$ for all t.

The last equation can be written in a more elucidative form as

$$\ddot{\theta} = -\frac{\partial U}{\partial \theta} + F(\theta) \tag{4}$$

where $U = \frac{g}{l}\cos\theta$ and $F(\theta) = \frac{\ddot{z}(t)}{l}\sin\theta = -\frac{\sin\theta}{l}\sum_{i=1}^{N} A_i\omega_i^2\cos(\omega_i t)$. The physical interpretation is straightforward here, given that $U(\theta)$ is the gravitational potential, while $F(\theta)$ is an external force due to vibrations at the pendulum suspension point.

We start assuming that the solution of Eq. 4 can be separated into two aditive components [15], [6]:

$$\theta(t) = \overline{\theta}(t) + \xi(t). \tag{5}$$

We are considering that the pendulum motion is composed by a non-perturbated path $\overline{\theta}$ plus a noise ξ composed by multiple frequencies $\{\omega_i\}_{i=1}^{N}$and amplitudes $\{A_i\}_{i=1}^{N}$. Another way to think is that $\overline{\theta}(t)$ has a large amplitude but slow frequency while $\xi(t)$ has small amplitude but fast frequency.

By the Taylor expansions of $U(\theta)$ and $F(\theta)$ around the slow path $\overline{\theta}$, we have:

$$\begin{aligned} \frac{\partial U}{\partial \theta} &= \left.\frac{\partial U}{\partial \theta}\right|_{\theta=\overline{\theta}} + \left.\frac{\partial^2 U}{\partial \theta^2}\right|_{\theta=\overline{\theta}} \xi + \frac{1}{2}\left.\frac{\partial^3 U}{\partial \theta^3}\right|_{\theta=\overline{\theta}} \xi^2 + ... \\ \frac{\partial F}{\partial \theta} &= F(\overline{\theta}) + \left.\frac{\partial F}{\partial \theta}\right|_{\theta=\overline{\theta}} \xi + \left.\frac{\partial^2 F}{\partial \theta^2}\right|_{\theta=\overline{\theta}} \xi^2 + ... \end{aligned} \tag{6}$$

Considering these approximations up to the first order term, we can obtain from Eq. 4 that

$$\ddot{\overline{\theta}} + \ddot{\xi} = -\left.\frac{\partial U}{\partial \theta}\right|_{\theta=\overline{\theta}} - \left.\frac{\partial^2 U}{\partial \theta^2}\right|_{\theta=\overline{\theta}} \xi + F(\overline{\theta}) + \left.\frac{\partial F}{\partial \theta}\right|_{\theta=\overline{\theta}} \xi \tag{7}$$

Now it is crucial to consider the nature of motion to distinguish the important terms in Eq. 7. The only candidates associated with the perturbative effects on the right side of this equation are $-\left.\frac{\partial^2 U}{\partial \theta^2}\right|_{\theta=\overline{\theta}} \xi$, $F(\overline{\theta})$, and $\left.\frac{\partial F}{\partial \theta}\right|_{\theta=\overline{\theta}} \xi$. Therefore, given that the terms $-\left.\frac{\partial^2 U}{\partial \theta^2}\right|_{\theta=\overline{\theta}} \xi$ and $\left.\frac{\partial F}{\partial \theta}\right|_{\theta=\overline{\theta}} \xi$ are small when compared with $F(\overline{\theta})$ we have

$$\ddot{\xi} = F(\overline{\theta}) = -\frac{\sin\overline{\theta}}{l} \sum_{i=1}^{N} A_i \omega_i^2 \cos(\omega_i t) \tag{8}$$

By integrating the equation 8 twice with respect to time we obtain

$$\xi(t) = \frac{\sin\overline{\theta}}{l} \sum_{i=1}^{N} A_i \cos(\omega_i t) + c_1 t + c_0 \tag{9}$$

Here, c_0 and c_1 are arbitrary constants and must be assumed null given that we want ξ to be an oscillatory term, so that it should not increase as a function of time. This is a constraint that can be imposed as initial condition. For a set $\{\omega_i\}_{i=1}^N$ the superposition $\sum_{i=1}^N A_i \cos(\omega_i t)$ does not necessarily results in a periodic function. For this to occur, there must be a period T, such that: $\omega_i T = 2n_i\pi$ and $\omega_j T = 2n_j\pi$, for every pair $i \neq j = 1,...,N$, or simply

$$\omega_i/\omega_j = n_i/n_j, \tag{10}$$

i.e., the ratio between frequencies must be a rational number where n_i and n_j are the smallest possible integers, so that, n_i/n_j is an irreducible fraction.

Let us focus our analysis only in situations where this condition is satisfied. It is important to recall this is a problem for which an analytical solution is not typically known. Therefore, our aim here is to derive a stability criteria given our choices for the perturbative functions. In order to do that, we start taking a time average of Eq. 7 and assuming that the unperturbed part are not significantly altered in a first order

approximation. Within these assumptions we find:

$$\ddot{\overline{\theta}} \approx -\left.\frac{\partial U}{\partial \theta}\right|_{\theta=\overline{\theta}} + \left\langle \left.\frac{\partial F}{\partial \theta}\right|_{\theta=\overline{\theta}} \xi \right\rangle \tag{11}$$

Where $\langle\cdot\rangle$ denotes a time average that results in

$$\begin{aligned}\left\langle \left.\frac{\partial F}{\partial \theta}\right|_{\theta=\overline{\theta}} \xi \right\rangle &= -\frac{\sin\overline{\theta}\cos\overline{\theta}}{l^2}\left(\sum_{i=1}^{N} A_i^2\omega_i^2\left\langle\cos^2(\omega_i t)\right\rangle + \sum_{i\neq j=1}^{N} A_iA_j\omega_i^2\left\langle\cos(\omega_i t)\cos(\omega_j t)\right\rangle\right) \\ &= -\frac{\sin 2\overline{\theta}}{2l^2}\left(\frac{1}{2}\sum_{i=1}^{N} A_i^2\omega_i^2\left(\frac{\sin(2\omega_i T)}{2T\omega_i}+1\right) + \sum_{i\neq j=1}^{N}\frac{A_iA_j\omega_i^2}{T}\left[\frac{\sin\left(\omega_i-\omega_j\right)T}{\left(\omega_i-\omega_j\right)} + \frac{\sin\left(\omega_i+\omega_j\right)T}{\left(\omega_i+\omega_j\right)}\right]\right)\end{aligned} \tag{12}$$

Now, given that $\ddot{\overline{\theta}} = -\frac{\partial U effective}{\partial \overline{\theta}}$, where

$$U_{effective} = \frac{g}{l}\cos\overline{\theta} - \frac{\cos 2\overline{\theta}}{4l^2}\left(\frac{1}{2}\sum_{i=1}^{N} A_i^2\omega_i^2\left(\frac{\sin(2\omega_i T)}{2T\omega_i}+1\right) + \sum_{i\neq j=1}^{N}\frac{A_iA_j\omega_i^2}{T}\left[\frac{\sin(\omega_i-\omega_j)T}{(\omega_i-\omega_j)} + \frac{\sin(\omega_i+\omega_j)T}{(\omega_i+\omega_j)}\right]\right) \tag{13}$$

the stability criteria, $\frac{\partial^2}{\partial\theta^2}U_{effective} > 0$, leads to

$$\left(\frac{1}{2}\sum_{i=1}^{N} A_i^2\omega_i^2\left(\frac{\sin(2\omega_i T)}{2T\omega_i}+1\right) + \sum_{i\neq j=1}^{N}\frac{A_iA_j\omega_i^2}{2T}\left[\frac{\sin(\omega_i-\omega_j)T}{(\omega_i-\omega_j)} + \frac{\sin(\omega_i+\omega_j)T}{(\omega_i+\omega_j)}\right]\right) > gl \tag{14}$$

where without loss of generality, we have assumed $\overline{\theta} = 0$. Here it is important to separate our analysis in three distinct parts: $N = 1$, $N = 2$ and for an arbitrary number of cosines $N > 2$.

2.1. $N = 1$;

This case has been widely studied under different analysis [1], [12]. When $N = 1$, the result from Eq. 14 is simply:

$$A^2 > A^2_{\min} = \frac{2gl}{\omega^2} \tag{15}$$

valid in the small oscillations regime. As we will show in section 4, this stability condition is not enough to cover all of the stability regions in a diagram $\omega \times A$. Unfortunately, it represents only one part of the history since there is a upper bound for the amplitude that can be observed by numerical simulations.

2.2. $N = 2$;

This is the simplest case where the perturbative analysis cannot be rigorously applied to all possible situations since the periodicity of the superposition $A_1\cos(\omega_1 t) + A_2\cos(\omega_2 t)$ depends on certain restrictions. As it will be shown in section 4, this case becomes particularly interesting when the amplitudes are

set equal, that is, $A_1 = A_2 = A$. Then, we find the condition:

$$\left(\omega_1^2 \frac{\sin(2\omega_1 T)}{2T\omega_1} + \omega_2^2 \frac{\sin(2\omega_2 T)}{2T\omega_2} + \frac{2}{T}\left(\omega_1^2 + \omega_2^2\right)\left[\frac{\sin(\omega_1 - \omega_2)T}{(\omega_1 - \omega_2)} + \frac{\sin(\omega_1 + \omega_2)T}{(\omega_1 + \omega_2)} + \frac{T}{2}\right]\right) > \frac{2gl}{A^2}. \tag{16}$$

If besides having equal amplitudes we also set $\omega_1 \approx \omega_2$, then we get from Eq. 16 that the condition $A^2 > A_{\min}^2/4$, certainly fulfills the requirements for stabilization given a frequency ω. However, for certain ranges of frequencies, stabilization can be attained for amplitudes A that are slightly smaller.

2.3. $N > 2$;

For an important and trivial case is when the frequencies are close enough $\omega_1 \approx \omega_2 \approx ... \approx \omega_N \approx \frac{2\pi}{T}$. This leads to $\sin(\omega_i - \omega_j)T \approx (\omega_i - \omega_j)T \approx 0$. Moreover, we also have $\sin 2\omega_i T \approx 0$ for all $i = 1, ..., N$. In this case we have a simplified condition: $\sum_{i=1}^N A_i^2 \omega_i^2 > 2gl$. For N asymptotically large and for a set of frequencies such that the $\{\omega_i\}_{i=1}^N$ are equally distributed according to some probability density function $f(\omega)$ we can replace: $\sum_{i=1}^N A_i \cos(\omega_i t) \to \overline{\cos(\omega t)} \sum_{i=1}^N A_i$, where $\overline{\cos(\omega t)} = \int_0^\infty \cos(\omega t) f(\omega) d\omega$ denotes the ensemble average. A standard case, could be an uniform distribution for the frequencies choosen in an interval $[\omega_{\min}, \omega_{\max}]$, so that:

$$\overline{\cos(\omega t)} = \frac{\sin(\omega_{\max} t) - \sin(\omega_{\min} t)}{t\ (\omega_{\max} - \omega_{\min})} \tag{17}$$

Here an interesting choice is to make $A_i = A(t)$, which leads to $\sum_{i=1}^N A_i = NA(t)$. So we have $\overline{z(t)} = NA(t)\frac{\sin(\omega_{\max} t) - \sin(\omega_{\min} t)}{t\ (\omega_{\max} - \omega_{\min})}$. In this case if we denote $f(t|\omega) = \frac{A(t)}{t}\sin(\omega t)$, we have

$$\begin{aligned} \frac{d^2 f}{dt^2} &= \ddot{A}(t)\sin\omega t + 2\dot{A}(t)\left(\frac{\omega\cos\omega t}{t} - \frac{\sin\omega t}{t^2}\right) + \\ &\quad A(t)\left(\frac{2\sin\omega t}{t^3} - \frac{2\omega\cos\omega t}{t^2} - \frac{\omega^2\sin\omega t}{t}\right). \end{aligned} \tag{18}$$

If $A(t)$ does not depend on time, then $f(t|\omega) \overset{t\to\infty}{\to} 0$. There is no parametric excitation and the pendulum is asymptotically unstable as $t \to \infty$. An alternative is to consider a linear dependence as $A(t) = Ct$. In this case, we have $\frac{d^2 f}{dt^2} = -CN\omega^2 \sin\omega t + O(\frac{1}{t})$, and reescaling $CN = a\omega_{\max}$:

$$\overline{\ddot{z}(t)} = \frac{-a\ \omega_{\max}^3}{\omega_{\max} - \omega_{\min}}\sin(\omega_{\max} t) + \frac{a\ \omega_{\min}^2\ \omega_{\max}}{\omega_{\max} - \omega_{\min}}\sin(\omega_{\min} t) \tag{19}$$

For the sake of the simplicity, let us consider $\omega_{\min} = 0$, so that

$$\overline{\ddot{z}(t)} = -a\omega_{\max}^2 \sin(\omega_{\max} t). \tag{20}$$

It is very surprising here that we recover the stability condition obtained for the case $N = 1$, by simply replacing ω^2 by $\omega_{\max}^2$ in eq. 15, that is:

$$a^2 > \frac{2gl}{\omega_{\max}^2} \tag{21}$$

At this point, it is worth emphasizing that the time-dependent amplitude can start contributing positively for stabilization by extending the length of time in which $\cos\theta > 0$. However this favorable effect soon becomes undesirable since this monotonically increasing amplitude will dominates the scenario leading to a loss of stability. Therefore, the real important question to be made here is whether the system is capable of keeping the memory of stabilization according to eq. 21 under this amplitude normalization procedure. We will show numerically in section 4 that such condition is preserved. However, to show that the condition 21 is held, we have to analyze the survival times instead of the survival probabilities.

3. Numerical Simulations

In this work, after a detailed observations in the numerical simulations, we defined a simple stability criterion definition:

Definition: Given a inverted pendulum governed by eq. 2 we say that this pendulum is stable during a window of time up to time $t_{\max}$ if given an initial angle $-\pi/2 < \theta_0 < \pi/2$, all θ_t, $t = 1,2,...t_{\max}$, obtained by integration of the motion equations via Runge-Kutta method of fourth order satisfy:

$$\cos\theta_t > 0 \tag{22}$$

This simple stability criterion leads to algorithms that although relatively simple they can describe the stability mapping in the inverted pendulum problem. Basically, we consider 4 procedures in our numerical simulations. All of them are based on a main algorithm (see Table 1) which describes a generic Runge-Kutta procedure for the inverted pendulum problem considering as input:

a) **Parametric excitation**: determined by N amplitudes: $A[N] : (A_1,...,A_N)$ and N frequencies $\omega[N] : (\omega_1,...,\omega_N)$;

b) **Maximal number o iterations in the Rung Kutta procedure**: N_{iter} – This number can or cannot be attained depending on stability condition given by eq. 22;

c) **Time interval for Runge Kutta iteration**: Δt

d) **Pendulum Characteristics**: g – gravity acelaration, l – pendulum lengh. In this paper was considered $g = 9.81$ m/s^2 and $l = 1.2$ m, which corresponds to a standardized broomstick lenght.

	Main_Runge_Kutta_Routine$(N, N_{iter}, \Delta t, g, l, \omega[N], A^*[N], \nu, f[N_{iter}], \theta_0, \dot{\theta}_0, i, \theta)$
1	**input**:$N, N_{iter}, \Delta t, g, l, \omega[N], A^*[N], \nu, f[N_{iter}], \theta_0, \dot{\theta}_0$
2	**output**:i, θ
3	**Initilizations**: $\theta = \theta_0$; $\dot{\theta} = \dot{\theta}_0$; $i = 0$;
4	**While** $[(\cos(\theta) > 0).\text{or.}(i < N_{iter})]$ **do**
5	$i := i + 1$; $t := i\Delta t$;
6	$\theta_1 := \theta$; $\dot{\theta}_1 = \dot{\theta}$
7	**For** $j = 1, ..., N$
8	$A_j = \frac{(1-\nu)\ A_j^*}{N}[\frac{2}{\omega_j} + t \cdot \tan(\omega_j t)] + \nu A_j^*$
9	**Endfor**
10	$a_1 = \omega_0^2[1 - \sum_{j=1}^{N} \frac{A_j \omega_j^2}{g} \cos(\omega_i t)] \sin\theta_1 + f(i)$
11	$\theta_2 := \theta_1 + \frac{1}{2}\dot{\theta}_1 \Delta t$
12	$\dot{\theta}_2 := \dot{\theta}_1 + \frac{1}{2} a_1 \Delta t$
13	$a_2 = \omega_0^2[1 - \sum_{j=1}^{N} \frac{A_j \omega_j^2}{g} \cos(\omega_i (t + \frac{\Delta t}{2}))] \sin\theta_2 + f(i)$
14	$\theta_3 = \theta_1 + \frac{1}{2}\dot{\theta}_2 \Delta t$
15	$\dot{\theta}_3 = \dot{\theta}_1 + \frac{1}{2} a_2 \Delta t$
16	$a_3 = \omega_0^2[1 - \sum_{j=1}^{N} \frac{A_j \omega_j^2}{g} \cos(\omega_i (t + \frac{\Delta t}{2}))] \sin\theta_3 + f(i)$
17	$\theta_4 = \theta_1 + \dot{\theta}_3 \Delta t$
18	$\dot{\theta}_4 = \dot{\theta}_1 + a_3 \Delta t$
19	$a_4 = \omega_0^2[1 - \sum_{j=1}^{N} \frac{A_j \omega_j^2}{g} \cos(\omega_i * (t + \Delta t))] \sin\theta_4 + f(i)$
20	$\theta = \theta + \frac{\Delta t}{6}(\dot{\theta}_1 + 2(\dot{\theta}_2 + \dot{\theta}_3) + \dot{\theta}_4)$
21	$\dot{\theta} = \dot{\theta} + \frac{\Delta t}{6}(a_1 + 2(a_2 + a_3) + a_4)$
22	**EndWhile**
23	**Return** i, θ
24	**End Main_Runge_Kutta_Routine**

Table 1: Main Procedure: performs the Runge Kutta iterations for the problem considering the all possible ingredients: excitation parameters and external noise

e) **Reescaling parameter**: ν– If $\nu = 0$, the amplitudes are rescaled as $A_i \to t\frac{A_i}{N}$, elsewhere ($\nu = 1$) they remain unchanged.

f) **External noise vector**: A string with N_{iter} random Gaussian variables with standard deviation σ and mean zero.

g) **Initial conditions**: θ_0 and $\dot{\theta}_0$– Without lost of generality we consider $\dot{\theta}_0 = 0$, i.e., the pendulum starts from rest.

As **output** of this generic procedure we have:

a) **Survival time**: i – Time (integer number) for which the pendulum remains stable.

b) **Final angle**: θ –If $\cos\theta > 0$, so necessarily $i = N_{iter}$, elsewhere the pendulum cannot be maintained stable until the maximal time considered as stop criteria (N_{iter})

Now, we will present all procedures used in our work by reporting specifically each one of them showing pseudo-codes.

3.1. Procedure 1

For $N = 1$, we change A and ω in the respective ranges $[A_{\min}, A_{\max}]$ and $[\omega_{\min}, \omega_{\max}]$. For $\sigma = 0$ we look for each pair (ω, A) if the pendulum stabilizes or not by calling the main procedure (sub routine): **Main_Runge_Kutta_Routine**. For $\sigma \neq 0$ we run N_{run} times the program for different seeds and we calculate the survival probability of pendulum, i.e., $p_{survival} = n_{survival}/N_{run}$, where $n_{survival}$ is the number of times that system stabilizes. In our procedure 2 $p_{survival}$ is denoted by $prob_{k,m}$ since it is associated to pair (ω, A), parametrized as $\omega = \omega_{\min} + k\Delta\omega$ and $A = A_{\min} + m\Delta A$, where $k = 1, ..., N_1$ and $m = 1, ..., N_2$ (see again the pseudo-code– described in Table 2).

Here (and in the other procedures) $H(\theta)$ is the Heaviside function in the cosine argument:

$$H(\theta) = \begin{cases} 1 & \text{if} \quad \cos\theta > 0 \\ \\ 0 & \text{if} \quad \cos\theta \leq 0 \end{cases}$$

Similarly, $iaver_{k,m}$ corresponds to survival time average over N_{run} repetitions, which is interesting only when $\sigma \neq 0$. It is important to notice that $p_{survival}$ is either 0 or 1 when $\sigma = 0$ (in this case we make $n_{run} = 1$ necessarily). Here $idum$ is the seed of uniform random variables generator: rand$[idum]$. In this paper we used the generator **ran2** of numerical recipes [14] as well as gasdev(rand$[idum]$) that has as input rand$[idum]$. This last routine is the Gaussian random numbers generator according to Box-Muller method which also is described in [14].

3.2. Procedure 2

For $N = 2$, we fix $A_1 = A_2 = A$ and we pick up ω_1 and ω_2 by chance. When $\sigma = 0$, for each pair (ω_1, ω_2) spanned in the invervals $[\omega_{\min}^{(1)}, \omega_{\max}^{(1)}]$ and $[\omega_{\min}^{(2)}, \omega_{\max}^{(2)}]$ respectively, we look whether the pendulum stabilizes or not. For $\sigma \neq 0$ we run N_{run} times the program for different seeds and we estimate the pendulum survival probability, i.e., $p_{survival} = n_{survival}/N_{run}$, as shown in procedure 1. This procedure can be observed in pseudo-code described in table 3.

3.3. Procedure 3

Here we analyze the problem with arbitrary $N > 2$. More precisely, we analyze the effects for $N \to \infty$ by a amplitude renormalization such that $A(t) \to \frac{At}{N}$. It is worth notice that in doing so, we realize this is a similar problem to $N = 1$, as previously described in section 2. For each selected A which varies in the range

Procedure 1 : Diagram_$N=1$

Input: $A_{\min}, A_{\max}, l, g, \omega_{\min}, \omega_{\max}, \sigma, \Delta\omega, \Delta A, \Delta t, N_{iter}, idum, N_{run}$

Parameters: $N=1, \nu=1$

$\cdot\ N_1 = (\omega_{\max} - \omega_{\min})/\Delta\omega;$

$\cdot\ N_2 = (A_{\max} - A_{\min})/\Delta A;$

For $i_{run} = 1, N_{run}$

  For $ic = 1, ..., N_{iter}$

    $f_{ic} = \sigma \cdot \text{gasdev}(\text{rand}[idum])$

  EndFor

For $k = 1, N_1$

 For $m = 1, N_2$

  $\omega_1 = \omega_{\min} + k\Delta\omega$

  $A_1^* = A_{\min} + m\Delta A$

Call Main_Runge_Kutta_Routine$(N=1, N_{iter}, \Delta t, g, l, \omega[N], A^*[N], \nu, f[N_{iter}], \theta_0, \dot{\theta}_0, i, \theta)$

  $iaver_{k,m} = iaver_{k,m} + i/N_{run}$

  $prob_{k,m} = prob_{k,m} + H(\theta)/N_{run}$

 EndFor

EndFor

EndFor

For $k = 1, N_1$

 For $m = 1, N_2$

  $freq = \omega_{\min} + k\Delta\omega$

  $Ampl = A_{\min} + m\Delta A$

  Print $freq, Ampl, iaver_{k,m}, prob_{k,m}$

 EndFor

EndFor

End Procedure

Table 2: This procedure is used to build data for a diagram of survival probability for each pair (ω, A) considering the parametric excitation (oscillation at the suspention) with um cossine ($N=1$) and an additive (white) noise

Procedure 2: Diagram_$N=2$

Input: $A, l, g, \omega_{\min}^{(1)}, \omega_{\max}^{(1)}, \omega_{\min}^{(2)}, \omega_{\min}^{(2)}, \sigma, \Delta\omega, \Delta t, N_{iter}, idum, N_{run}$
Parameters: $N=2, A_1^* = A; A_2^* = A; \nu = 1$
$\cdot\ N_1 = (\omega_{\max}^{(1)} - \omega_{\min}^{(1)})/\Delta\omega;$
$\cdot\ N_2 = (\omega_{\max}^{(2)} - \omega_{\min}^{(2)})/\Delta\omega;$
For $i_{run} = 1, N_{run}$
  For $ic = 1, ..., N_{iter}$
    $f_{ic} = \sigma \cdot \text{gasdev}(\text{rand}[idum])$
  EndFor
For $k = 1, N_1$
 For $m = 1, N_2$
  $\omega_1 = \omega_{\min}^{(1)} + k\Delta\omega$
  $\omega_2 = \omega_{\min}^{(2)} + m\Delta\omega$
Call Main_Sub_Routine$(N, N_{iter}, \Delta t, g, l, \omega[N], A^*[N], \nu, f[N_{iter}], \theta_0, \dot{\theta}_0, i, \theta)$
  $iaver_{k,m} = iaver_{k,m} + i/N_{run}$
  $prob_{k,m} = prob_{k,m} + H(\theta)/N_{run}$
 EndFor
EndFor
EndFor
For $k = 1, N_1$
 For $m = 1, N_2$
  $freq1 = \omega_{\min}^{(1)} + k\Delta\omega$
  $freq2 = \omega_{\min}^{(2)} + m\Delta\omega$
  Print $freq1, freq2, iaver_{k,m}, prob_{k,m}$
 EndFor
EndFor
End_Procedure

Table 3: This procedure produces data for the diagram of survival probability for each pair (ω_1, ω_2) considering the parametric excitation (oscillation at the suspention) with a superposition of two cosines ($N=2$) and an additive (white) noise. Here the amplitudes are $A_1 = A_2 = A$, which is also a input of the algorithm

$[A_{\min}, A_{\max}]$ according to lag ΔA, we attribute $A_1 = A_2 = ... = A_N = A$ and we choose N random uniform variables ω_1, ω_2, ..., ω_N in the interval $[0, \omega_{\max}]$. The value maximum frequency to be drawn $\omega_{\max}$, assumes values in the interval $[0, \omega_{\max}^{\sup}]$ varying according to a shift $\Delta\omega$. So this procedure calls the main sub-routine Table: 1 with $\nu = 0$ (which makes the rescaling). Here N is an arbitrary input, since we study the effects of N in the asymptotic limit $N \to \infty$.

In this case, the algorithm with this rescaling, computes the survival time (the time up destabilization) in order to compare with stabilization diagrams with $N = 1$. This procedure is summarized according to pseudo-code described in table 4.

3.4. Procedure 4

Finally, we look for an optimum number of cosines N in the stabilization of the inverted pendulum. For arbitrary N, we also perform an optimization algorithm. Given the frequencies ω_1, ω_2, ..., ω_N and A_1, A_2, ..., A_N randomly chosen uniformily in the respective intervals $[\omega_{\min}, \omega_{\max}]$ and $[A_{\min}, A_{\max}]$, we search for the number N that maximizes the stabilization probability. Therefore the algorithm run N_{run} different formulas with parametric excitation $z(t) = \sum_{i=1}^{N} A_i \cos(\omega_i t)$ and call the main sub-routine that solves the Runge-Kutta for each set: $\{(A_1, \omega_1), ..., (A_N, \omega_N)\}$. From that, we calculate the $p_{survival} = n_{survival}/N_{run}$. The procedure also computes the average time survival for completeness, but it is not used in this work.

4. Results

First of all we start looking at the phase diagrams for $N = 1$, $\frac{d^2\theta}{dt^2} = \frac{g}{l}\left(1 - \frac{1}{g}A\omega^2\cos(\omega t)\right)\sin\theta + \xi(t)$, in Fig. 2. Here we will show that our simple stability criteria $\cos\theta(t) > 0$ is in accordance with results obtained from literature (see for example [1][12])) which are based on perturbative analysis as shown in section 2. Based on our stability criteria we initially integrate the equations according to algorithms described in section 3, in order to check the main results and to verify some important points not explored in literature yet. The results for $N = 1$ are also important to give insights to the other cases ($N \geq 2$).

In Fig. 2 we show results of simulations starting from a small angle, $\theta_0 = 0.018$, and using frequency $\omega = 15$ rad/s and $A = 0.17$ m. In our simulations, $l = 1.2$ m and $g = 9.81$ m/s^{2}which brings in our imagination the typical situation of a child trying to stabilize a broomstick on its hand. Other dimensions deserve discussion for large N which will be considered in other contribution [18].

In all the following results, we have used $t_{\max} = 10^6$ iterations and $\varepsilon = \Delta t = 10^{-5}$. These parameter values were settled after the observation that for $t \geq t_{\max}$ and $\varepsilon' < \varepsilon$ no significant variations were detected. Fig. (2 a) and (2 b) show the time evolution and the corresponding phase diagram respectively. In this

Procedure 3 : Reescaling

Input: $A_{\min}, A_{\max}, N, l, g, \omega_{\max}^{(\sup)}, \Delta\omega, \Delta A, \Delta t, N_{iter}, idum, N_{run}$
Parameters: $\nu = 0$
$\cdot\ N_2 = (A_{\max} - A_{\min})/\Delta A;$
$\cdot\ N_1 = \omega_{\max}^{(\sup)}/\Delta\omega$
For $i_{run} = 1, N_{run}$
For $k = 1, N_1$
$\omega_{\max} = k\Delta\omega$
For $i = 1, N$
$\omega_i =$rand$[idum] \cdot \omega_{\max}$
End For
For $m = 1, N_2$
$Aux = A_{\min} + m\Delta A$
For $i = 1, N$
$A_i^* = Aux \cdot \omega_{\max}$
EndFor
Call Main_Sub_Routine$(N, N_{iter}, \Delta t, g, l, \omega[N], A^*[N], \nu, f[N_{iter}], \theta_0, \dot{\theta}_0, i, \theta)$
$iaver_{k,m} = iaver_{k,m} + i/N_{run}$
$prob_{k,m} = prob_{k,m} + H(\theta)/N_{run}$
EndFor
EndFor
EndFor
For $k = 1, N_1$
For $m = 1, N_2$
$freq = k\Delta\omega$
$Ampl = A_{\min} + m\Delta A$
Print $freq, Ampl, iaver_{k,m}, prob_{k,m}$
EndFor
EndFor
End Procedure

Table 4: Giving a superposition of N cosines exciting the basis of pendulum, this procedure calculate the average survival time of pendulum calling the main subroutine when the amplitudes are rescaled. The plots must recover in some instance, the plots the standard plots for $N = 1$

Procedure 4 : Optimization

Input: $A_{\min}, A_{\max}, N_{\max}, l, g, \omega_{\min}, \omega_{\max}, \Delta\omega, \Delta A, \Delta t, N_{iter}, idum1, idum2, N_{run}$
Parameters: $\nu = 1$
For $N = 1, N_{\max}$
  For $i_{run} = 1, N_{run}$
    For $i = 1, N$
      $\omega_i = \omega_{\min} + \text{rand}[idum1] \cdot (\omega_{\max} - \omega_{\min})$
      $A_i = A_{\min} + \text{rand}[idum2] \cdot (A_{\max} - A_{\min})$
    End For
    Call Main_Sub_Routine$(N, N_{iter}, \Delta t, g, l, \omega[N], A^*[N], \nu, f[N_{iter}], \theta_0, \dot{\theta}_0, i, \theta)$
    $iaver_N = iaver_N + i/N_{run}$
    $prob_N = prob_N + H(\theta)/N_{run}$
  EndFor
EndFor
For $N = 1, N_{\max}$
  Print $N, iaver_N, prob_N$
EndFor
End Procedure

Table 5: Procedure that determines the N that maximizes the probability of stabilization considering different ensemble of formulas

simulation $\xi(t) = 0$, so that there is not any stochastic noise. The corresponding plots to (2 a) and (2 b) when we use the small angle approximation $\sin\theta \approx \theta$ (known as Mathieu equation [19])

$$\ddot{\theta} - \frac{g}{l}\left(1 - \frac{1}{g}A\omega^2\cos(\omega t)\right)\theta = 0 \tag{23}$$

are observed in (2 c) and (2 d) respectively.

The fact that this figure illustrates a case where the initial condition leads to a non-stable outcome is not relevant here, since they do not satisfy eq. 15. However what call ones attention is the fact that small initial angle leads to a different different divergence for $\theta(t)$ for large times (instability) whether the one replaces $\sin\theta$ by θ or not. The plot (2 c) is in mono-log scale since there is a exponential divergence (straight line in this scale) which is more pronounced than in (2 a). Such aspect although seems very simple is simply discarded by some authors in literature. The very different phase diagrams (b) and (d) obtained for these different regimes shows even more our thesis about this topic.

In the results shown in Fig. 2, we consider a larger amplitude $A = 0.50$ m. Now, that Eq. 15 is satisfied, we can see a periodic behavior for θ and $\dot{\theta}$ as function of time in Fig. (3 a) and now beautiful Lissajous plot in the phase space shown in Fig. (3 b).

Differently from the Fig. 2 the plots (3c) and (3d) corresponding to small oscillations regime are here

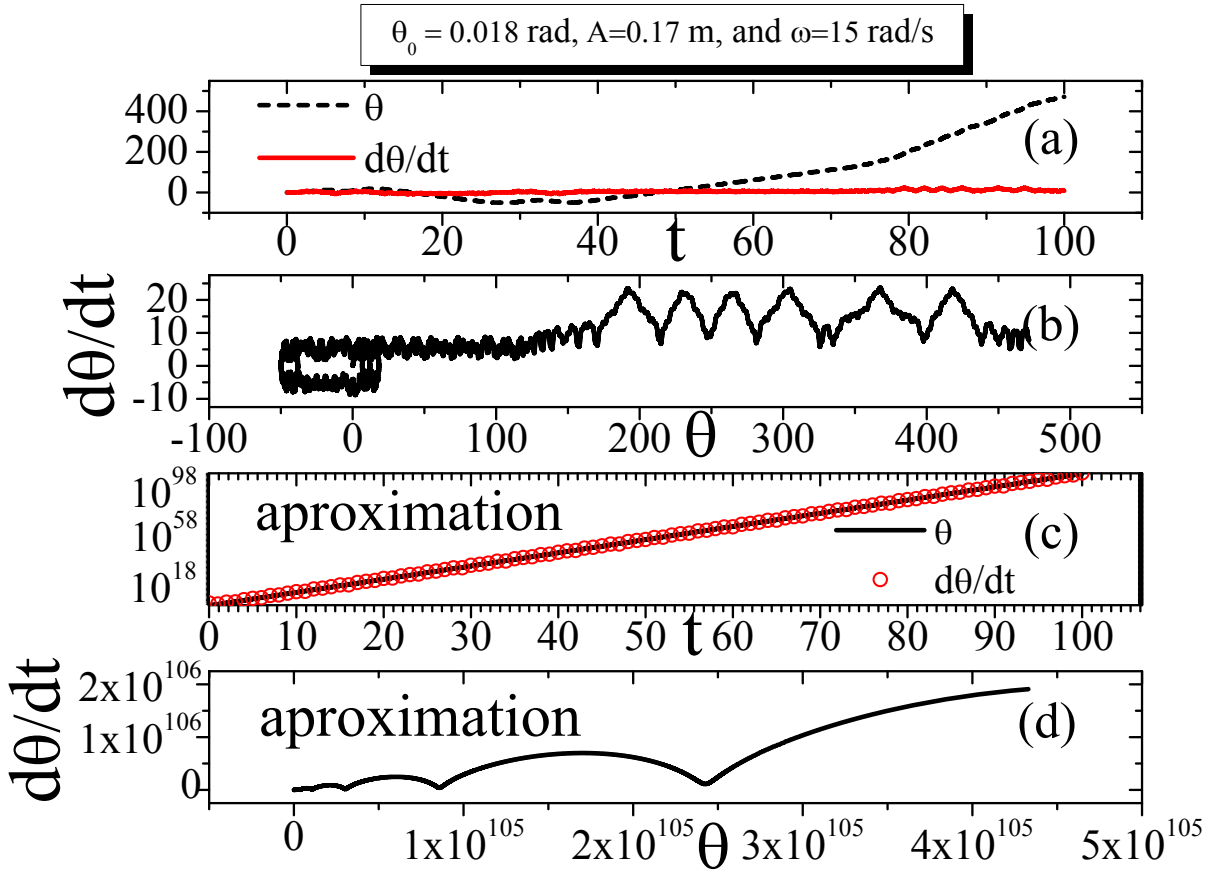

Figure 2: Results for time evolving and phase diagram considering $\theta_0 = 0.018$ rad, $\omega = 15$ rad/s and $A = 0.17$ m. (a) Time evolving θ and $\dot{\theta}$. (b) Corresponding phase diagram $\dot{\theta} \times \theta$ (c) The corresponding Fig. (a) in small oscillations approximation $\sin\theta \approx \theta$– Mathieu equation. (d) Corresponding phase diagram in this approximation.

omitted since there is no significant difference in the simulations.

In order to study initial angles' effects, we analyze the phase diagram $\omega \times A$ obtained via numerical simulations. The diagrams are shown in Fig. 4, and which they correspond to results from Procedure 1: Table 2 (in this case we make $N_{run} = 1$). It is important to consider that Eq. 15 determines a lower bound for amplitude: $A_{\min} = \frac{\sqrt{2gl}}{\omega}$. On the other hand, when the amplitude A is increased beyond a certain critical value $A_{\max}$, the pendulum loses its stability again [16, 17, 12] and its evolution cannot be described by effective potential method (perturbative analysis). It is shown in Butikov [12], based in simulation (heuristic) arguments, shows that the solution over the upper boundary of stability has a simple spectral decomposition in only two frequencies: $\omega/2$ and $3\omega/2$, such that $\theta(t) = A_1\cos(\omega t/2) + A_3\cos(3\omega t/2)$. By using this hypotesis and substituting this solution in Eq. 23 (instead of the exact equation Eq. 2) we

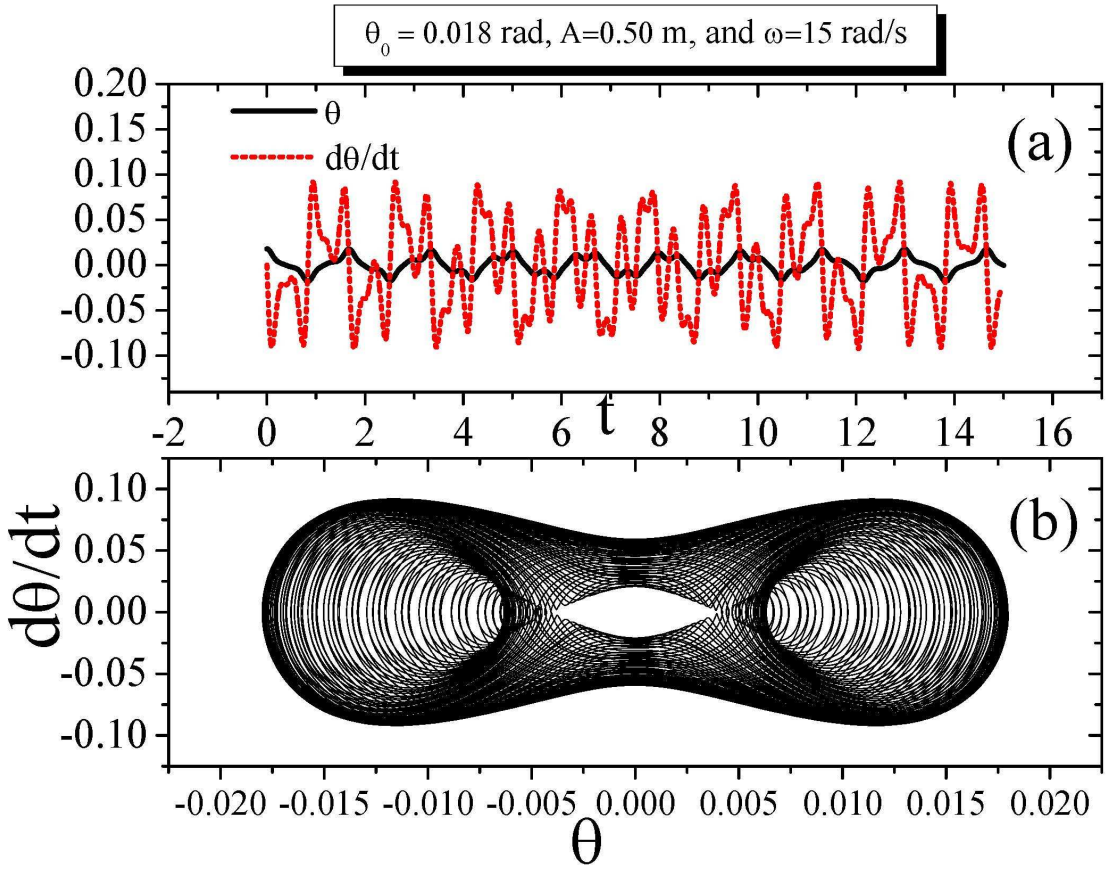

Figure 3: Results for time evolving and phase diagram considering $\theta_0 = 0.018$ rad, $\omega = 15$ rad/s and $A = 0.50$ m. (a) Time evolving θ and $\dot{\theta}$. (b) Corresponding phase diagram $\dot{\theta} \times \theta$.

have:

$$A < A_{\max} = \frac{l}{4}\left[\sqrt{117 + 232(\omega_0/\omega)^2 + 80(\omega_0/\omega)^4} - 9 - 4(\omega_0/\omega)^2\right] \tag{24}$$

The solid and dashed black curves show respectively the lower (Eq. 15) and upper (Eq. 24) stability domain boundaries. First, we see that the blue region is being destroyed as the initial angle increases, but we need to pay attention to the way it happens. We can observe an interesting effect: there is a set of conditions in the primary stability region that loses its stability so that the region becomes fragmented, while another set above the upper limit becomes stable. The upper limit, established in [12], is really restricted to small angles showing that is based in the approximated equation, which again indicates the importance of the numerical work here. However the lower bound obtained by the effective potential is absolutely respected (not invaded by stability region).

In Fig. 5 we show the effects of an additive random noise. We are interested in seeing how the stability

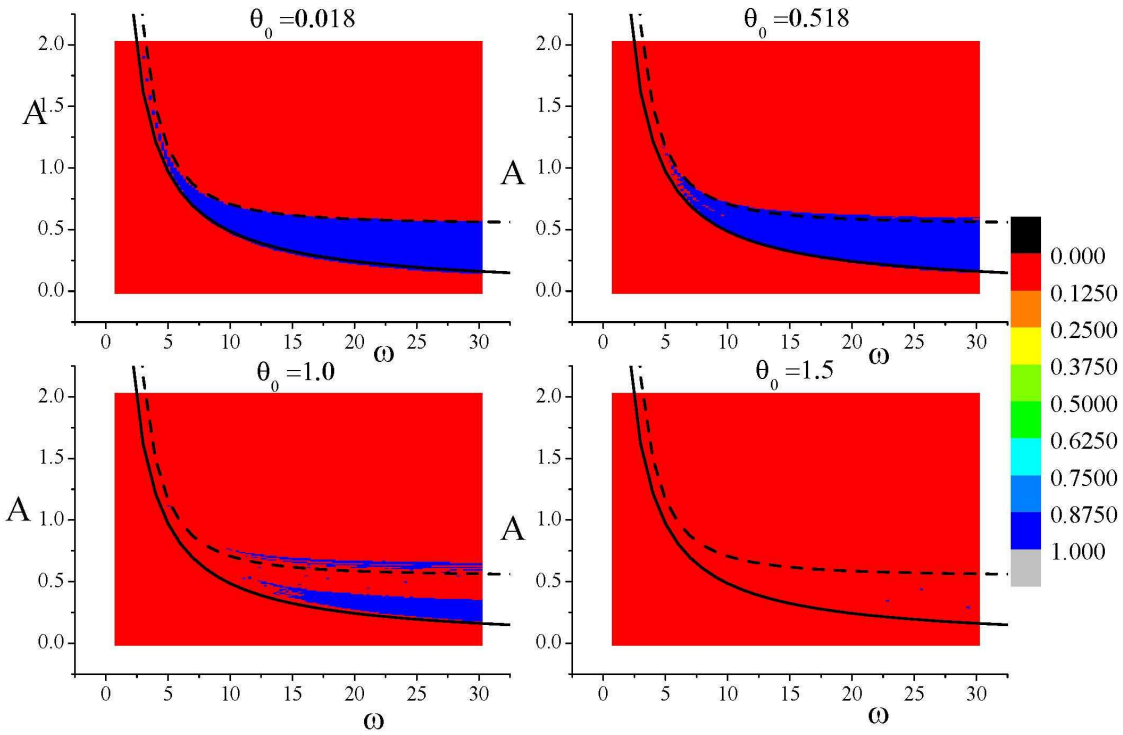

Figure 4: Initial angle effects on the diagram phases $\omega \times A$. The upper (solid) and lower (dashed) curves correspond respectively to the limits established by Eqs. 15 and 24.

diagram is degraded according to the increase of noise variance. Each plot corresponds to a different variance (σ^2). So, we run procedure I (see table 2) with N_{run} = 50 times with different seeds and we calculate an interesting statistical quantity developed in the context of survival analysis, which has a wide application in the dynamical systems framework, when we analyze the escape from an unstable fixed point (see for example the [13]), known as survival probability and here defined by:

$$p_{survival} = \frac{n_{survival}}{N_{run}} \tag{25}$$

where $n_{survival}$ is the number of times in which our pendulum stabilizes.

The color scale are graduated according to the $p_{survival}$-values that were obtained.

Now we focus our analysis in the case $N = 2$, where we make $A_1 = A_2 = A$ according to Procedure II: Table 3. The results show a rich structure as we can see in Fig 6. We illustrate two different initial angles

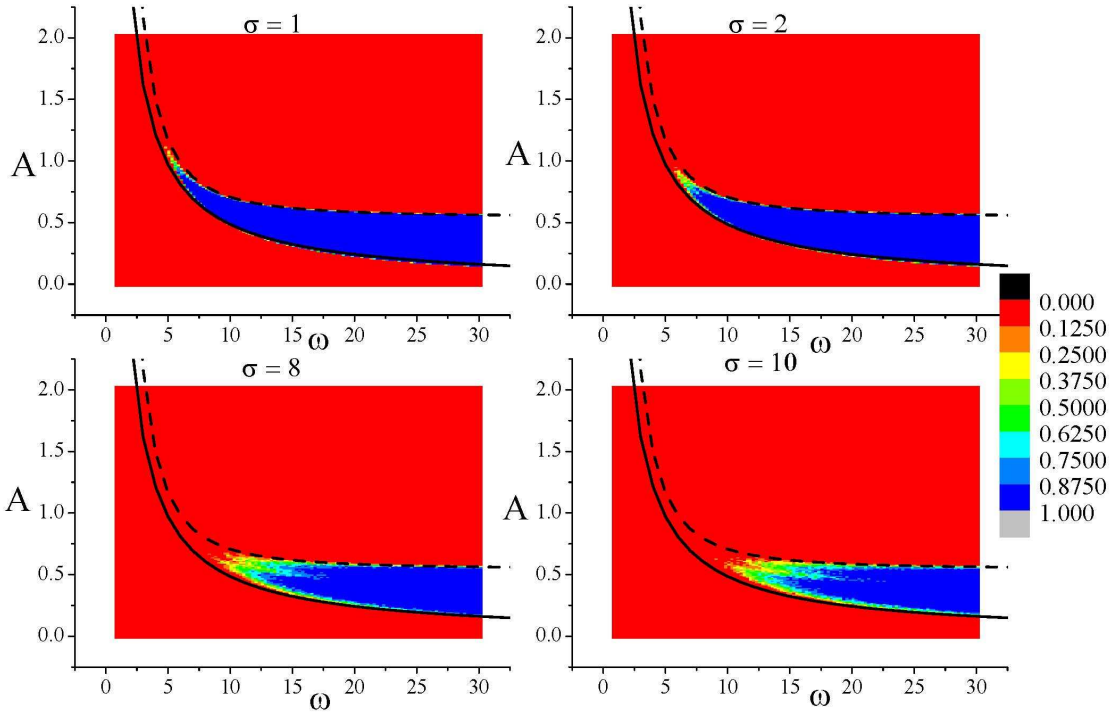

Figure 5: External (additive) stochastic noise effects on the diagram phases $\omega \times A$. The different plots correspond to different standard deviations (σ) of noise $\phi(t)$.

for $A = 0.17$ recalling that red stands for unstable regions, while blue denotes stabilization. Comparing the figures on the left with the ones on the right (small angles approximation) we can see that it is important to consider $\sin\theta$ and not to make the approximation $\sin\theta \approx \theta$, even for very small angles $\theta_0 = 0.018$ rad $\approx 1^o$. We can observe a less restrictive condition $\omega_1^2 + \omega_2^2 \leq \frac{2gl}{A^2}$ (a quarter circle, plotted in all figures), which corresponds a condition that $\omega_1 \approx \omega_2 = \omega$. Exactly in diagonal the condition goes to $\omega^2 \leq \frac{gl}{A^2}$, which asserts the diagonal line penetrating the 1/4-circle. But, we have more stability regions inside this semi-circle which depend on the proximity of the diagonal. However for $\theta_0 = 0.518$ the system recover the restriction and all quarter of circle is completed but not for the small angles approximation.

However, even more interesting, one should note that it is not always the case that ω_1 and ω_2, both large, will lead to stabilization. We see branches of unstable regions that remind us of Arnold tongues [20] breaking the stability sea, specially around diagonal the diagonal. It is not our task in this paper to describe

the properties of these unstable branches, but they are certainly very rich sets of fractal dimensions [21].

This fractal structure set is deeply modified when $\theta_0 = 0.518$ but only when the numerical solution is not performed in small angle approximations.

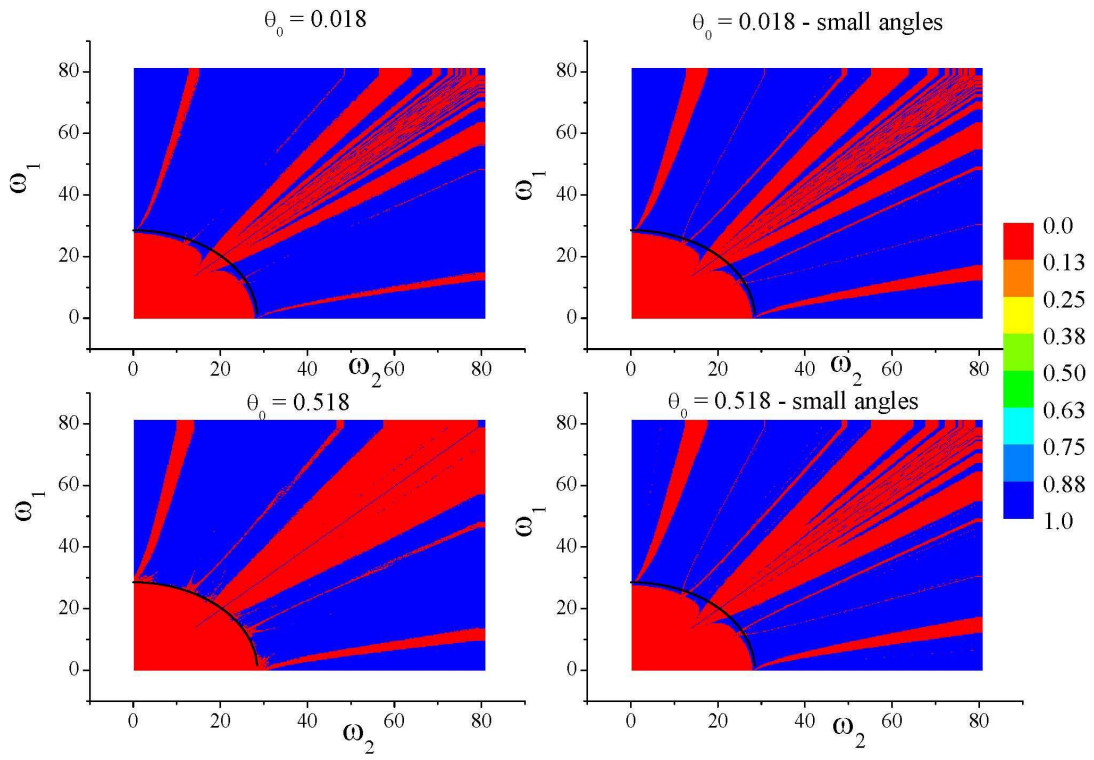

Figure 6: Initial angle effects $N = 2$. We used $A = 0.17$.

In the Fig. 7 we show the same simulation of Fig. 6 for a larger amplitude $A = 0.34$. Now we have a larger instability region. Details of the complexity of unstable branches look less pronounced on the scale of this figure, but it does not mean that they are not there.

In Fig. 8 we also analyze the effect of noise on the stabilization diagram similar to the case shown in Fig. 5 for $N = 1$. Again, $N_{run} = 50$ and we observe only one case one case ($\sigma = 6$), since the behavior is similar to the case $N = 1$, that is, the degraded region enlarges as σ enlarges. The case $A = 0.34$ m is less sensitive to degradation than $A = 0.17$ m.

At this point it is important to analyse the results from the perspective of the effective potential method according to Eq. 16. Recall that we are dealing with the case of $N = 2$ and equal amplitudes so that Eq. 16

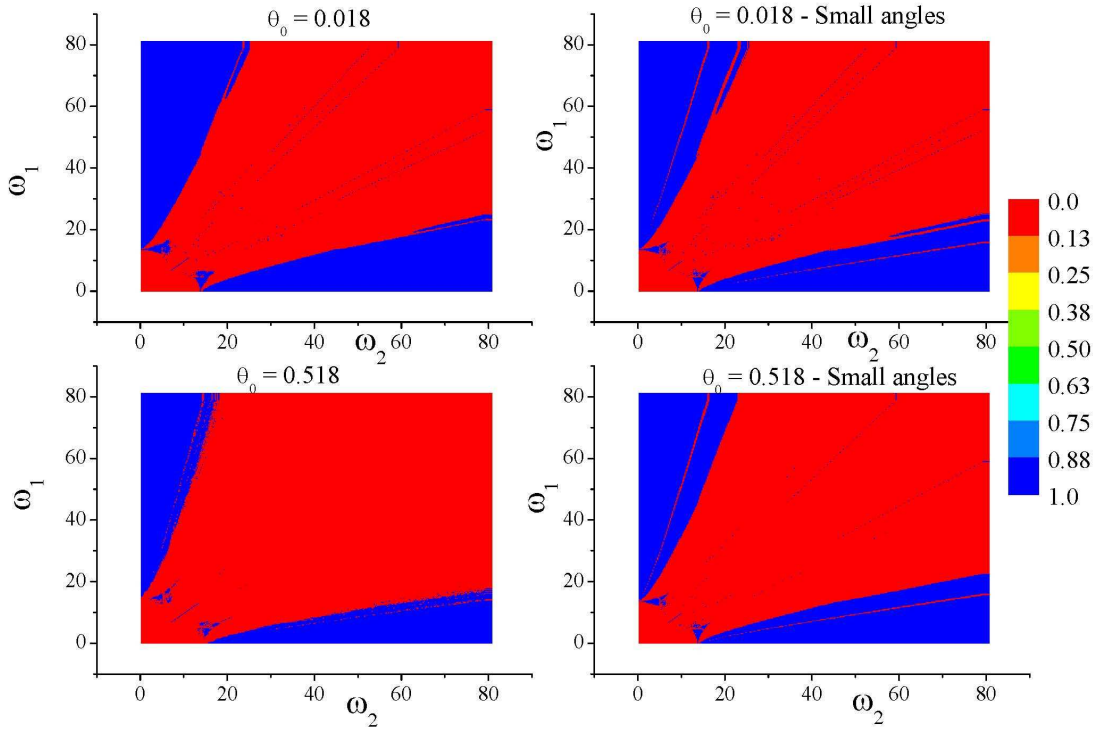

Figure 7: Initial angle effects $N = 2$. We used $A = 0.34$. Similar to Fig. 6.

depends on a variable T, which must be function of ω_1 and ω_2 not always easily determined. So, first we consider what we think that are reasonable choices of T as shown in Fig. 9.

It is clear from these results that the stability diagrams obtained from the effective potential approximation depends strongly on the choice of T. From all the numerical simulations, the best option is the choice $T = \max(T_1, T_2)$. Another limitation of Eq. 16 is shown in Fig. 10. Here, for different amplitudes we have the same stabilization pattern, except by the fact that the pattern is rescaled with A. On the contrary, however, simulations show that $A = 0.17$ and $A = 0.34$ (please see again Figs. 6 and 7 have completely different diagrams than ones which are shown in the Fig. 10. Just as in the case $N = 1$, we must also have an upper limit for the amplitude A, however a formulas like Eq. 24 is beyond of our expectations.

Now let us studying the stochastic stabilization considering $N > 2$. Dettman, keating and Prado [11] studied this problem in the context of stochastic stabilization of chaos. And they showed not using our pendulum inverted equation: $\frac{d^2\theta}{dt^2} = \frac{g}{l}\left(1 - \frac{A}{g}\sum \omega_i^2 \cos(\omega_i t)\right)\sin\theta$ but so $\frac{d^2\theta}{dt^2} = \left(1 - A\sum_{i=1}^{N}\sin(\omega_i t + \varphi_i)\right)\theta$

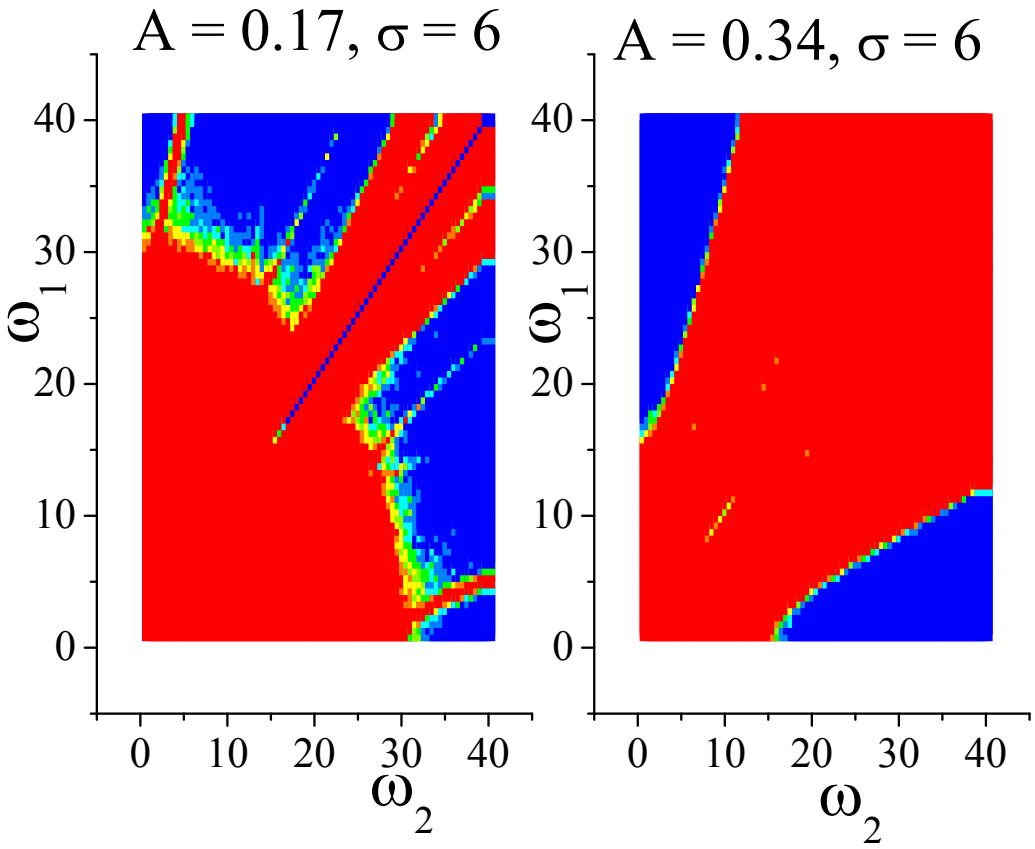

Figure 8: External Noise effects for effects $N = 2$. Comparison for $A = 0.17$ and $A = 0.34$ for $\sigma = 6$. We consider $\theta_0 = 0.018$.

that θ pendulum should be stabilized. Indeed for this particular equation this indeed occurs. We tested this equation with parameters used in this paper: $A = 38$, by changing sin by cos (to bring even more proximity with our case) and moreover making $\varphi_1 = \varphi_2 = ... = 0$ which they did not used but which bring even more to similarity with our case. So we also perform 100 frequencies chosen at random from [120, 600] and we do stabilize. However this means to make $g = l = 1$ in our case which is not real parameters for our problem. By making $g = l = 1$ we also numerically stabilize θ even considering ω_i^2 term in the sum which does not appear in [11], but the same does not ocurrs with real values in our case ($l = 1.2$ m and $g = 9.81$ m/s^2). The general arbitrary case $\omega_0^2 = g/l$ with the presence of term ω_i^2 deserves an special attention and the problem is being studied by the authors in another contribution (see [18]).

So, this negative case leads to look the problem in a alternative point of view which we presented in section 2.

For that we consider the case for N large considering a normalization for amplitude: $A(t) = Ct$, with

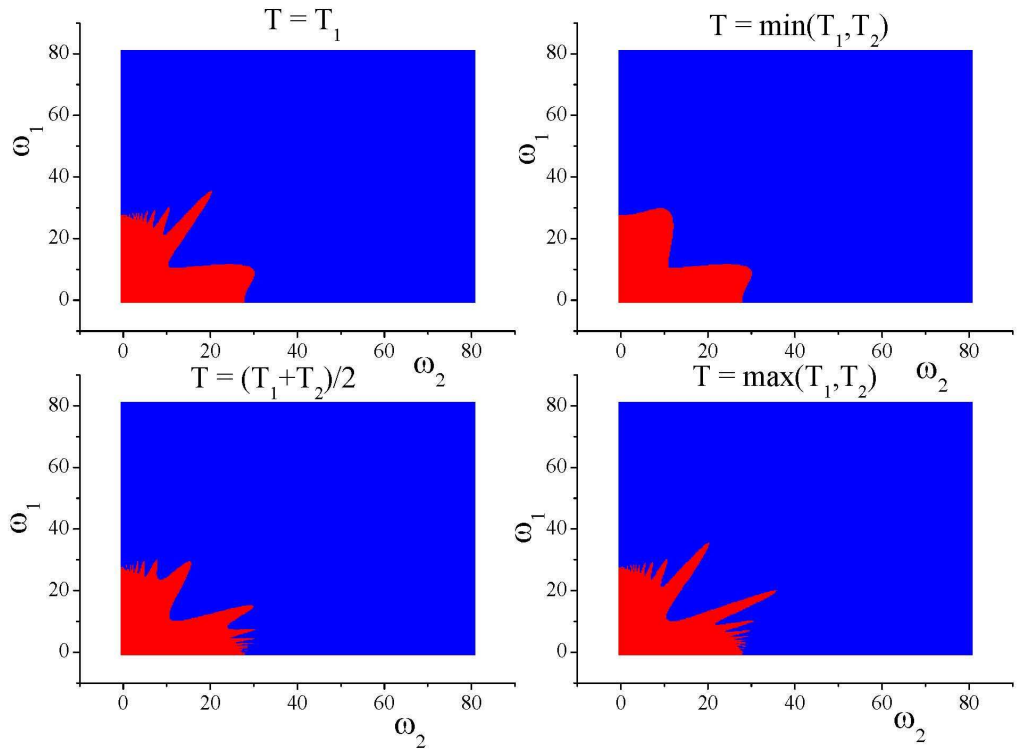

Figure 9: Potential effective for $N = 2$ according to Eq. 16. We show some choices for T. The best one (that better fits with simulations is to consider the maximal between periods.

$CN = a\omega_{\max}$ where ω_1, ω_2,..., ω_N are randomly chosen in interval $[0,\omega_{\max}]$. Here it is important to notice that $z(t) = C\sum_{i=1}^{N} t\cos(\omega_i t)$, and the equations must be originally integrated by Runge-Kutta by using $\ddot{z}(t) = -2C\sum_{i=1}^{N}\omega_i\cos(\omega_i t) - C\sum_{i=1}^{N}\omega_i^2 t\sin(\omega_i t)$. Such choice as previously reported must captures the case $N = 1$ at least for survival time. So we perform simulations (Procedure III - Table 4) that performs a random formula with N cosines. So we build diagrams a versus $\omega_{\max}$ for survival time (time that pendulum remains stable according the established condition) which can be observed in Fig. 11.

After this interesting phenomena that brings N large for $N = 1$, we concentrate our ideas for an interesting optimization process related to stability of pendulum. What the best N for a stabilization of inverted pendulum. This question when performed so free seems to be no interesting. However, the question is, if we would consider an ensemble of formulas by randomly chosen $\omega_1,...,\omega_N$ and $A_1,...,A_N$ in the intervals $[\omega_{\min} = 0, \omega_{\max}]$ and $[A_{\min} = 0, A_{\max}]$ by repeating $N_{run} = 2000$ different formulas and for each choise we

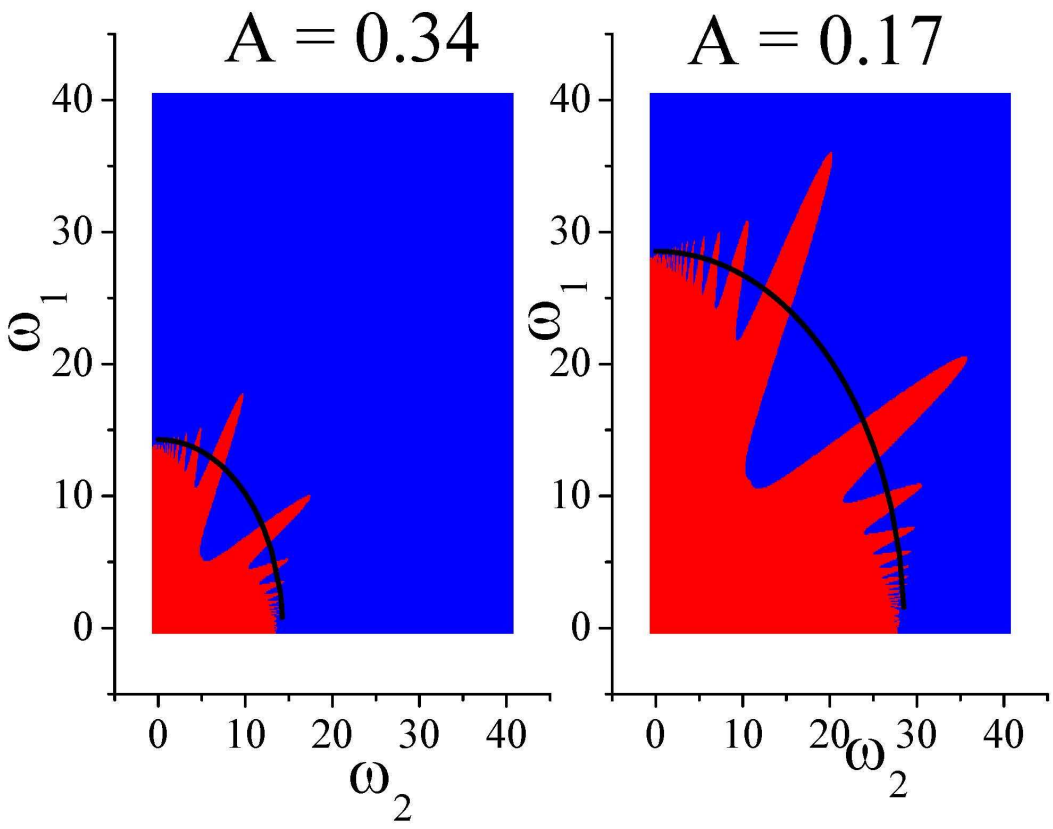

Figure 10: Potential effective for $N = 2$ according to Eq. 16. We show that for different amplitudes we have the same behavior which shows that effective potential as case $N = 1$ has a limitation since numerically we have very different diagrams considering $A = 0.17$ and $A = 0.34$.

observe the stability or not of the pendulum by calculating with this sample a survival probability. We used our Procedure 4: table 5 to calculate such probability. The Fig. 12 shows the survival probability in different situations.

The upper plot in this figure by keeping $A_{\max} = 0.17$m and we plot the probability for different values of $\omega_{\max}$. The different frequencies does not change the $N_{\max}$(value that maximizes the survival probability). However the middle figure, shows that keeping $\omega_{\max}$ fixed and by plotting the survival probabilities for different values $A_{\max}$. In this case we change the $N_{\max}$. But it is important to notice that different initial angles does not change $N_{\max}$ as reported in the lower plot in same Fig. 12.

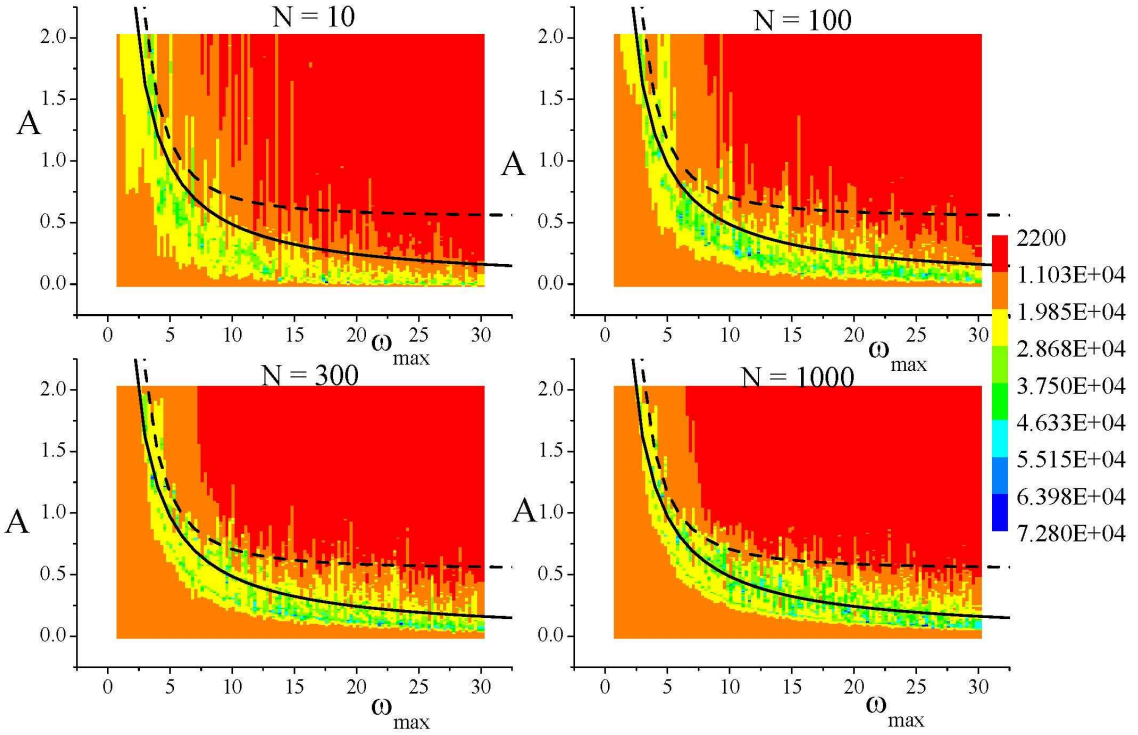

Figure 11: Diagram $a \times \omega_{\max}$. Each point corresponds to survival time (necessary time for the pendulum loses its stability) according to procedure 3. We can observe a better agreement of the points with region determined by the bounds (continuous and dashed curves) as N enlarges. This shows that case $N = 1$ has the pattern captured according to the amplitude normalization if we exchange the survival probability by the survival time.

5. Conclusions

In this paper we have detailed the study of inverted pendulum under a parametric excitation in its basis which is described by a superposition of N cosines. In case $N = 1$ we explore diagrams $A \times \omega$. We show that depending of initial conditions the effective potential method diverges from the numerical simulations, which also occurs in $N = 2$ that presents an interesting diagram where stability regions are alternated with no stability ones in a fractal structure. The diagonal $\omega_1 = \omega_2 = \omega$ has an important hole in the stability due to the known bating problem in waves. Although the method of effective potential is extended for arbitrary N, its applicability depends on choice of a common period existence and its utility has several limitations by showing the necessity of Runge Kutta integration of equations which in this paper is separated in four procedures used in each part of our manuscript and showed in details.

For $N > 2$ we perform two kind of analysis: a) a discussion about stochastic stabilization and b) optimization of survival probability of pendulum. In this first part (a), starting from hypothesis that inverted pendulum with real parameters cannot be stabilized for N large (this does not occur with a suitable choice of parameters) we show that problem for N large can be reduced to $N = 1$ if we look for survival time, i.e., the properties of survival time diagram which via a suitable scale in the amplitude are preserved when compared with regular, $N = 1$ diagram. In second part (b) we choose randomly choose amplitudes and frequencies in ranges and we calculate the survival probability of pendulum in order to observe the optimal N that maximizes such probability. We have two important conclusions here by observing our numerical studies : a) By fixing the upper limit of the frequencies chosen and changing the amplitude, N_{opt} depends on amplitude b) By fixing the upper limit of the amplitude and changing frequency, N_{opt} remains the same. The initial angles seems to be does not change N_{opt}.

We believe that many relevant questions are not completely understood and deserve more attention in future works. As an example, whether there is a general amplitude condition capable of stabilizing an inverted pendulum in the limit of a large number N of cosines with random frequencies by extending the particular result obtained in [11]. In this case, will it be necessary to introduce random phases in the modeling? Other important question is the real connection between the additive external noise and the parametric excitation in pendulum basis. This composition of different perturbations and the emerging phenomena by including resonance and other effects can bring more light to the problem of the control of noise systems.

Acknowledgments – This research was partially supported by the Conselho Nacional de Desenvolvimento Cientifico e Tecnologico (CNPq), under the grant 11862/2012-8. The authors would like to thank Prof. L.G. Brunet (IF-UFRGS) for kindly providing the computational resources from Clustered Computing (ada.if.ufrgs.br) for this work

[1] R. A. Ibrahim, Excitation-Induced Stability and Phase Transition: A Review, J. Vib. Control **12**(10), 1093-1170 (2006)
[2] R. A. Ibrahim, Stabilization and Stochastic Bifurcation with applications in ocean structures, chapter 1, page 1-52 in the Collection: Stochastically Excited Nonlinear Ocean Structures edited by M. F. Shlesinger, T. Swean (1998)
[3] Y. Kim, S. H. Kim, Y. K. Kwak, Dynamic Analysis of a Nonholonomic Two-Wheeled Inverted Pendulum Robot,Journal of Intelligent and Robotic Systems, **44**(1), 25-46 (2005)
[4] R.N. Gasimov, A. Karamancıoglu, A. Yazıcı, A nonlinear programming approach for the sliding mode control design, Applied Mathematical Modelling **29**, 1135–1148 (2005)
[5] A. Stephenson, On induced stability, Philosophical Magazine Series **15** (86), 233-237 (1908)
[6] P. L. Kapitza, Dynamical stability of a pendulum when its point of suspension vibrates, and Pendulum with a vibrating suspension, in "Collected Papers of P. L.Kapitza", Ed. by D.ter Haar, Pergamon Press (1965)
[7] J. L. Bogdanoff, S. J. Citron, Experiments with an inverted pendulum subjected to random parametric excitation, J. Acoust. Soc. Amer. **38**, 447-452 (1965)
[8] R. Yang, Y. Peng, Y. Song, Stability and Hopf bifurcation in an inverted pendulum with delayed feedback control, Nonlinear Dyn. **73**, 737–749 (2013)
[9] C.A. Hurst, The Indian rope trick explained, Australian Mathematical Society Gazette **23**, 154-159 (1996)

[10] D. J. Acheson, A pendulum theorem, A pendulum theorem, Proc. R. Soc. Lond. A **443**, 239–245
[11] C. P. Dettmann, J. P. Keating, S. D. Prado, Stochastic stabilization of chaos and the cosmic microwave background, Int. J. Mod. Phys. D. **13**(7) 1-8 (2004)
[12] E. I. Butikov, On the dynamic stabilization of an inverted pendulum, Am. J. Phys. **69**(6) 1-14(2001)
[13] J. G. Milton, J. L. Cabrera, T. Ohira, Unstable dynamical systems: delays, noise and control, EPL, **83** 48001(2008)
[14] W. H. Press, S. A. Teukolsky, W. T. Vetterling, B. P. Flannery, Numerical recipes in Fortran 77: the art of scientific computing, Cambridge University Press, 1992
[15] L. D. Landau, E.M. Lifshitz, Mechanics (Volume 1 of A Course of Theoretical Physics) Pergamon Press,1969
[16] J. A. Blackburn, H. J. T. Smith, N. Groenbech-Jensen, Stability and Hopf bifurcations in an inverted pendulum, Am. J. Phys. **60**(10) 903-908 (1992)
[17] H. J. T. Smith, J. A. Blackburn, Experimental study of an inverted pendulum, Am. J. Phys. **60**(10) 909-911 (1992)
[18] R. da Silva, S. D. Prado, H. A. Fernandes, Is it really possible to stochastically stabilize an inverted pendulum under real parameters?, arXiv:1608.00558 (2016)
[19] N. W. McLachlan, Theory and Application of Mathiey Functions, Clarendon Press, Oxford (1947)
[20] V. I. Arnold, Mathematical Methods of Classical Mechanics, Springer New York (1978)
[21] E. Ott, Chaos in Dynamical Systems, Cambridge University Press (1993)

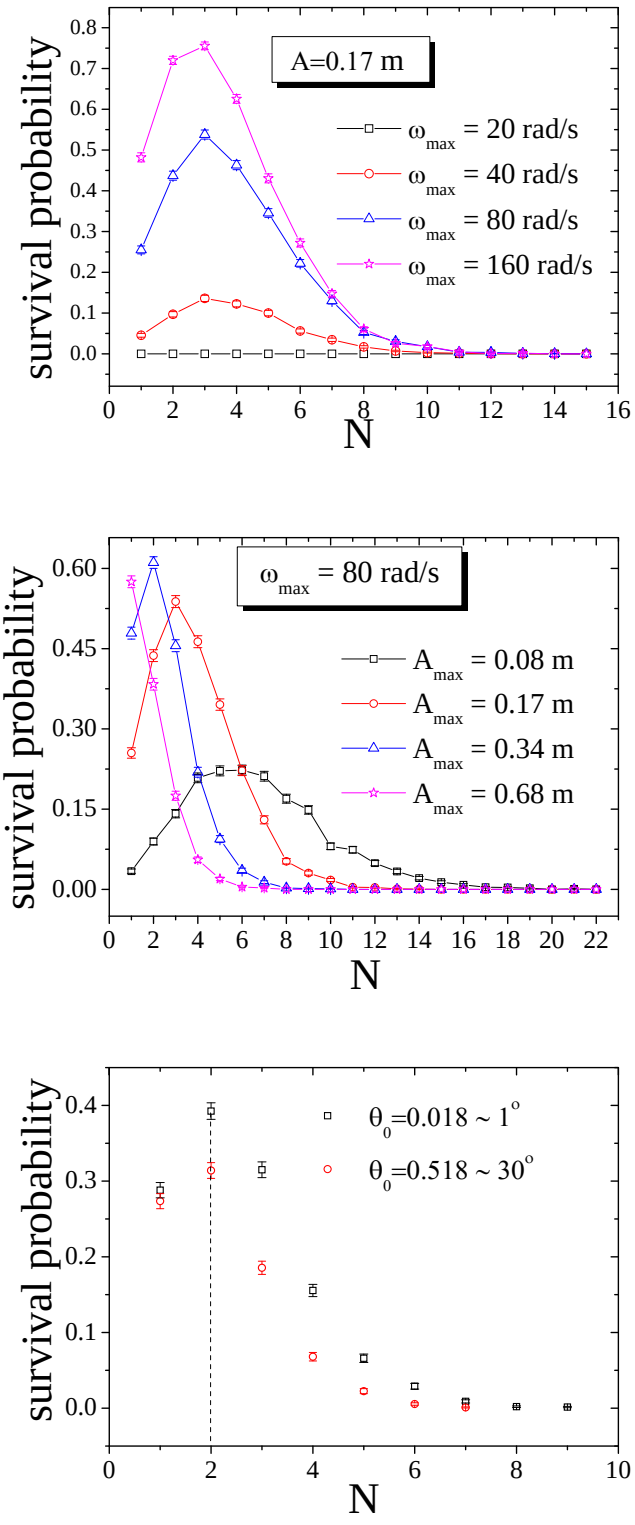

Figure 12: Survival probability obtained according to Procedure 4. From top to bottom: First plot shows curves corresponding to the different maximal frequencies considering the same maximal amplitude. In the second plot, we can observe the different curves corresponding to the different maximal amplitudes with the same maximal frequency. Finally, in the third plot, effects of initial angle is explored.